UNIVERSITÀ DEGLI STUDI DI PADOVA

Dipartimento di Fisica e Astronomia "Galileo Galilei"

Master Degree in Physics

Final Dissertation

Cellular dosimetry using GEANT4

in the context of the ISOLPHARM project

Thesis supervisor

Prof. Marcello Lunardon

Thesis co-supervisor

Dr. Alberto Arzenton

Dr. Alberto Andrighetto

Candidate

Emma Reniero

Academic Year 2022/2023

Abstract

The aim of the ISOLPHARM Project, and in particular the ADMIRAL experiment, is to develop a new radiopharmaceutical exploiting the properties of the ^{111}Ag isotope. The research program is subdivided into 4 different work packages. The first passages are devoted to the production of the radionuclide and the β and γ imaging, while in the fourth work package WP4 a set of radiobiological *in vitro* experiments will be performed to assess the new radiopharmaceutical. These experiments will be integrated with dosimetry simulations.

This thesis in particular will focus on dosimetry simulations using Geant4 in the context of the WP4 package. A dedicated code to simulate the energy absorbed by cells with different geometries and with different activity distributions of the isotope will be developed. After the library choice and the evaluation of the stability of results, the code will enable the study of the energy absorbed by a spherical and ellipsoidal cell in various configurations due to the decay of ^{111}Ag.

The second step of the thesis regards preliminary studies of the Lethal and Potentially Lethal (LPL) model. There will be the development of a code to simulate an experimental set-up that could be compared to the one that will be used for the studies of ^{111}Ag. This experiment is conducted at the LENA nuclear reactor in Pavia and it consists in the 2D *in vitro* cells irradiation with ^{60}Co sources. This first experiment allows to validate the code. After this validation, the data obtained through another experiment consisting in the irradiation of 2D *in vitro* colonies and the values obtained with simulations will be summed to evaluate the biological parameters (repair and misrepair) and to obtain the survival curve considering the LPL model. This process could be adapted in the case of an experiment with ^{111}Ag irradiation.

Contents

Chapter 1

The ISOLPHARM Project

Nuclear medicine is a widely expanding field where radioactive nuclides are exploited for both diagnosis and therapy. These radionuclides are mainly produced in nuclear reactors and cyclotrons, most of the times with a high production cost, reduced specific activity and possible significant contaminations [1].

In this context the aim of the ISOLPHARM (ISOL technique for radioPHARMaceuticals) Project is the production of a wide range of β-emitters with a high purity that are difficult to obtain in standard facilities. Moreover, compared to the standard production facilities, the production cost is expected to be lower and have less impact on the environment. Some of these radionuclides can be used to develop new radiopharmaceuticals having the purpose to kill specific tumor cells.
ISOLPHARM is a part of the SPES (Selective Production of Exotic Species) Project, which is based in the Istituto Nazionale di Fisica Nucleare (INFN) in Legnaro and it is part of the INFN Road Map, which is supported by the National Laboratories of Legnaro (LNL) and Catania (LNS).
SPES has in fact the aim to produce beams of neutron-rich nuclei with both high purity and intensity. These beams will then be used for nuclear physics researches and studies in other correlated fields, as medical physics [1] [2].
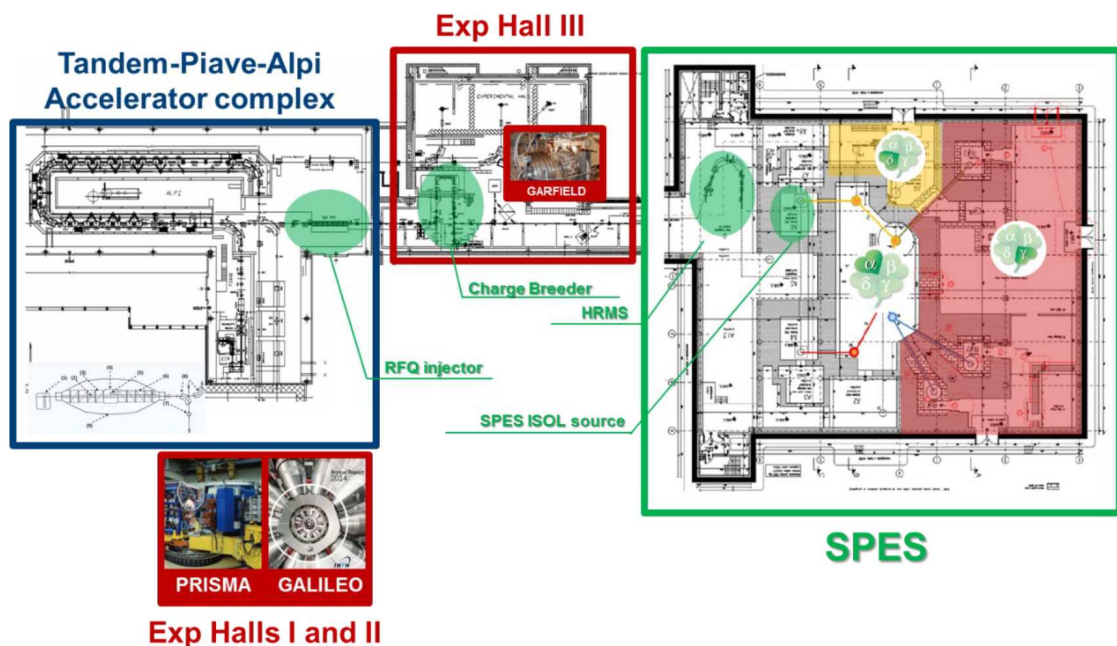

Figure 1.1: Layout of the SPES facility and the accelerator complex in Legnaro [3]

The structure of the facility is visible in Figure 1.1 together with the Tandem-Piave-Alpi accelerator complex. Currently the SPES facility is still under construction and its development can be divided in four different phases: α, β, γ and δ. The first two phases α and β comprehend the beam acceleration and the production and post acceleration of the RIB, while in the γ phase the beams are used to carry out experiments. SPES-δ will produce secondary neutrons.

Going more into details, the first phase SPES-α consists in the acceleration of the proton beam. This acceleration is done inside a cyclotron (that is currently under commissioning) and the beam energy can range from 35 to 70 MeV with a maximum total current of 700 µA. In the case of the ISOLPHARM Project the proton beam will have initially an energy of 40 MeV.

After the beam production, the second step SPES-β covers the production and post acceleration of the generated RIB (Radioactive Ion Beam) for Nuclear Physics researches [3].

The beam impinges on a multifoil thick target made of Uranium Carbide (UC_x) and it allows the production of radioactive isotopes, mostly neutron rich, with a mass number ranging of about Z=28-57. Changing the target's material one could also obtain proton-rich nuclei [4] [6].

Figure 1.2: Scheme of the ISOL method at SPES [5]

There are two different methods to separate the radionuclides from the target and to accelerate them: the In-Flight Separation and the ISOL (Isotope Separation On-Line) technique, which is the one used at SPES.

As one can see in the Figure 1.2, the Radioactive Ion Beam produced will follow diffusion and effusion processes at temperatures of about 2000°C (in vacuum conditions), to be extracted via evaporation from the target and to migrate to the ion source, where it will be ionised. This process can happen because the nuclear reactions reheat the primary target.

The RIB will then be then accelerated by a potential difference up to 40 kV in the Front-End. To eliminate the undesired contaminants and to get an Isobaric Ion Beam of the desired mass, the beam will pass through an electromagnetic mass separator, positioned after the ion source [5].
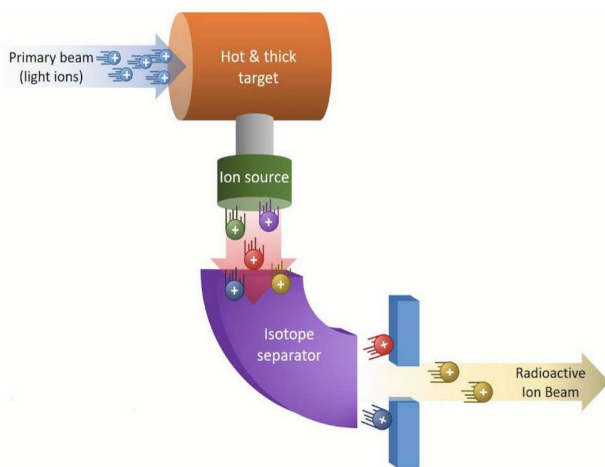
The isotopic RIB can then be implanted in a secondary target where the wanted isotopes, as ^{111}Ag, can be deposited.

The ultra pure RIB impinges in a substrate, which is processed to recover the radionuclides. To eliminate the residual contaminations, there is also a chemical separation [5].

SPES-γ exploits these intense and pure beams to carry out studies in different fields, in particular in Nuclear Medicine. In this step there are two initiatives regarding the medical field: the LARAMED and ISOLPHARM projects.

The SPES-δ step will be used to produce secondary beams of neutrons for studies in applied science [3].

1.1   ISOLPHARM_Ag and ISOLPHARM_EIRA

ISOLPHARM is a multidisciplinary project headed by INFN-LNL with the collaboration of different other Sections, as the ones in Pavia, Padova, Trento, Pisa, Bologna and LNS. It can also account for the cooperation with various university departments, as the Physics and Astronomy Department "Galileo Galilei" and the Departments of Pharmaceutical and Pharmacological Sciences and of Chemistry of the University of Padova, and the collaboration with the hospitals Santa Maria Nuova (Reggio Emilia) and Sant'Orsola (Bologna). This project is in fact based on the collaboration between researchers from different fields, as physicists, chemists, biologists and engineers [5].

After a preliminary feasibility study (ISOLPHARM_Ag, 2018-2019), the project started the research and development phase with the experiment ISOLPHARM_EIRA (2020-2022), continuing now as ADMIRAL (2023-2025).
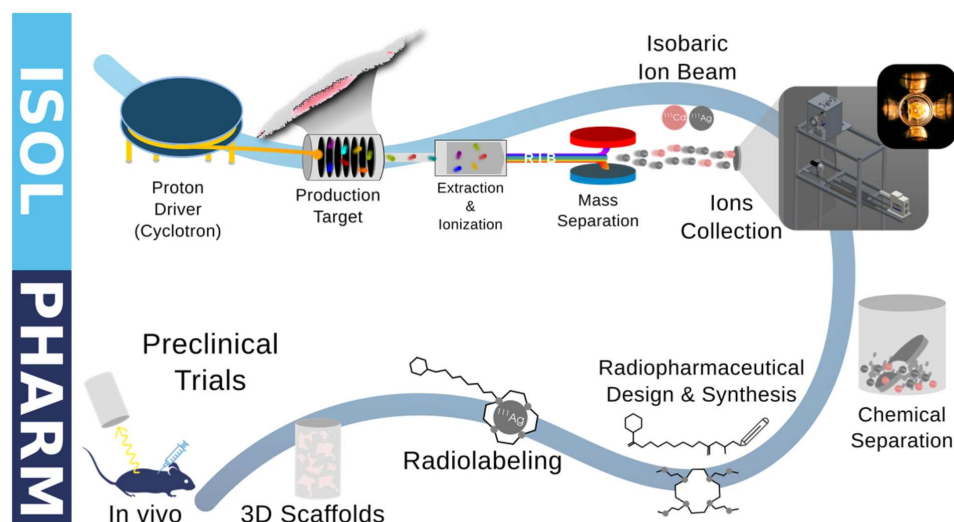

Figure 1.3: ISOLPHARM method scheme [1]

The ISOLPHARM Project is subdivided into two different stages:

- the ISOL step, in which the radionuclides, generated from the nuclear reactions triggered by the protons colliding with the target, follow the ISOL method path, obtaining a RIB with high specific activity [1];

- the PHARM stage, where macromolecules are radiolabelled with the radionuclides to produce radiopharmaceuticals (see Figure 1.4) [1].

Waiting for the SPES facility to enter in operation, the radionuclides are produced in the TRIGA Mark-II reactor available at LENA in Pavia.

The efficiency of these radiopharmaceuticals will then be tested in pre-clinical studies including *in vitro* and *in vivo/ex vivo* trials. The aim of these experiments is to study the uptake of the radiopharmaceutical in cellular colonies and in mice.
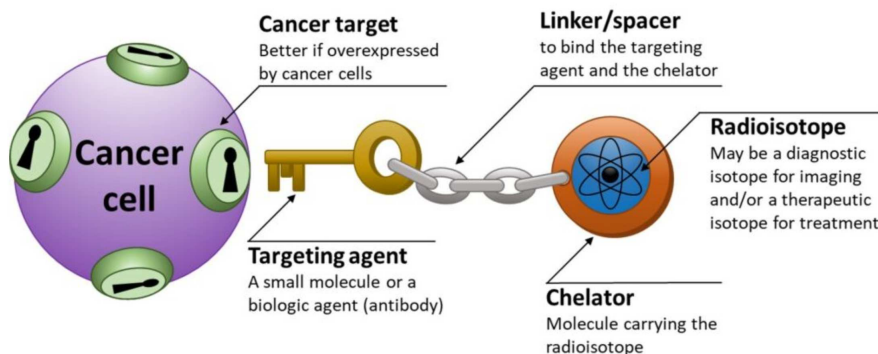
Figure 1.4: Radiopharmaceutical composition: the radioisotope is connected to a chelator which, thanks to a linker, is connected with the target agent that allows the bound between the disease cell and the radionuclide [7]

One promising isotope for radionuclide therapy is ^{111}Ag. In general this radionuclide can be produced in nuclear reactors in carrier-free form if a target of ^{111}Pd is irradiated. One of the cons of this process is the fact that this target has a high cost. With the ISOL technique instead, there could be the possibility to obtain a pure form of ^{111}Ag at a lower cost. This type of production is in fact under investigation [8]. Considering a UC$_x$ target and a 40 MeV proton beam, 5 days of irradiation could produce 80 GBq of ^{111}Ag. Moreover, the only contaminant that should be chemically separated is ^{111}Cd, that is a stable isotope.

These studies were at first conducted in ISOLPHARM_Ag and, due to the promising results, they were continued in another experiment: ISOLPHARM_EIRA (Experiment on Interdisciplinary research on Radioactive Ag). The latter project, as one can see schematized in Figure 1.5, is divided into different areas: physics, chemistry and biology [1].
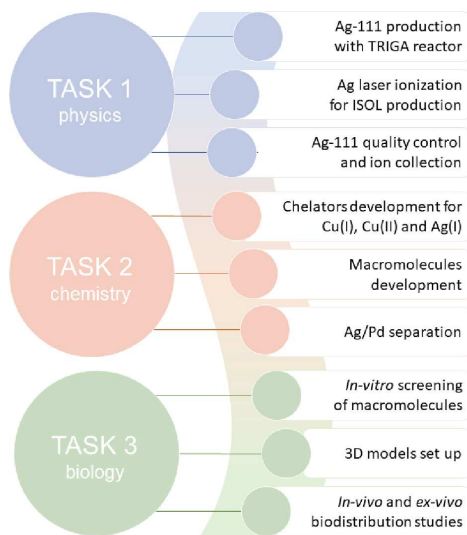

Figure 1.5: Scheme of the ISOLPHARM_EIRA tasks [5]

The aim of the first task was to produce and to conduct studies on ^{111}Ag. The production of the radionuclide was supposed to happen with the ISOL method in LNL, but for the preliminary studies, while the SPES facility is under construction and development, the ^{111}Ag is produced in the TRIGA nuclear reactor.

The chemistry step consists in the production and characterization of chelators, linkers and targeting agents. Moreover, another task is the purification of the radioisotope.

The biology task aims to develop at first *in vitro* evaluations regarding the effect of the targeting agents, followed by preliminary *in vivo* and *ex vivo* studies of radiopharmaceutical biodistribution [1].

The ISOLPHARM_EIRA project is currently completing the last task because of delays due to Covid. The *in vivo* and *ex vivo* experiments with chelated ^{111}Ag are scheduled at the end of 2023.

1.2 ADMIRAL

Since 2017, ISOLPHARM has conducted some studies regarding the development of radiopharmaceuticals labelled with a silver isotope: ^{111}Ag.

To continue and to enrich the preceding activities, the new experiment ADMIRAL (Advanced Dosimetry Methods and In-vitro Radiobiology of Ag-111 Labeled radiopharmaceuticals) has the aim to study ^{111}Ag, to verify its diagnostic and therapeutic properties.

^{111}Ag is a β^- emitter:

$$^{111}Ag \rightarrow\, ^{111}Cd + \bar{\nu}_e + e^- + \gamma \tag{1.1}$$

The associated γ-emission has a low probability to happen ($\simeq$ 8 %) and the average β energy (with an intensity of 92%) is of 360 keV. It penetrates through the tissues of about 1.1 mm and its half-life $t_{\frac{1}{2}}$ of 7.45 d is suitable for Targeted Radionuclide Therapy.

The properties of ^{111}Ag are similar to other radionuclides already approved by the European Medicines Agency EMA and the United States of America Food and Drug Administration FDA, such as ^{177}Lu [8].
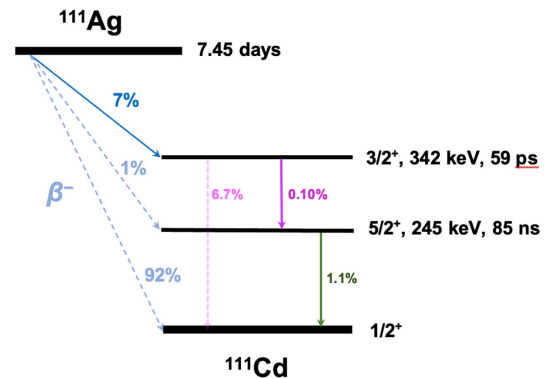

Figure 1.6: ^{111}Ag decay scheme

To study the ^{111}Ag features and to verify its efficiency for therapeutic and diagnostic purposes, the research program has been subdivided into four different work packages (WP), as it can be seen in Figure 1.7.
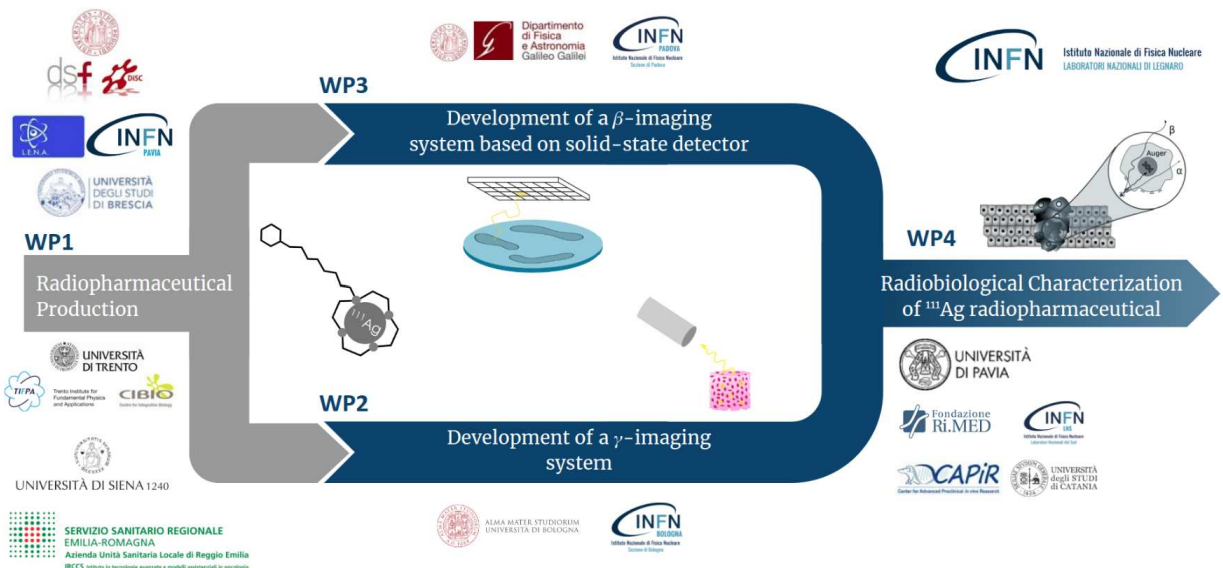

Figure 1.7: Work packages of ADMIRAL [9]

The first step WP1 has the aim to produce the ^{111}Ag-labelled radiopharmaceutical. The SPES facility is currently under construction and so the production of the nuclides is made with traditional methods in the nuclear reactor TRIGA Mark II at the Laboratory of Applied Nuclear Energy (LENA) in Pavia. Once ^{111}Ag is produced, radiochemistry experiments will be conducted to optimize the purification of ^{111}Ag, which requires the dissolution of the irradiated target. At the end of the process, the silver

isotope needs to be inserted in a macromolecular context. The aim of this macromolecule is to allow the bind and the transport the radionuclide through the body and to the disease site. This study has to focus on the choice of chelators, spacers and targeting agents to build the radiopharmaceutical. The latter have to be chosen to have a binding affinity with the cholecystokinin B receptor. This receptor results in fact over-expressed in several tumors.

The choice of a stable chelator and of the macromolecules was already done in the ISOLPHARM_EIRA project [9].

The WP2 package focuses on the β-imaging. The main task is to design and to construct a 2D detector with high resolution. This detector will use a technology developed during the ALICE experiment: the monolithic silicon pixels called ALPIDE chips.

At first it will be needed the design of the electronic and mechanic parts, followed by Monte Carlo simulations. To study its behavior, fluorescence tests and detector characterization will then be done.

Most of the experiments will be carried out with 3D scaffolds. These structures can in fact mimick disease tissues [9].
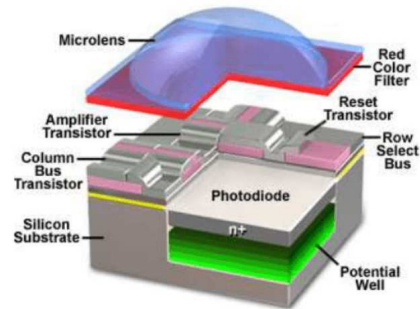

Figure 1.8: Monolithic silicon pixel schema [9]

WP3 has the aim to evaluate the diagnostic features of the ^{111}Ag. This can be done with the development of a system for γ-imaging to detect the γ-decay that follows, in some cases, the β emission.

This task can be done with the use of scintillators coupled with SiPMT and with the use of electronics and the structure is called γ-camera. Also in this case, phantoms injected with the labelled radionuclide will be used to study the features of the device [9].

The last step of the ADMIRAL proposal, WP4, consists in the test of the produced radiopharmaceutical, to have a radiobiological characterization of it. The *in vitro* tests will take place at the biology laboratory already present at LENA. The location's choice will avoid problems correlated to the transport of the radioactive isotope. Labelled ^{111}Ag will be tested in 2D cultures (see Fig. 1.9) and 3D scaffolds (see Fig. 1.10) with different levels of activity and time of exposition [9].

Figure 1.9: Cellular survival studies in 2D *in vitro* cultures [9]

The tests will be then associated with simulations made with Geant4, PHITS and MCNP of the experimental setup. The latter will allow to perform studies about the associated dosimetry.
Both the simulations and the *in vitro* studies aim to improve the predictivity and the strategies of the tests, to collect as many information as possible and to decrease the *in vivo* and *ex vivo* experiments on animals.
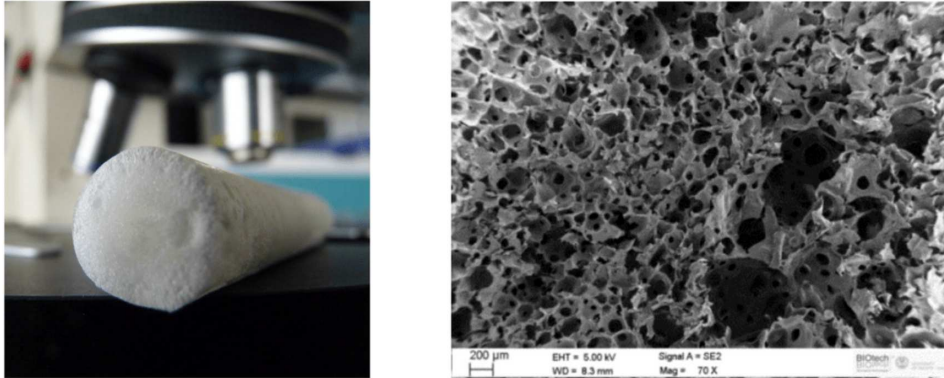

Figure 1.10: 3D scaffold for cell cultures [9]

1.3 Simulation studies using Geant4

Figure 1.11: Geant4 logo [10]

Geant4 (GEometry ANd Tracking) is a toolkit able to simulate the passage of both radiation and particles through matter. It was developed independently at CERN and at KEK Accelerator Laboratory in 1993 at first for High Energy Physics. Later on, it was adapted for the optimal use in different science fields, as Space and Radiation Science and Medical Physics.
It is based on Monte Carlo method and it includes a large range of functionalities as tracking, physics models, various geometries and hits. A wide set of particles is present and the energy range implemented goes from eV to TeV.
Its graphic interface (in relatively simple cases) allows to visualize set-up geometries and to view the tracks generated by the interactions of radiations and particles with the environment [9] [12].

1.4 Aims of the thesis

The contents of this thesis are mainly divided into two different sections.

Calculations of the S-values   The initial section of the thesis is dedicated to examining the absorbed dose within a cell exposed to varying activity configurations. This investigation is facilitated by a Geant4-based code developed *ad hoc*. The geometries considered for the cell are spherical and ellipsoidal (see Fig. 1.12) and the radionuclides simulated are ^{111}Ag and ^{177}Lu. The silver isotope is in fact studied to develop a new radiopharmaceutic for Radionuclide Therapy. The values of absorbed dose obtained will be then compared with the values simulated for ^{177}Lu. This comparison can be useful to assess the therapy efficiency of ^{111}Ag in relation to the well-established ^{177}Lu, a widely utilized radionuclide within the field of Nuclear Medicine.

An additional comparison of the absorbed dose resulting from the decay of ^{111}Ag, simulated with the Geant4-based code, will be conducted with the values obtained using the MIRDcell applet with the same radionuclide.

MIRDcell is a free software used for the modelling of radiopharmaceutical distributions in tissues and for the estimation of the cell absorbed dose [11]. This applet is a widely recognized software within the field of Medicine. By comparing the doses obtained through the code developed in this thesis with those available in MIRDcell, a first code validation can be established.
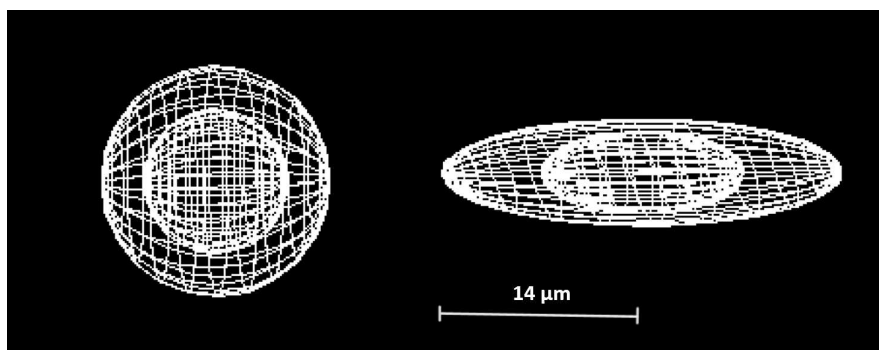

Figure 1.12: Graphical interface of Geant4 in which it can be seen a spherical and an ellipsoidal cell

The activity distributions studies regard the self-absorbed dose (the radionuclides decay on the membrane, in the whole cell or in the cytoplasm), the cross-absorbed dose (the emitting cell is moved at increasing distances from the target cell) and the environmental dose (the events are homogeneously distributed outside the target cell).

Dose and survival fraction estimations   The subsequent section of the thesis starts with the comparison between the absorbed dose acquired from an experiment conducted at LENA (Pavia) and the dose simulated employing the identical experimental configuration. This experiment involves the irradiation of flasks containing the U-87 GM cell line with ^{60}Co. Comparing the doses obtained through calibration with the simulated ones allows to validate the developed code (see Fig. 1.13).

When this thesis project started, a test experiment with a standard radiopharmaceutical was forseen, but due to external reasons only the ^{60}Co irradiation could be realized.
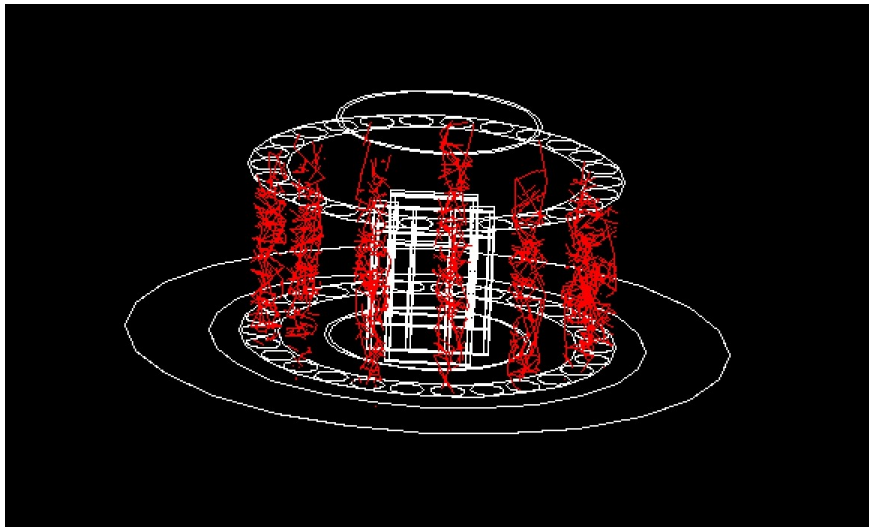
Figure 1.13: Photo of the graphical Geant4 interface during the simulation of the *in vitro* colonies irradiation

A second experiment, conducted at the nuclear reactor of Pavia, has the aim to study the cells survival fraction of the UMR-106 cell line after the irradiation with ^{60}Co. The experiment allows to obtain the absorbed dose for different irradiation times. The dose can be related to the cells survival fraction with different models. In particular, the two survival models considered in this thesis: the Linear-Quadratic (LQ) model and the Lethal and Potentially Lethal (LPL) model. Specifically, the aim is to examine the survival fraction curve generated by the LPL model using parameters acquired in the experiment and comparing it with the LQ model's curve.

Chapter 2

Brief introduction to RNT

The usage of radiation in any field needs an accurate measurement of it. In particular, in the context of Nuclear Medicine, the radiation measurement is necessary for both diagnosis and therapy. In the first case, one needs to obtain a good quality image, keeping the radiation dose as low as possible. For radiotherapy, the radiation has to be delivered in an accurate and precise way to the target, to maximize the dose to the disease side, while avoiding as much as possible dose to the healthy tissues. The radiation given to healthy tissues could in fact cause damages to the DNA that could bring to the development of cancer.

To study the energy released in matter, depending on the deepness one can introduce the absorbed dose D_{em}, defined as:

$$D_{em} = \frac{dE_{ab}}{dm} \tag{2.1}$$

where dE_{ab} is the mean energy absorbed by a certain volume (that can be the target organ or adjacent tissues) of mass dm. The absorbed dose unit is the Gray (Gy) that, in SI unit, can be written as 1 Gy=1 J $\cdot$ kg^{-1}. D_{em} depends on both the absorber and the type of radiation. In most cases, the human body can be represented as water and so the effect produced by radiation passing through a human tissue can be approximated to the one in water [13].
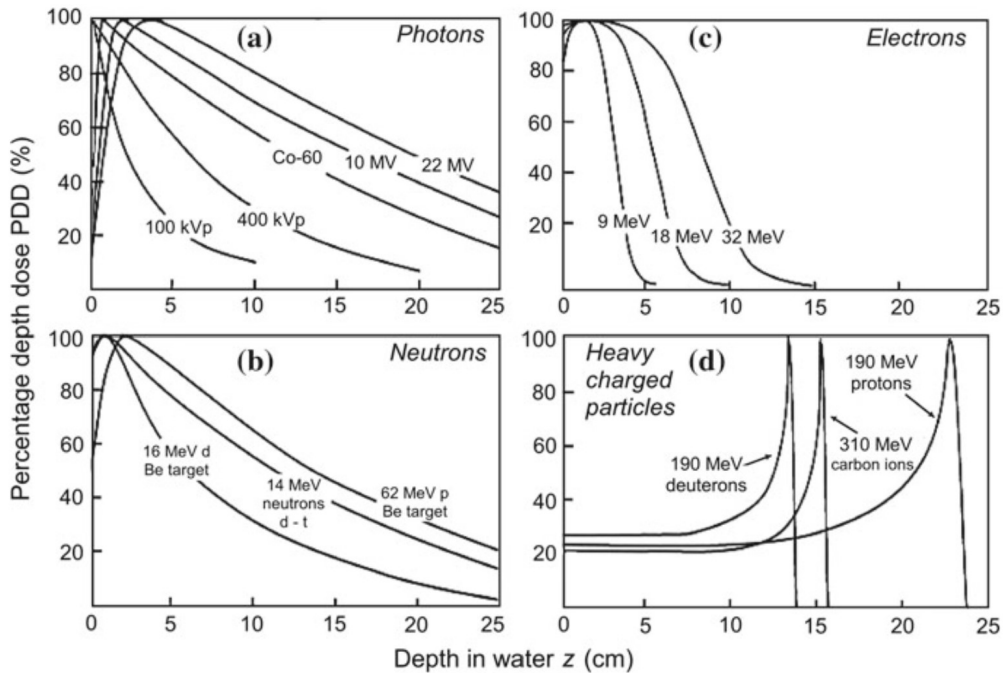

Figure 2.1: Dose-depth curves of different kind of ionizing radiation [23]

The main categories usually taken into account during the study of the dose distribution in water are photons, neutrons, electrons and heavy ions.

As one can see in Figure 2.1, the dose released at a certain depth highly depends on the kind of radiation. In all the curves it is visible a maximum, which varies for shape, sharpness and deepness; this fact can be exploited to maximise the release of the energy in the disease site, sparing the healthy tissues [13].

2.1   Radiation Therapy

A widely applied branch of Nuclear Medicine is Radiation Therapy. In this therapy the patient receives radiation locally for the treatment of a disease. In particular, it is commonly used as a tool for cancer treatment. Radiation Therapy can be subdivided into 3 different modalities [14]:

- External Beam Radiation Therapy (EBRT), in which the patient receives an external beam that can be of γ-rays from a radioactive source as ^{60}Co, e^-, X-rays or hadrons from accelerators. The dose is usually given in multiple fractions (the standard is 2 Gy/fx) and the radiation received is homogeneous and so it is possible to have a well-defined dosimetry [14] [15];

- the second modality is Brachytherapy. This technique consists in the placement of sealed radiation nearby the disease inside the body. This placement can be made manually through a catheter, that is a small and stretchy tube, or through an applicator, that is instead a larger device. These capsules can stay inside the body from 1 to 7 days or they can be left for 10-20 minutes at a time and the treatment can go on for some days. In other cases the capsules are left inside the body [14] [16];

- the last technique is Radionuclide Therapy (RNT), that exploits unsealed radiation sources to treat tumors and other diseses [14].
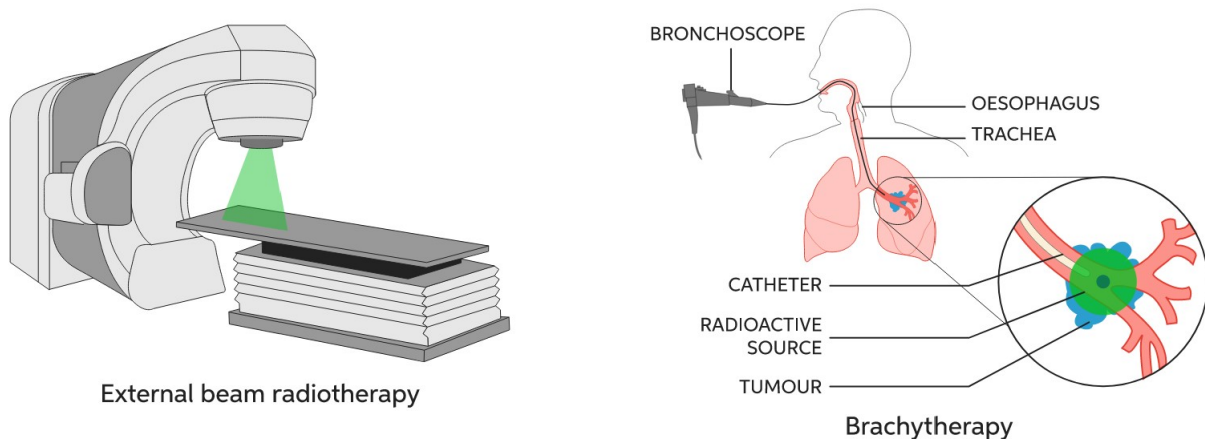

Figure 2.2: Scheme of EBRT [16] (on the left) and of Brachytherapy [16] (on the right)

RNT is currently an expanding technique of treatment. It consists in the delivery of radiopharmaceuticals at cellular level, to kill the disease cells. This method aims to minimize the damage to the surrounding tissues that are non-targeted cells.

The radiopharmaceutical that is used can be a simple ion, as for example the widely used ^{131}I, or a complex one. In Targeted Radionuclide Therapy (TRNT), a modern branch of RNT, one uses a carrier molecule labelled with a particular radionuclide [14].

The ions can be injected intravenously or administrated orally to the patient. The mechanisms used for targeting the radionuclides to the disease tissue are multiple.

Moreover, this method is characterized by an extended exposure with a declining dose rate, described by the exponential decay law. The absorbed dose is not homogeneous and the particles used have different ionization densities that modify the quality of the therapy.

Radionuclide Therapy is used when the conventional External Beam Therapy can not be used. This

happens when the latter method causes unacceptable toxicity to the surrounding healthy tissues as in the case of disseminated disease, metastases or cancers located in the vicinity of sensitive organs, as liver and kidney [17].

2.2 Discovery and development

The history of Radionuclide Therapy started in 1898 with the discovery of Radium. Shortly after, it was noted that the exposure or the contact of this radionuclide with living tissues generated adversed effects. They depended on the duration of the exposure and on the distance from the source. In particular, it was noted that scientists who used to carry the radionuclides in the pocket of their jacket developed a burn in the chest.
This observation was used for example to cure certain types of skin diseases. However, this technique was limited by the fact that only natural radionuclides were available [20].
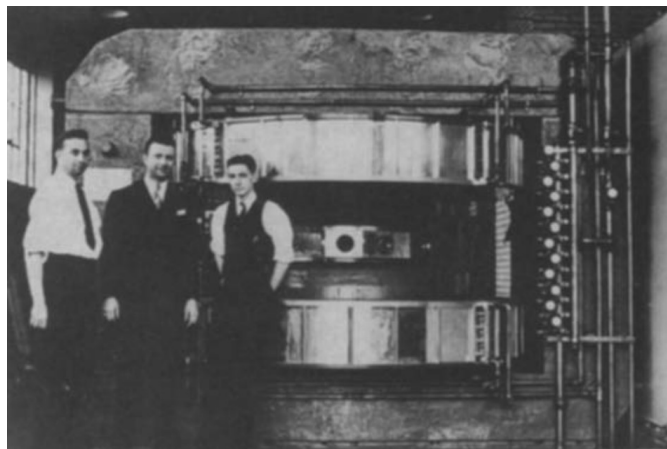
Figure 2.3: Photo of the construction of a cyclotron at MIT for medical purposes [21]

The major step forward happened in 1934, when they discovered that it was possible to produce unstable versions of stable nuclei. This technique consisted in the exposure of stable elements to the emission of highly radioactive ones.
At the same time they built the first cyclotron, in which charged particles are accelerated at energies high enough to penetrate the nuclei of stable elements to get unstable ones [19].
Speculations were made about the possibility to use these radionuclides in medicine. In particular, in 1936 Dr.-Karl Compton, President of MIT, had a lecture ad Harvard University, "What Physics can do for Biology and Medicine", where he discussed about potential uses of artificial radionuclides to study metabolic mechanisms. The Massachusetts's General Hospital thyroid group was interested in obtaining iodine radioisotopes.
They started a joint project to obtain and use radioactive isotopes of iodine. At first, they were able to obtain ^{128}I and after various studies they managed to get ^{131}I. They started therapeutic treatment in 1941 and cancer treatments in 1942 [20] [21].

2.3 Radionuclides selection

To be a candidate for Radionuclide Therapy the isotope needs to satisfy certain criteria. In primis it needs to cause a notable damage to the disease cells. The target of this kind of therapy is the DNA and the interaction with the radiation can happen with direct or indirect mechanisms (see Fig. 2.4) [14].

In the first case, the radiation interacts directly with the DNA helix and it is dominant for high LET
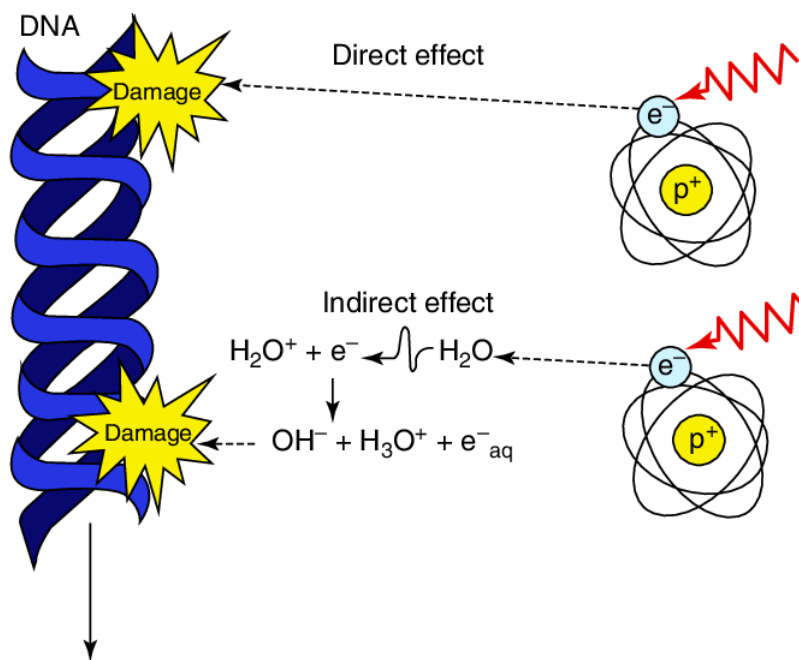
Figure 2.4: Scheme of radiation interacting directly and indirectly with the DNA

particles. In the indirect case, the radiation dissociates the water generating reactive oxygen species (ROS). This interaction generates various radiolytic reactive products, such as O_2, H_2O_2 and free radicals.

These products are able to break chemical bonds and this process generates changes that can bring to DNA damages. In particular, the most lethal lesion for the cell is the Double-Strand DNA Break in which both the strands are damaged. This lesion can be repaired or, in case of misrepair, it can bring to a cell mutation.

The ionization distribution and the lesion depend on the type of radionuclides and on their energy. Potentially, the highest therapeutic efficiency is expected in the case of α-emitters, β-emitters and Auger electrons [14].
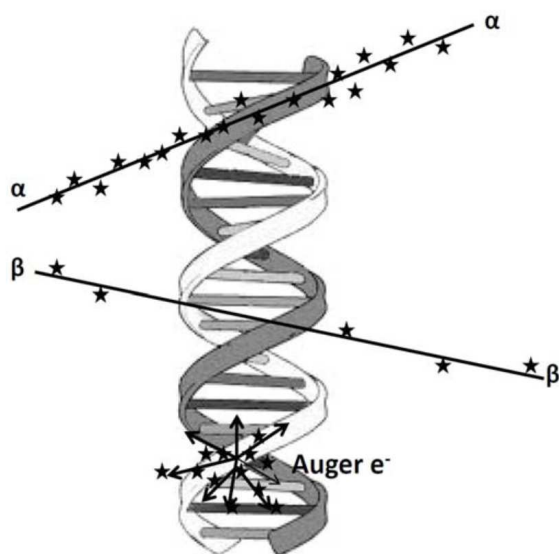
Figure 2.5: Scheme α, β radiations and Auger electrons interacting with a DNA helix [14]

α-particles from nuclear decays have energies in the range of 5-9 MeV and their deposited energy is of 80-100 keV/µm (except for the end, where it reaches about 300 keV/µm). Their trajectory is straight and usually they can travel for 50-100 µm in biological tissues. They cause irreversible DNA lesions and, due to their high energy transfer, only 2-3 tracks are enough to cause cell death.

β-emitters are the most commonly used for Radionuclide Therapy. Their trajectory is contorted. Their linear energy transfer is of about 0,2 keV/µm (except for the last nm of the range), which is low respect to the energy transferred by the α particles. Because of that it is needed a higher density in the disease site to be therapeutically efficient. The tracks needed to kill a disease cell are in fact typically $10^2 - 10^3$ [18].

Usually, β-decay is followed by the emission of one or more γ-photons. The γ emission at low energies (70-300 keV) can be useful in the case of theranostics, but it can be a problem at high

energies.

In the case of electron capture or internal conversion there is the formation of a vacancy inside the isotope. This vacancy is usually in the inner shells. To fill it there is an electron rearrangement and an e^- of the outer shells is dropped. Each electron transition is followed by the release of energy that can be in the form of an Auger electron or a characteristic X-ray photon.

On average the number of Auger electrons emitted is 30-50 with energies from a few eV to 1 keV. The low energy causes a contorted trajectory and it is possible to observe a multiple ionization nearby. Due to the short range, proximity to the target is needed [18].

One also needs to consider the radionuclide half-life $t_{\frac{1}{2}}$. To have a good therapeutic efficiency, the half-life should be longer than the time that is required for the radiopharmaceutic preparation, the delivery to the clinic, the injection and the path through the body to the disease site.

The optimal half-life of radionuclides for this kind of therapy ranges from a few hours to about a week. More short- and long-lived isotopes present some problems.

The short-lived ones may have a shorter half-life than the time needed for their storage and delivery to the disease, while the long-lived ones can cause an increment of the absorbed dose in the healthy tissues. In this case the patient can also become a radioactive source and isolation is needed.

However, in clinical practice it is usually considered the complete life-span T that can be written as:

$$T = \frac{1}{t_{\frac{1}{2}}} + \frac{1}{t_{hc}} \tag{2.2}$$

where t_{hc} is the half-clearance time of a radiopharmaceutical from the organism or the disease site. This time highly depends on the delivery system of choice [19].

The choice of the emitters depends also on the tumor size, its heterogeneity and the pharmacokinetics. Another important requirement is the chemical purity. In particular, the absence of metal impurities. This is due to the fact that metals inhibit the process of labelling in the case of Targeted RNT of carriers with metal radionuclides [14].

It is also necessary to have a large-scale production. This production can follow three different methods.

2.4   Radionuclides production

Radionuclides in Nuclear Medicine are produced with different methods: the most common are nuclear reactors, accelerators and radionuclide generators.

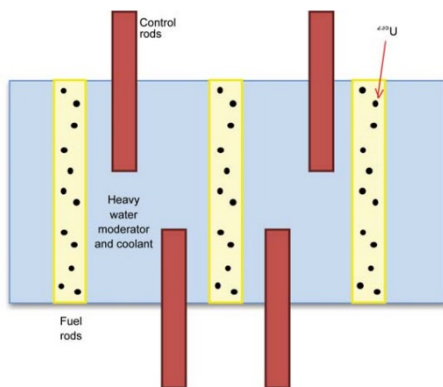In nuclear reactors fission and neutron activation are exploited [22].

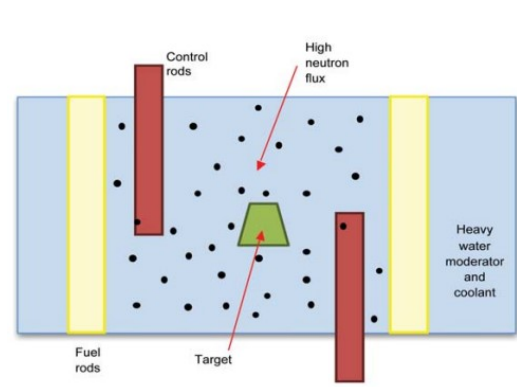Figure 2.6: Scheme of fission mechanism [22]

Figure 2.7: Scheme of neutron activation [22]

The fission process (see Figure 2.6) consists in the split of a nucleus into two pieces. Usually the nuclides

used are ^{235}U and ^{239}Pu. It happens spontaneously in nature, but in nuclear reactors the process starts adding energy in the form of a neutron. Fission fragments move apart really fast. Fragments produced are various but the probability says that most of the fragments have different mass number and they can be called fission pairs. A single fission reaction is uncommon in reality and instead a wide variety of nuclei are produced simultaneously.

As a by-product of the reaction fast and high energetic neutrons are produced. These neutrons can be slowed down in scatter reactions with moderators, such as water or heavy water. After the thermalisation they can be used again to start new fission reactions that gives birth to a reactions chain. This chain can bring to an uncontrollable production of nuclei that can be slowed down and controlled by control rods made usually of boron or cadmium.

The second reaction is nuclear activation (see Figure 2.7), in which the neutron high flux, produced as a by-product during the fission, can be exploit to bombard stable nuclei. These nuclei need to be placed inside the nuclear reactor. Most reactions are (n, γ) [22].
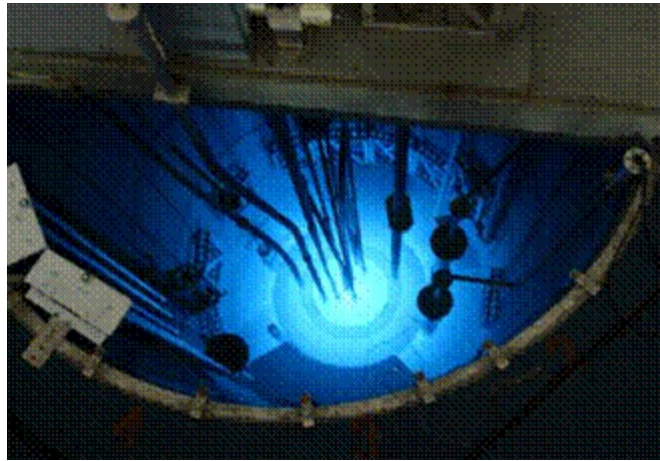
Figure 2.8: Nuclear reactor at LENA [24]

As far as the production of ^{111}Ag is concerned, the SPES cyclotron is now in phase of construction and it is not possible to generate radionuclides (in particular ^{111}Ag) with this method. To conduct preliminary studies, the nuclear reactor situated in Pavia is currently exploited. This reactor is called TRIGA Mark II and it is part of the Laboratory of Applied Nuclear Energy (LENA).

The nuclear reaction used to produce ^{111}Ag via radiative neutron capture is:

$$^{110}Pd(n,\gamma)^{111}Pd \rightarrow {}^{111}Ag \tag{2.3}$$

After the irradiation, ^{111}Ag has to be extracted by the Pb sample by chemical separation [23].

The second way to produce radionuclides for TRNT is through cyclotrons. Cyclotrons generate high energy particles (as protons, deuterons and alphas) that bombard a target made of stable nuclei (see Figure 2.9).

In the classic configuration, a cyclotron is made of two semi-circular electrodes Ds separated by a gap inside the vacuum within a magnetic field.

The source is placed at the centre of the cyclotron and a high frequency oscillator generates a high voltage in both the electrodes. The particles, attracted by the D with the opposite charge, pass through the gap and arrive to the electrode. When they reach it, the high-voltage is switched and so they are attracted to the opposite one. This process generates an acceleration and it goes on until the particles reach the wanted speed. When the velocity is reached they exit the cyclotron to collide with the target of stable nuclei [22].
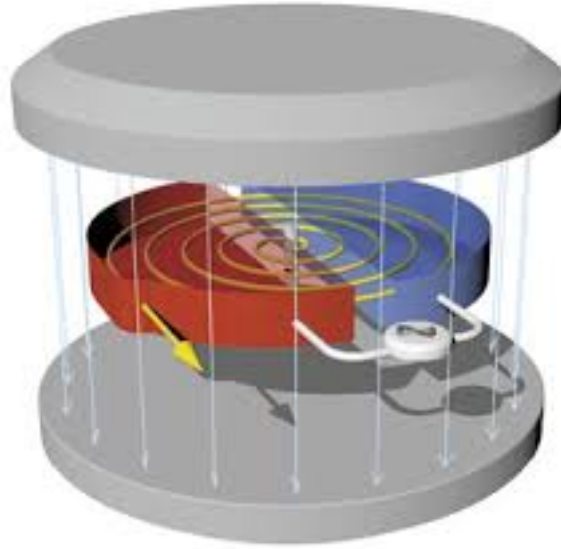
Figure 2.9: Schematic structure of a cyclotron

The SPES cyclotron (currently under construction) is visible in Figure 2.10. This cyclotron will be exploited for the production of neutron-rich isotopes, in particular of ^{111}Ag for the ADMIRAL experiment. This silver isotope can be produced with the collision of the high energy protons with a target of ^{238}U [23].

Figure 2.10: Picture of the SPES cyclotron at INFN-LNL [25]

The last method to produce radioactive isotopes is the radionuclide generator. It is used when there is the necessity of a weekly supply of a certain isotope. The isotope in this case is available on site and it is mainly used when the transportation results difficult and when the half-life is short.
Inside the radionuclides generator a pair of parent-daughter radionuclides are present. The first is a long-lived isotope, while the second is a short-lived one. The process of separation of the daughter from the parent nucleus and the extraction is called elution and it depends on the half-life of both. The elution efficiency, that is the percentage of daughter nucleus extracted with elution, is usually of about 90 % [22].

The classification of generators is based on the kind of equilibrium between the parent-daughter pair. In the case in which the half-life of the parent nucleus is at least 100 times longer than the one of the daughter it is defined as secular equilibrium (see Figure 2.11). In this case after 5-6 half-lives (after the last elution) the activity of the two isotopes is the same. The other case is called transient equilibrium (see Figure 2.12) and one has that the half-life of the parent is not considerably longer than the daughter one. The daughter activity increases until it reaches a maximum (after about 4 half-lives) and then it decreases with the activity of the parent [22].
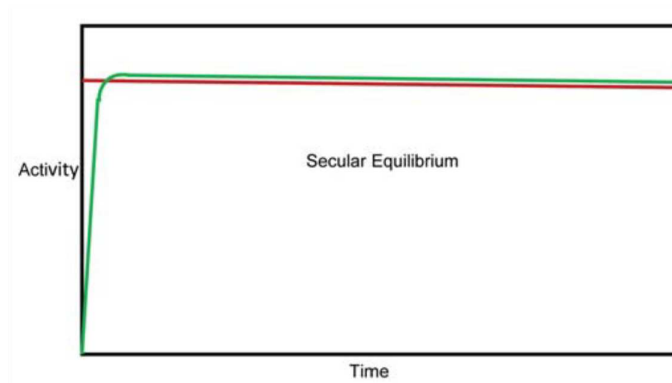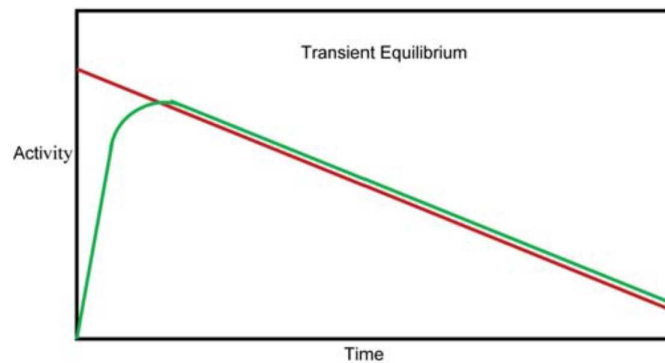
Figure 2.11: Secular equilibrium [22]

Figure 2.12: Transient equilibrium [22]

2.5 Targeted RNT

To treat different kind of diseases, a new technique was developed: Targeted Radionuclide Therapy (TRNT). The goal of this method is to deliver the radiopharmaceuticals with more selectiveness and to cause as less damage to the healthy tissues as possible. In this way the side effects could be less severe and frequent.

In TRNT the radiopharmaceutic is made of multiple components that can be seen in Figure 2.13 [19].
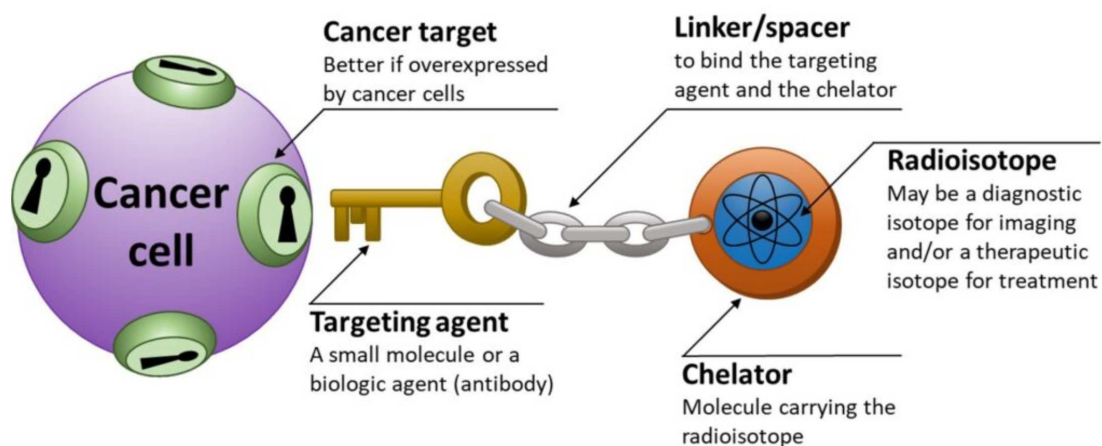
Figure 2.13: Radiopharmaceutical scheme composition and its way of binding with the malignant cell [7]

First of all there is the radioisotope, that in case of the ADMIRAL experiment is the β-emitter ^{111}Ag. The radioactive isotope is carried by a chelator. The chelator needs to be stable when passing through physiological medium to arrive to the disease site carrying the ^{111}Ag intact [7]. It is connected to the targeting agent thanks to a linker.

The targeting agent needs to follow certain criteria: it needs not to be immunogenic and neither toxic. Moreover, it needs to have a high affinity to the targets that are situated on the surface of the disease cells and simultaneously it should be able to bind to different radionuclides. Another important requirement is its resistance to biodegradation, while travelling inside the human body. Chemical purity and low production costs are also necessary [14].

The targets are molecules that are localized in all the tumor surface. They are usually over-expressed by the disease and in particular by tumors and they should be easily reachable through extracellular fluids or blood but at the same time they need to stay in the tumor site.

To avoid side effects, they should not be expressed or should be present minimally in healthy cells.

These requirements bring to a high specific activity labelling. This means that the radiopharmaceutic binds to the higher number of tumor cells as possible.

Currently, the most exploited molecules are peptides and antibodies. In fact most of the malignancies over-express certain peptide receptors or antigens [14].

Chapter 3

Survival models

3.1 Mechanisms of DNA damage and repair

The DNA damages can be divided into two different categories, depending on their origin: endogenous and exogenous. In the first case, the DNA undergoes hydrolitic and oxidative reactions with ROS (reactive oxygen species) and water that are already present in the cell. These damages are the cause, for example, of hereditary diseases. The endogenous damages instead are due to the external environment. In this case in fact there are chemical and physical agents that interact (directly and indirectly) with the DNA [26].

One of these agents is ionizing radiation (IR), that is used in Nuclear Therapy to damage and possibly kill disease cells [27]. As it can be seen in Fig. 3.1, the IR can bring to different types of damages. The damage depends mainly on the amount of energy that is transferred to the human body when the IR passes through it. In particular, there are two classes: high and low LET (linear energy transfer) [26].

High LET radiation has more probability to cause a damage to a base or to generate a Single-Strand Break (SSB). The latter happens when only one strand of the DNA is broken. Low LET radiation can generate the same lesions and also has more probability than high LET to also cause Double-Strand Break (DSB), which happens when both the strands are damaged by radiation. Other damages that happen with different amount of energies are the sugar damages and DNA-DNA and DNA-protein cross links [28]. The DSB, due to misrepairs, seems to be the most effective for the cell death.
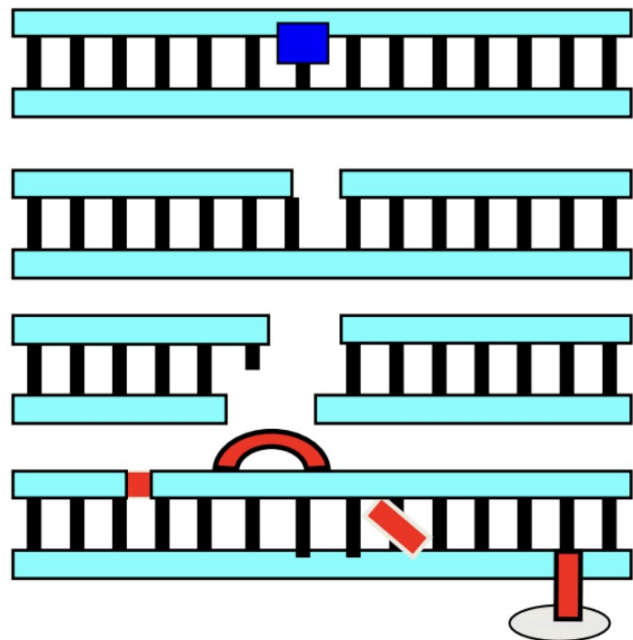
Figure 3.1: Scheme of DNA damages [28]

When a human cell is damaged, there is a signal that interrupts momentously the cellular cycle. The DNA can then be repaired, depending on the conditions, with different repair mechanisms:

- Base Excision Repair (BER);

- Nucleotide Excision Repair (NER);

- Mismatch Repair (MMR);

- Homologous Recombination (HR);

- Non-Homologous End-Joining (NHEJ);

- Translesion DNA Synthesis (TLS).

To repair the DSB the main mechanisms are HR and NHEJ [28].

In the case of the Homologous Recombination, the cell can exploit the redundancy of the information of the genome and it is enabled to copy an intact sequence of DNA from another chromatid with an almost identical DNA sequence. This process allows to repair the DNA lesions due to IR. This kind of repair mechanisms is based on the use of a sister chromatid and this implies a high fidelity [28, 29].
During meiosis, that is the phase in which the chromosomes are duplicated and there is the generation of the gametes, this mechanism can produce new combinations in the DNA that bring to variations. This is due to the fact that the DNA sequences have small differences and are not completely identical [29].
In Non-Homologous End-Joining, the DNA is repaired without the information contained in a sister chromatid. In this case the break ends are directly connected. This mechanism has less fidelity and it generates more errors but it is still tolerated. DSBs in fact happen usually in non-coding sections [30].
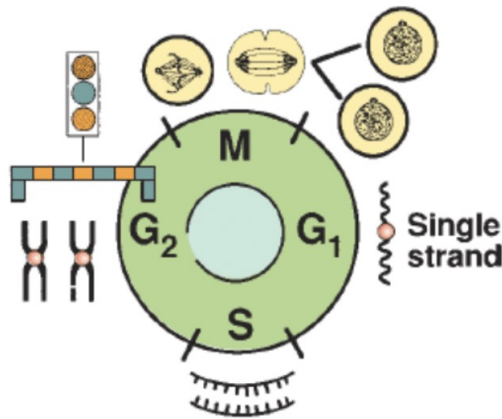
Figure 3.2: Scheme of the cellular cycle [28]

Depending on the phase of the cellular cycle, one of them dominates over the other. During the G1 phase, that is the longest phase, the repair mechanism is the NHEJ (in this phase there is in fact only one single strand), while in the S, G2 and M the repair is mainly through HR. After the cell correct repair it re-enters the cellular cycle.
In general, when the cell is misrepaired, there are two scenarios: the cell can die or it can generate a mutation. In the latter case, it re-enters the cellular cycle giving birth to a malignant cell.

3.2   Linear-Quadratic Model

The Linear-Quadratic Model is a quasi-empirical model
to connect the absorbed dose to the survival fraction.
Knowing this relation could be useful to develop an
optimal treatment plan for the patient. It is one of the
first models elaborated and it is currently adopted in
both clinical and laboratory studies.
It is based on the assumption that the Double-Strand
Break is a lethal event and it can happen in two cases:
when there is one hit that damages both the strands
or when two different hits break the DNA strands.
In the first case, one has that the yield Y_S scales linearly
with the dose D, while in the second case Y_D scales
quadratically with D. The total yield will be then: $Y_{tot} = Y_S + Y_D = \alpha D + \beta D^2$ [28,31].
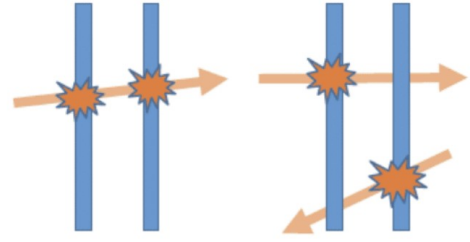
Figure 3.3: Scheme of DSB damages [28]

The distribution of the DSB damage in a cell population is given by the Poisson statistics [28]. With
this statistics one has that the probability P for a cell to be damaged depends on the number n of hits
by the following relation:

$$P(n) = \frac{Y^n e^{-n}}{n!} \tag{3.1}$$

The probability for the cell to receive no hits, that is the case S in which the cell survives, is given by:

$$S = P(0) = e^{-Y_{tot}} = e^{-\alpha D - \beta D^2} \tag{3.2}$$

This equation can be expressed in a log-scale as in the following plot:
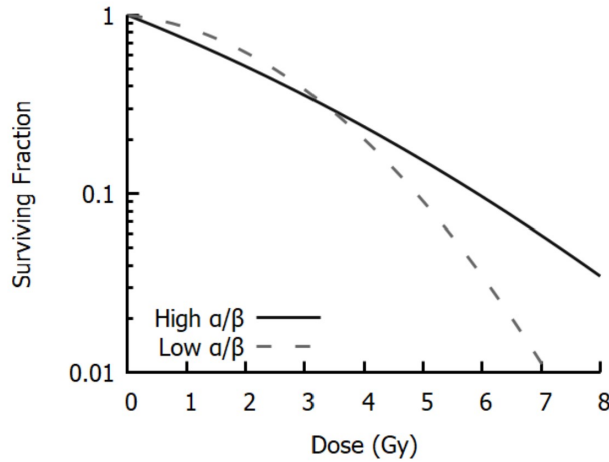
Figure 3.4: Survival fraction as a function of the absorbed dose [31]

This is a quadratic response curve. For low doses, the graphic is dominated by the linear component,
while if one increases the dose, the D^2 starts to dominate. In this model it can be defined the degree of
curvature that is expressed as the ratio α/β, whose unit is Gy. As it can be seen in Fig. 3.4, depending
on this ratio the curvature changes.
In the case of high ratio the rate of cell death is almost constant and the curve resemble an almost
straight line, while when α/β is low, there is a pronounced curvature. This kind of behavior represents
the case in which the radiation is given in one single administration. In reality for treatments the dose
is subdivided into different exposures with lower dose than the single one (range of 1.5-8 Gy and usually
the dose per fraction is 2 Gy) [28,31].

When the cells have enough time to recover after the irradiation ($\simeq$ 6-24 h), at the next exposure they will respond as they have not already received a certain dose. This fractionating method is based on the fact that most of the diseases cells seem to have a reduced repair capacity respect to the healthy cells. The expression for the survival fraction will in this case be written as:

$$S = e^{-n(\alpha d + \beta d^2)} \tag{3.3}$$

where n is the number of fractions and d the dose for each fraction ($D = nd$). This process, as it can be seen in Fig. 3.5, increases the survival fraction. In fact, in this case the magnitude of D^2 is reduced [31].
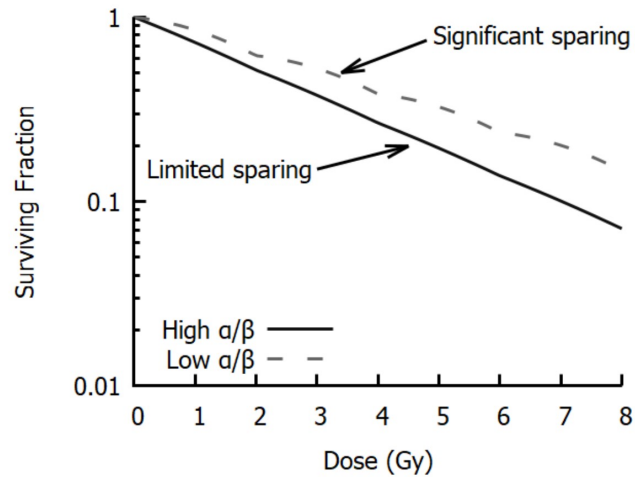
Figure 3.5: Survival fraction as a function of the absorbed dose, comparison between fractionated and not fractionated dose exposure [31]

The LQ model is a widely used model. Nonetheless, due to its simplicity, there are doubts in some cases about its applicability. This model in fact does not take into consideration the complexity of the human body biology. The cell sensitivity is regulated in fact by phenotypic and intrinsic genetics characteristics. Moreover, one should also consider external factors and, as seen in the above chapter, the type of radiation therapy [28].

The ratio between α and β also depends on the phase of the cell cycle. In G2 and S phases, for example, the cell seems to have a greater resistance to radiation. This characteristic should be considered when one irradiates a cell population where the cells are in different phases. In LQ model, instead, the population is thought to have a constant α/β ratio. To have a more reliable curve, one should consider a range of sensitivities for an heterogeneous cell colony [31].

3.3 Lethal and Potentially Lethal Model

The Lethal and Potentially Lethal (LPL) Model is a radiobiological model developed to try to describe, from a qualitative point of view, the results found in experiments using parameters that consider biological, chemical and physical processes [32]. In this model the DNA damages are divided into two different classes:

- **potentially lethal lesions** are damages that do not kill the cell. The cell death happens only when two of them interact with each other. This process is called binary misrepair.
  The lesions are usually repaired individually by biochemical processes and, in the cases of misrepair, they do not bring to the cell death. This can happen, for example, when the section damaged by the radiation is point-like and it is not a critical part of the helix [33];

- **fatal lesions** are instead due to an irreparable mutation or a damage that can not be fixed. In these cases the cell can not reproduce itself anymore [33].
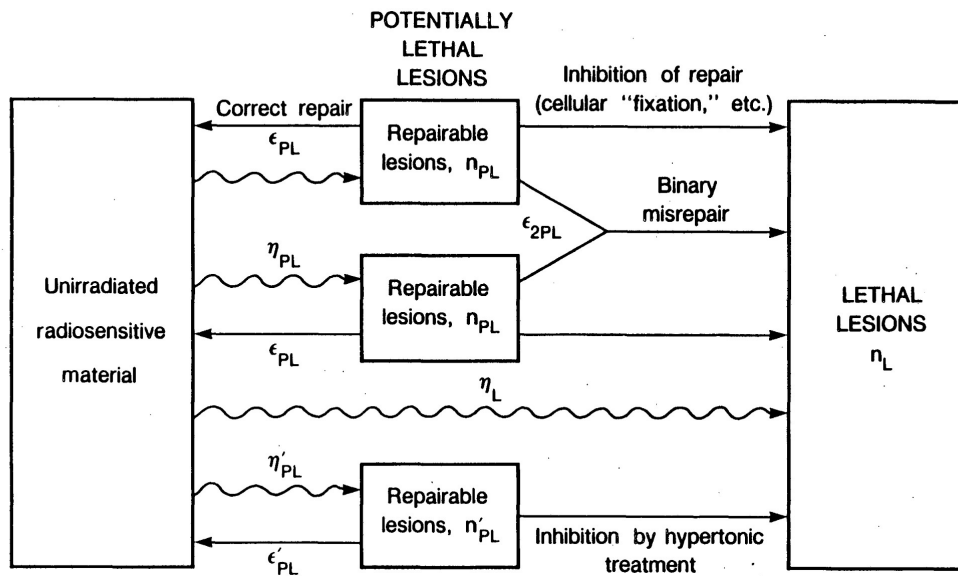
Figure 3.6: Scheme of the evolution of the events for the different DNA lesions in the LPL model [32]

The amount of lethal and potentially lethal lesions depend on the absorbed dose rate $\dot{D}$ and the rate of repair does not depend on the amount of damages inflicted to the cell.
After the first formulation of the model (1985), it was proposed by Curtis to associate the potentially lethal lesions to the DSBs and in the commonly used model version, the Double-Strand Breaks and its mechanisms of repair and misrepair are described by the following differential equation [33]:

$$\frac{d\bar{L}_{dsb}(t)}{dt} = 2\dot{D}(t)Y\Sigma_{dsb} - \{\lambda_{dsb} + \eta_{dsb}\bar{L}_{dsb}(t)\}\bar{L}_{dsb}(t) \tag{3.4}$$

where $\bar{L}_{dsb}(t)$ represents the average amount of Double-Strand Breaks in a single cell, $\dot{D}(t)$ is the rate of absorbed dose at the time t, Y the amount of pair of basis inside each cell and Σ_{dsb} is the quantity of DSBs generated by the radiation normalized per the number of nucleotides and per Gray.
λ_{dsb} represents the probability of the Double-Strand Break to be repaired, while the parameter η_{dsb} is the probability that two DSBs interact with each other.
When the average number of DSBs has an exponential behavior depending on the irradiation time, the latter parameter can be considered equal to zero. A useful process that can be done in this case is to relate λ_{dsb} to the half-time τ_{dsb} of repairing of the DSBs. This time is equal to half of the one that is needed to fix half of the initial damage generated inside a cell by an acute irradiation dose. The two quantities can be written as $\lambda_{dsb} = ln2/\tau_{dsb}$.

The fatal lesions behavior, especially the way they are accumulated in a cell, can be expressed by the following differential equation:

$$\frac{d\bar{L}_f(t)}{dt} = 2\dot{D}(t)Y\Sigma_f + \eta_{dsb}\bar{L}_{dsb}(t)\bar{L}_{dsb}(t) \tag{3.5}$$

In this case $\bar{L}_f(t)$ is equal to the amount of lethal lesions at a certain time t for each cell. Σ has the same meaning as above, but in this case related to fatal lesions. Looking at the Equations (3.4) and (3.5) one can see that this model has 4 parameters that depend on the system: Σ for DSBs and fatal lesions, λ_{dsb} and η_{dsb}.

When the irradiation stops, the equations regulating the repair result similar to the one describing the irradiation without the term related to the dose rate $\dot{D}(t)$.

The Equations (3.4) and (3.5) are the same as in the original version of the LPL model (see Fig.3.6) with some differences in the notation:

- $\eta_{PL} = 2Y\Sigma_{dsb}$ and $\eta_L = 2Y\Sigma_f$;

- $\epsilon_{PL} = \lambda_{dsb}$;

- $\epsilon_{2PL} = \eta_{dsb}$

$\bar{L}_{dsb}(t)$ and $\bar{L}_f(t)$ were referred respectively as $n_{PL}(t)$ and $n_L(t)$.

3.3.1   Mechanisms of action and their interpretation

In this model the production of DSBs is due to ionizing radiation and its rate depends on the absorbed dose. Both the repair and misrepair processes (1st- and 2nd-order) can fix Double-Strand Breaks, while the lethal damages can not be formed by 1st-order mechanisms, but can only be due to the 2nd-order ones. The latter lesions have also a rate depending on the absorbed dose. Moreover, IR bring to aberrations in the chromosomes, which are they in turn due to DSBs.

These mechanisms can be interpreted as follow:

Direct formation of lethal damage   Curtis speculated about the fact that the term $2\dot{D}(t)Y\Sigma_f$ could come from the interaction of 2 different DNA lesions. These lesions are situated one near each other and are due to the passage of the same track. This kind of interaction generates a damage that can not be repaired and that should result as the break of a chromosome.

Another hypothesis regarding the mechanism of production of lethal damages is that ionizing radiation happens to generate a DSB and nearby also another damage. These lesions together are so severe that the cell is not able to start the repairing process (and so neither the misrepairing one). In this way there is the formation of a lethal damage instantaneously.

A third possibility regarding the generation of this kind of damage is the formation and the misrepair of a DSB in a critical section of the DNA. In this case the cell death is due to the damage of a critical gene that, after the misrepair, undergoes a mutation that is then followed by its inactivation. Therefore, the mutation can not be instantaneously.

The last hypothesis is that $2\dot{D}(t)Y\Sigma_f$ represents the fixation of a Double-Strand Break from a physio-chemical point of view. The DSB interacts with a molecule connected to the DNA or a histone protein. These processes bring to the break of the chromosome. The DSB can also become a break that can not be repaired or can generate a damage by the interaction with another DSB or a protein. These processes can happen if the cell has been irradiated. This mechanism is an approximation: the fixation can not in fact happen simultaneously.

Binary misrepair of Double-Strand Breaks   This misrepair is expressed in the term $\eta_{dsb}\bar{L}_{dsb}(t)\bar{L}_{dsb}(t)$. This term expresses the proportionality between the rate of incorrect rejoining of break ends of two different DSBs and the square of the DSBs inside a cell that can not be repaired. The average number of broken ends at time t in a cell is equal to $2\bar{L}_{dsb}$.

The process of incorrect rejoining of two DSBs happens in a large segment of the DNA and the misrepair is related to various chromosome aberrations. They can be for example acentric and dicentric rings. These rings can be associated with 2 acentric fragments of chromosome when the process of interaction of DSB does not arrive to its end.

3.3.2   Survival curve

To evaluate the survival curve at time $t = T + t_r$ (where T is the irradiation time and t_r the repair one) one can assume that the total number of lethal lesions for each cell can be written as the sum of the potentially lethal and lethal damages. This assumption implies that, after the fixing time t_r, the potentially lethal damages still not fixed become lethal.

So it can be written:

$$\bar{L}_{tot}(t) = \bar{L}_{dsb}(t) + \bar{L}_f(t) \tag{3.6}$$

Supposing also that the lethal damages follow a Poisson distribution, the probability that a cell survives (i.e. it has no lethal lesions) is:

$$S = e^{-\bar{L}_{tot}(t)} = e^{-\bar{L}_{dsb}(t)}e^{-\bar{L}_f(t)} \tag{3.7}$$

The solutions of $\bar{L}_{dsb}(t)$ and $\bar{L}_f(t)$ after the irradiation are:

$$\bar{L}_{dsb}(t) = \frac{\bar{L}_{dsb}(T)e^{-\lambda_{dsb}t_r}}{1 + \bar{L}_{dsb}(T)/\epsilon(1 - e^{-\lambda_{dsb}t_r})} \tag{3.8}$$

where $\epsilon = \lambda_{dsb}/\eta_{dsb}$.

$$\bar{L}_f(t) = \bar{L}_f(T) + \bar{L}_{dsb}(T)\left(1 + \frac{\bar{L}_{dsb}(T)}{\epsilon}\right)\left(1 - e^{-\lambda_{dsb}t_r}\right)\Big/\left(1 + \frac{\bar{L}_{dsb}(T)}{\epsilon(1 - e^{-\lambda_{dsb}t_r})}\right)$$
$$- \epsilon \cdot ln\left[1 + \frac{\bar{L}_{dsb}(T)}{\epsilon(1 - e^{-\lambda_{dsb}t_r})}\right] \tag{3.9}$$

Equations (3.8) and (3.9) are obtained substituting $t = T$ in the solutions of the differential equations (3.4) and (3.5). Substituting Equations (3.8) and (3.9) in (3.7) one can write the survival probability as:

$$S = e^{-\bar{L}_{tot}(T)}\left[1 + \frac{\bar{L}_{dsb}(T)}{\epsilon(1 - e^{-\lambda_{dsb}t_r})}\right]^{\epsilon} \tag{3.10}$$

Chapter 4

Cellular S-values calculation

The Geant4 code allows to simulate the dose absorbed by a cell. The aim of it is to simulate this process in the case of the radioactive decay of ^{111}Ag in the context of the TRNT. Another radionuclide that will be evaluated is ^{177}Lu. This radioactive isotope is widely used in TRNT and the comparison of the results could give information about the efficiency of the silver isotope.

To verify the validity of the code, it will be adapted to simulate the absorbed dose of different systems. The dose values simulated can be compared with the quantities that can be obtained in dedicated experiments. In this case, two different experiments taking place at LENA in Pavia with the radionuclide ^{60}Co will be considered. This radionuclide decays via β^-, followed by γ emissions, into the stable nucleus ^{60}Ni.
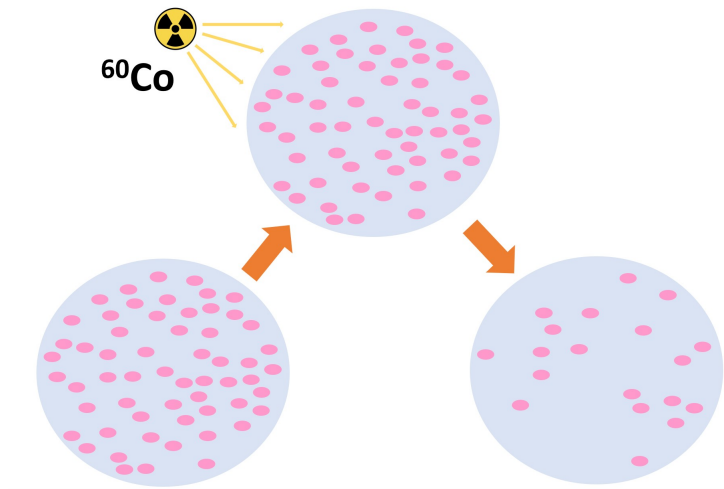
Figure 4.1: Schematic view of the irradiation of a 2d *in vitro* colony

During the experiments, the 2D *in vitro* colonies are positioned near ^{60}Co sources and they receive an external flux of radiation due to the cobalt decay. The exposed cells absorb a certain dose which can be confronted with the simulated one to validate the code.

The absorbed dose can be connected to the cellular survival fraction with many models. These models are based on different assumptions about DNA damages and repair mechanisms and in this thesis one will take into consideration two different models: the Linear-Quadratic (LQ) Model, that is the "classic" model, and the Lethal and Potentially Lethal (LPL) one.

4.1 MIRD schema

To standardize the nomenclature for the dose evaluation, the Medical Internal Radiation Dose (MIRD) Committee of the American Society of Nuclear Medicine proposed a schema, called MIRD schema, which will be used in this thesis. This schema allows to have a framework to evaluate the dose absorbed in the case of organs, tissues belonging to a organ, tissues subdivided into voxels and single cells for both diagnosis and therapy [34].

The absorbed dose $D(r_T, T_D)$, which is the mean energy received by the target r_T per mass unit over the period T_D, can be written as (in the hypothesis of time-independence of the masses):

$$D(r_T, T_D) = \sum_{r_s} \widetilde{A}(r_S, T_D) S(r_T \leftarrow r_S) \tag{4.1}$$

where $\widetilde{A}$ is the time-integrated activity in the tissue which has the role of the source r_S. $S(r_T \leftarrow r_S)$ is a quantity depending on the chosen radionuclide: it represents the mean absorbed dose rate that the target r_T receives from another organ or tissue, that is the source tissue r_S, per unit of activity. As one can see in the schematic example (see Fig. 4.2), targets are usually the organs near the emitting one and one can have more than one emitter.

It has to be taken into consideration that it varies also depending on the particular atomic model chosen to represent the tissue or the whole patients. In this thesis the cells will be considered equivalent to water and it will be focused on the simulation of the S-values in different cases [34].
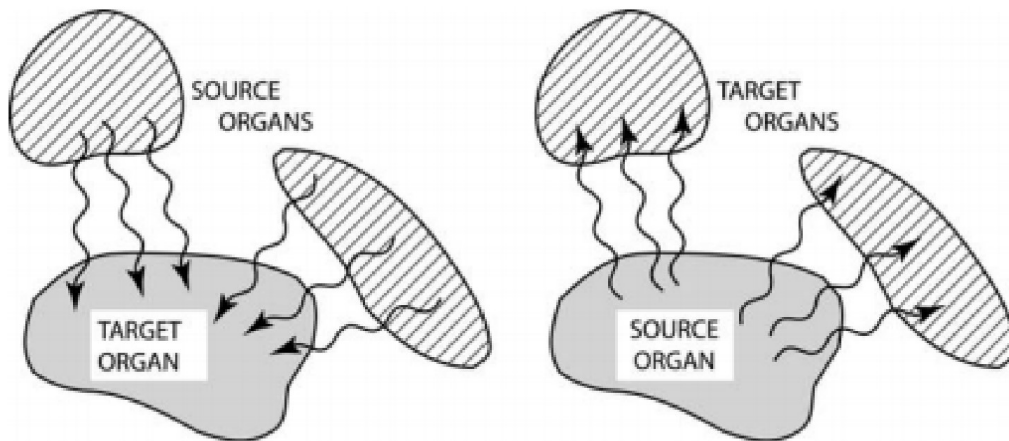
Figure 4.2: Scheme of the dose absorbed by target organs when the radiation comes from one or more source organs [35]

4.2 ^{111}Ag studies

As introduced before, ^{111}Ag is a radionuclide currently under evaluation for Radionuclide Therapy in the context of the ISOLPHARM project. When it decays there is the emission of a β and in some cases also of γ. As it has been observed in this thesis, due to the lower probability of the γ decay and to its much longer range, the main energy absorbed by the cells comes from the β radiation.

For these studies both spherical and ellipsoidal cells are considered with the following dimensions:

- Spherical cell with a radius of 8 µm and with the nucleus radius of 5 µm;

- Ellipsoidal cell with the same volume (two half-axes of 14 µm and the third of 2.5 µm; the nucleus has the shorter semi-axis of 2.5 µm, while the others have a length of 7.1 µm).
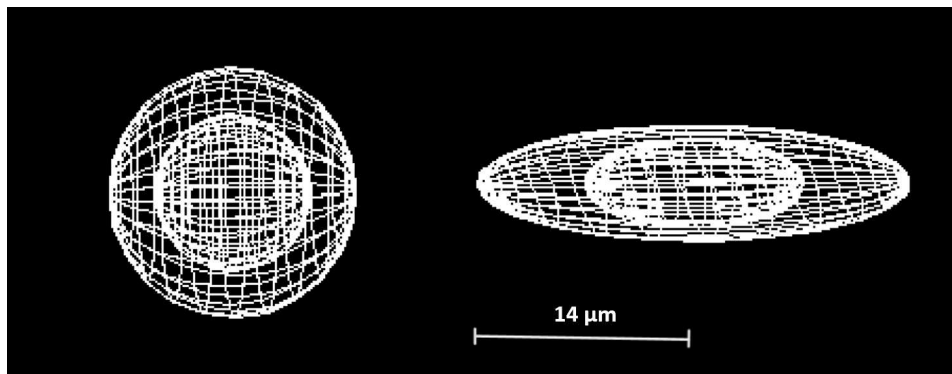
Figure 4.3: Picture of the graphic interface with the ellipsoidal and spherical cells

These dimensions are typical cells radii and are also the ones used in literature [35–37]. One has to take into account both geometries because cells have different kinds of shape (see as examples Fig. 4.4 and Fig. 4.5) and, as it has been observed with the simulations, the geometry influences the dose absorbed by both the whole cell and its nucleus. These information could be useful to decide where to deposit the radiopharmaceutical depending on the cell's shape.
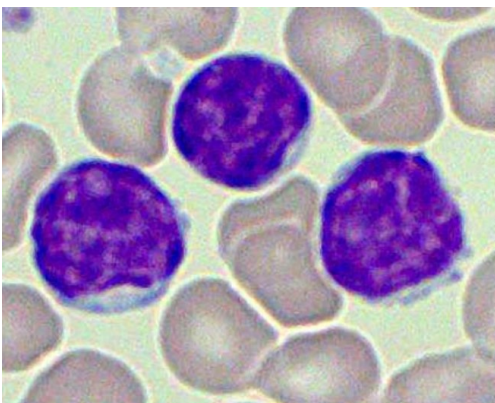
Figure 4.4: Example of spherical cells: lymphocytes [38]
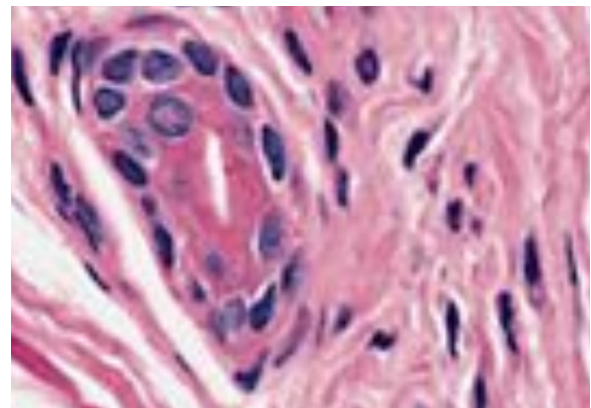
Figure 4.5: Example of ellipsoidal-like cells: fibroblasts [39]

The simulations regarding the estimation of the absorbed dose with ^{111}Ag can be subdivided into three main categories:

- Self-absorbed dose, when the events take place on the cellular membrane, inside the whole cell or in the cytoplasm;

- Cross-absorbed dose, that is the mean energy absorbed when the decays happen on the membrane or inside another cell;

- Environmental dose, coming from the space external to the cell.

In all these cases the event distribution is homogeneous and the absorbed dose is calculated for both the entire cell and its nucleus.

4.2.1   Physics libraries and statistics evaluation

Before starting the simulations, it is necessary to choose the Geant4 library that will be used for these estimations. The three candidates are: Low Energy, Livermore and Electromagnetic Std (option 3). These libraries, following the Geant4 website description, could all be good choices due to the energy range and the type of interactions considered [41].

The values of absorbed dose (nuclear and whole cell absorption) are calculated in the case of self-absorption of both ellipsoidal and spherical cells made of water and positioned in a water environment. Taking in consideration the ellipsoidal cells, in the case of membrane activity distribution one can evaluate the calculate dose as a function of the number of generated events (see Fig.4.6 and 4.7):
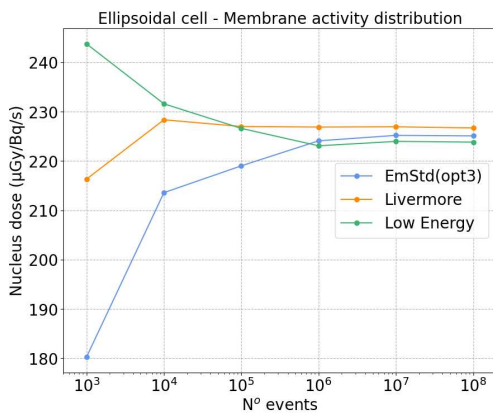
Figure 4.6: Nucleus normalized absorbed dose
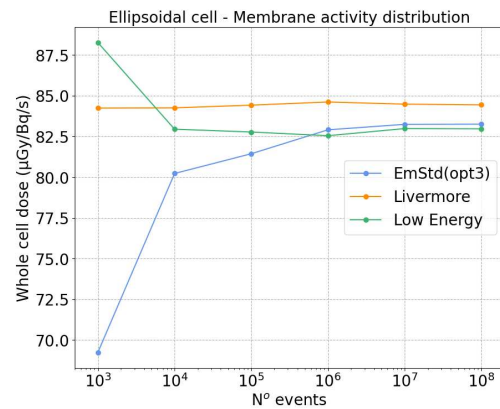
Figure 4.7: Whole cell normalized absorbed dose

While, for the whole volume activity distribution we obtain the results in Fig.4.8 and 4.9:
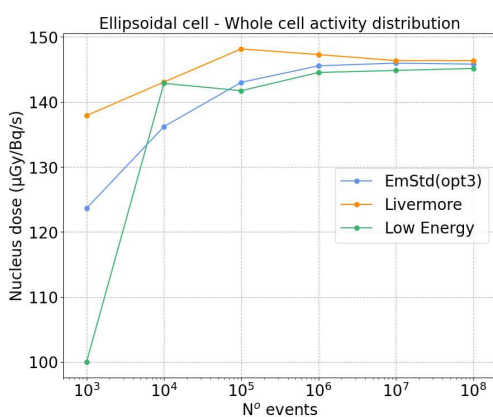
Figure 4.8: Nucleus normalized absorbed dose
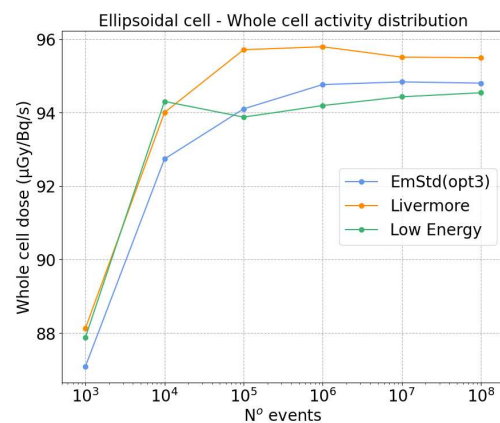
Figure 4.9: Whole cell normalized absorbed dose

The spherical cell values are visible in Appendix. As one can see in the Figures 4.6, 4.7, 4.8, 4.9, the doses per event obtained with the three libraries have higher differences for lower amount of events. This is due to the fact that these numbers of events are not statistically significant and one has to increase them at least up to 10^6 to have more reliable values. For this amount of events there is no significant difference between the dose values. In this thesis it has been chosen the Electromagnetic Standard (option 3) library. This library shows in fact values intermediate to the other two. The cut-off

range of the chosen library is 1 mm for the γs and 0.1 mm for the electrons [43].

Taken this library into account, one can simulate events up to 10^9 to study in details the stability of the absorbed dose per event and to evaluate the minimum value of generated events that are necessary to obtain a statistical uncertainty lower than 1%. The data simulated are visible, in the case of the ellipsoidal cell with membrane activity distribution, in Fig. 4.10. Looking at the percentage difference between the dose for a certain number of event and the one obtained for 10^9 events (see Fig. 4.11), one can see that, starting from 10^6, the dose differs of less than 1% respect to the one simulated with 10^9 events. This observation is valid for all the combinations of cellular geometry and activity distribution. This value results already stable but, due to the fact that the simulation is extremely fast, one can simulate 10^7 events to have a better dose evaluation in a reasonable time (see Fig. 4.12).
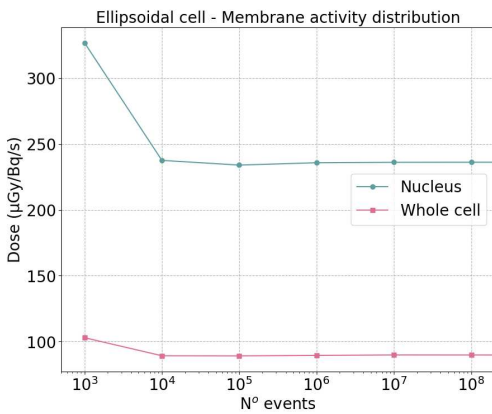
Figure 4.10: Nucleus absorbed dose
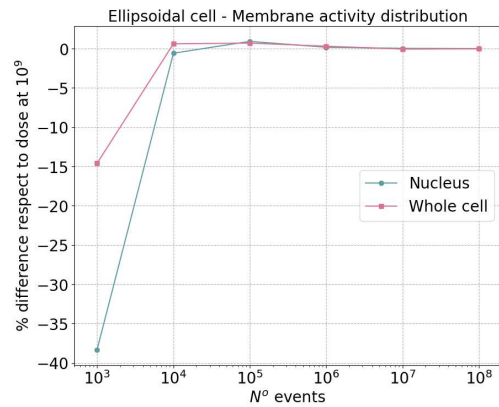
Figure 4.11: Whole cell absorbed dose
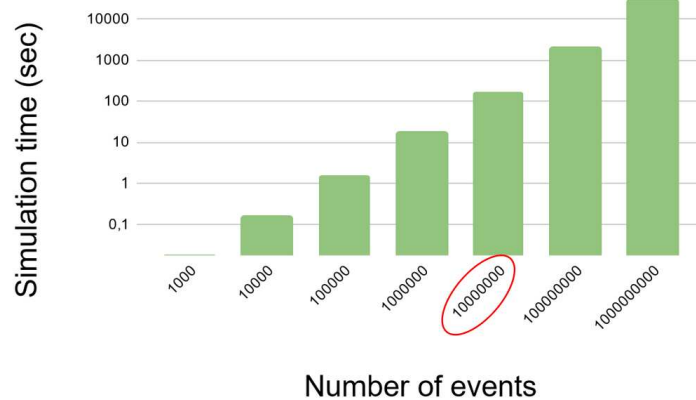
Figure 4.12: Histograms of the simulation times for different numbers of events for spherical cell with membrane activity distribution

One can compare the simulation time of the code developed for this thesis and the time taken by the example "molecularDNA", available on Geant4-DNA. The latter code allows to obtain different information regarding the DNA damages of an irradiated cell, among which there is the absorbed dose. The simulation time of Geant4-DNA is 4 orders of magnitude higher than the Geant4-based one [45]. The developed code allows to estimate the absorbed dose in a faster way than "molecularDNA", meaning that the code could be a really useful tool to get information about how to set the geometry, the dimensions of the environment and the number of events needed without the use of the time consuming G4DNA libraries. Taking for example the time needed to simulate 10^6 events one has that it takes $\simeq$ 17 seconds for the developed code and $\simeq$ 12 hours for "molecularDNA".

4.2.2 Self-absorbed dose

To study the self-absorbed dose, one needs to consider the values simulated before (in the case of membrane and whole cell activity distribution) and in addition the cytoplasm one. As one can see in the pictures, depending on the geometry of the cells, the absorbed dose can be higher for a certain distribution (see Fig. 4.14 and 4.15).
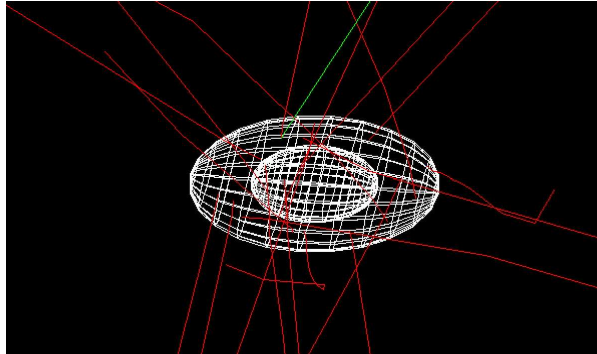
Figure 4.13: Picture of the graphic interface with the self-irradiation of the cell
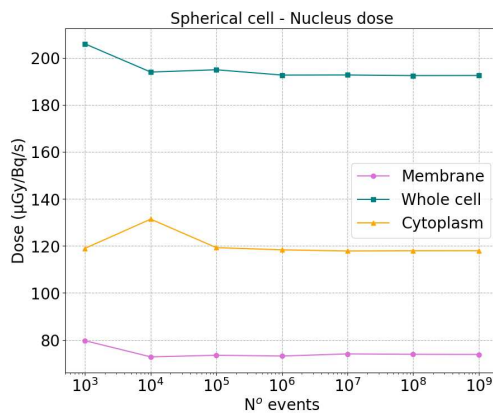
Figure 4.14: Nucleus dose for spherical cell
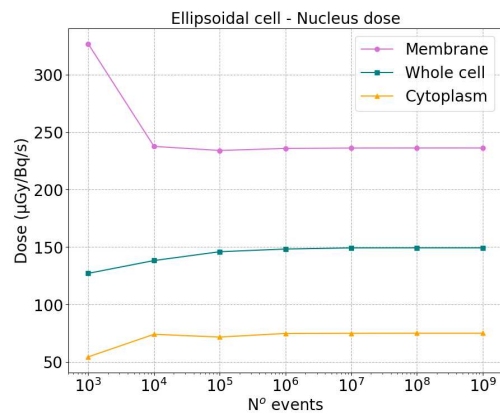
Figure 4.15: Nucleus dose for ellipsoidal cell

A fact that should be taken into consideration for future studies is that for the ellipsoidal cell (see Fig. 4.15), which is the one that better resembles the cells used for experiments with a 2D colony, the dose absorbed by the nucleus results higher with a membrane distribution than with decays distributed inside the whole cell. This could be a hint to keep studying the release of the radiopharmaceutical on the membrane, avoiding its internalization. In the other case, the internalization could bring to a higher dose (see Fig. 4.14).
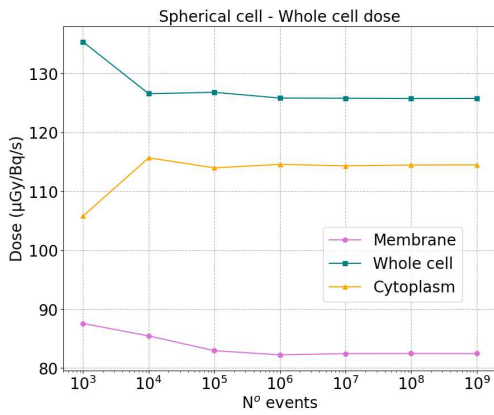
Figure 4.16: Whole cell dose for spherical cell
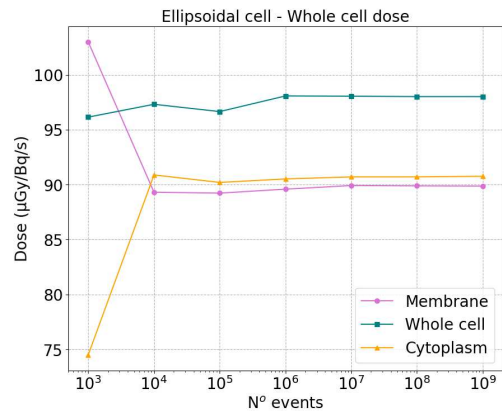
Figure 4.17: Whole cell dose for ellipsoidal cell

One can also observe that the dose absorbed by the cell is higher in the case of whole volume activity distribution for both geometries. For the ellipsoidal cell, the dose absorbed with cytoplasm and membrane activity distribution differs for a few μGy/Bq/s.

Figure 4.18: MIRDcell logo [11]

The values estimated with a spherical cell can be compared with the ones available in the MIRDcell applet. MIRDcell is a software widely used in the medical field to estimate the cell absorbed dose. As one can see in the Table 4.1, the difference between the Geant4 and the MIRDcell simulations is between 9 and 13% for self-absorbed dose. This result seems to agree with scientific literature regarding the differences between MIRDcell and Monte-Carlo based simulators [42] and it could be a first validation of the code developed in this thesis.

Spherical cell		D_G (μGy/Bq/s)	D_M (μGy/Bq/s)	% diff
Membrane	Nucleus	74	64	13
	Whole cell	83	91	10
Whole cell	Nucleus	193	168	13
	Whole cell	126	138	10
Cytoplasm	Nucleus	107	118	10
	Whole cell	128	145	11

Table 4.1: Comparison between the self-absorbed dose obtained with Geant4 D_G and with MIRDcell D_M and their percentage difference % diff

One could also evaluate the absorbed dose due to the γs that, in some cases, are emitted after the ^{111}Ag decay. This evaluation is possible comparing the absorbed dose with and without the γs. One could for example take into consideration the spherical cell with a membrane activity distribution.

As one can see in the Table 4.2, the γs do not contribute substantially to the self-absorbed dose. The main differences between the dose are in fact for numbers of events lower than 10^6. In this range the fluctuations are too high to consider the values of the dose reliable. From 10^6 events the differences between the doses are less that 1%.

Number of events	$D_\gamma(\mu Gy/Bq/s)$	$D_{no\gamma}(\mu Gy/Bq/s)$	% diff
10^3	80	86	8.0
10^4	79	80	1.6
10^5	76	76	0.6
10^6	76	76	0.2
10^7	76	76	0.1
10^8	76	76	0.1

Table 4.2: Comparison between the whole cell self-absorbed doses for a spherical cell with and without considering the γs and their percentage difference % diff between the two values

This observation is in agreement with the values obtained in the master thesis of A. Arzenton [43]. Looking at the Fig. 4.19, one can see that the γs, in the case of ^{111}Ag, start to contribute to the dose at about 4.5 mm.
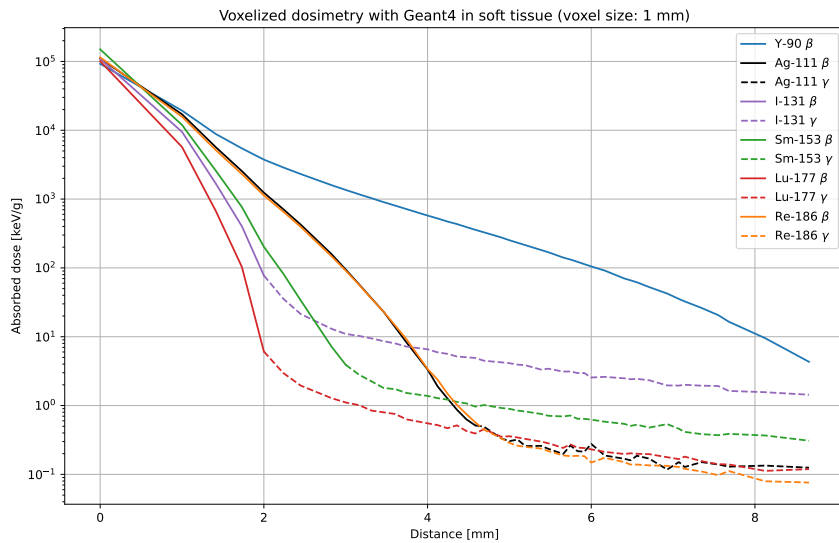
Figure 4.19: γ and β contributions to the absorbed dose [40]

Another interesting study that can be done in the case of the self-absorbed dose is the evaluation of the absorbed dose depending on the size of the cell's environment. This kind of information could be useful in the case of long and complex simulations, in which the changing in the environment's size could shorten the time needed (for example in the case of Geant4-DNA).

For this evaluation it is considered the self-irradiated dose (10^8 events) coming from the membrane with an ellipsoidal cell (this geometry is, as mentioned before, the situation that better resembles an experiment with 2D colonies). The world is considered ellipsoidal as well.

First of all, one will calculate the dose for wide surroundings (a cube with $\simeq 0.5$ mm for each side is considered) and then simulate the dose in an ellipsoidal environment at the decreasing of its size. The aim is to obtain the dimensions for which there is a changing in the dose of at least 1%.
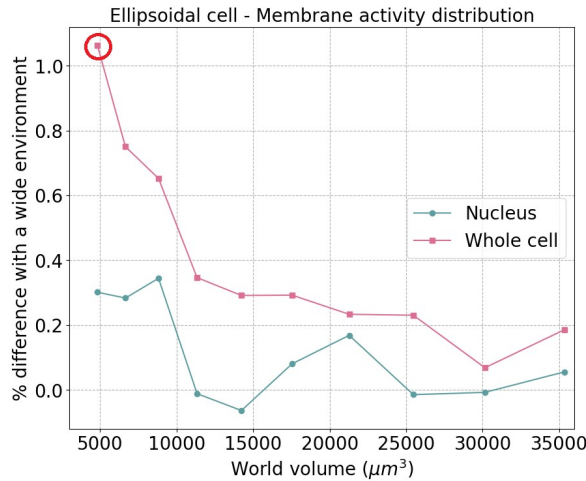
Figure 4.20: Percentage differences in the dose with different environments' size

As it is shown in Fig. 4.20, this value is reached when the environment has a volume of about 5000 µm^3 (with the semi-axes of 16 x 4.5 x 16 µm). An interesting fact is that, in the case of the nuclear dose, the difference does not reach the 1% for environments bigger than the cell itself. This means that a simulation with an environment of small volume gives a dose value as reliable as the one given by a simulation with wide environment. Knowing this information could be useful to optimize complex simulations due to the fact that, for wider environment, the simulation takes more time for running.

At this point one could compare the self-absorbed dose for the different geometries.
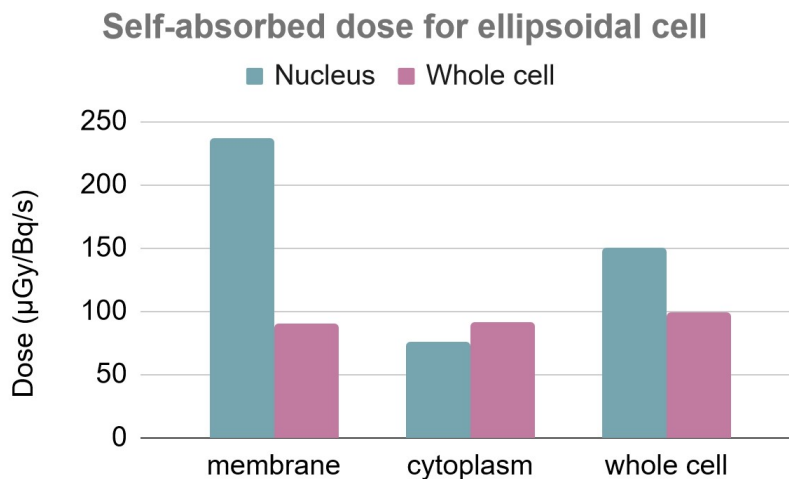
Figure 4.21: Comparison of the absorbed dose between the different distributions in the case of self-absorbed dose for the ellipsoidal cell

As one can see in the Fig. 4.21, the ellipsoidal nucleus receives a higher dose when the activity has a membrane distribution. The lower dose is given for cytoplasm activity. The whole cell doses differ of maximum 10 µGy/Bq/s between each other.

In conclusion, for ellipsoidal cells, according to the values obtained in this thesis, the distribution of the delivered radiopharmaceutical on the membrane results the most efficient: one obtains in fact the higher dose for the nucleus, while for the whole cell the dose differences are negligible.
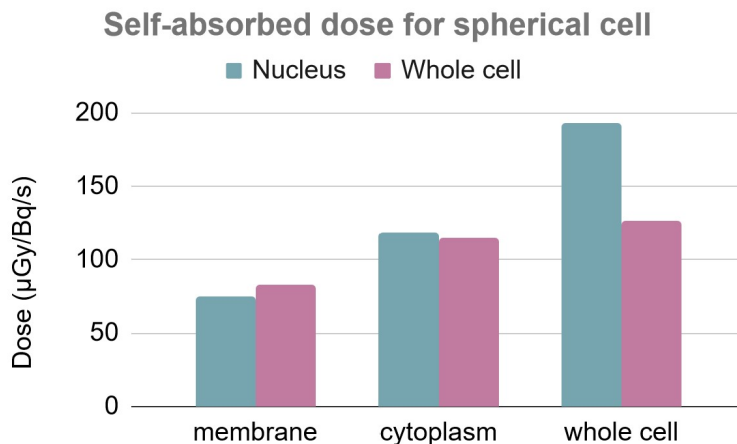
Figure 4.22: Comparison of the absorbed dose between the different distributions in the case of self-absorbed dose for the spherical cell

In the case of the spherical cell, the conclusions are different respect to the ellipsoidal one (see Fig. 4.22). The spherical nucleus gets more dose when the decays are in the whole cell. As in the ellipsoidal case, the dose difference in the case of the whole cell for different activity distributions is lower compared to the nucleus one, but in this case it should be kept into consideration. The maximum difference is in fact of about 50 µGy/Bq/s.

According to the simulations, for the spherical cell, the whole cell activity distribution (for both nucleus and cell absorbed dose) is the most advantageous.

4.2.3 Cross-absorbed dose

For the cross-absorbed dose evaluation, the cell is positioned adjacent to an emitting cell. For the ellipsoidal geometry, the cells touch each other in the plane of the 28 µm axes. In 2D *in vitro* experiments this is in fact the geometry that approximates the real situation [49].

The events distributions considered are the membrane and whole cell ones. This is due to the fact that the cytoplasm one generates always a dose in good agreement with the whole cell activity distribution. As one will see in this paragraph, also the membrane and the volume ones coincide after 2-3 diameters of distance (see Fig. 4.26).

The cross-absorbed doses d_D are calculated at different distances that are then compared with the dose d_0, given by the adjacent cell. This allows to evaluate up to which distance $d_D \leq 0,01 \cdot d_0$. Knowing this could be useful to understand at which distance one can neglect the dose contribution of another cell. The results obtained are:

- for the ellipsoids: 250 µm for the membrane distribution and 300 µm for the volume one;

- for the spherical cell 150 µm for both the distributions.
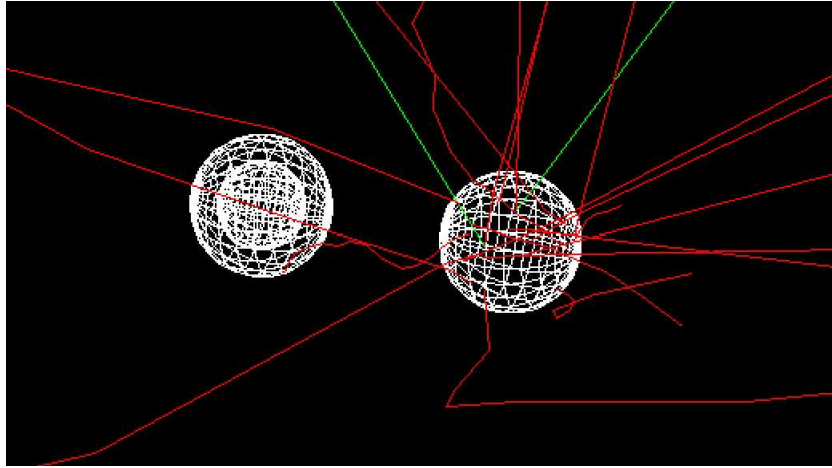
Figure 4.23: Picture of the graphical interface for cross-absorbed dose

In the case of the ellipsoidal cell, the distance is of about 100 µm more than for the spherical one. This could be addressed to the fact that the dose at a certain distance is compared to the one obtained when the cells touching each other. The spherical cell, due to geometrical observations, takes a higher dose d_0 than the ellipsoidal one and so d_D reaches before the 1% of d_0.

The dose absorbed by the whole cell results in general more stable. The nucleus has in fact a lower volume and one should consider a higher number of events to have smaller fluctuations.
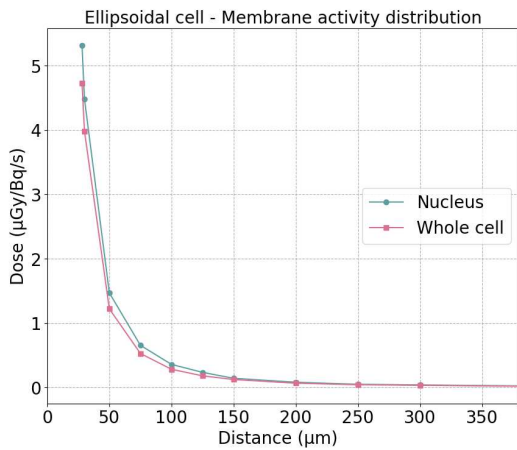
Figure 4.24: Cross-dose in a range of $\simeq$ 0-350 µm
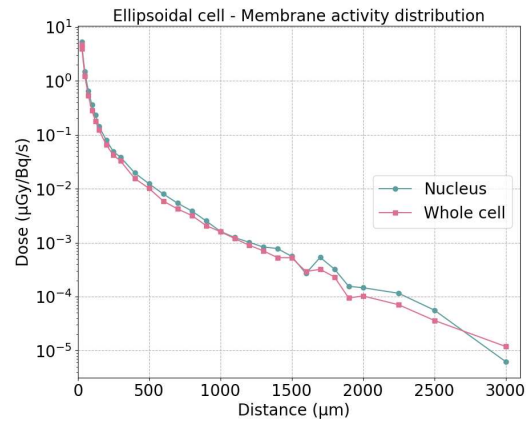
Figure 4.25: Cross-dose in a range of $\simeq$ 0-3000 µm

The maximum distance simulated is 3 mm (due to observations that will be highlighted during the study of the environment) and the logarithmic behavior of the dose is in accordance with the one in literature [43]. As mentioned before, in Fig. 4.26, it is possible to see that after about 2 diameters of distance, the dose differences between the membrane and the whole cell activity distributions are minimal.
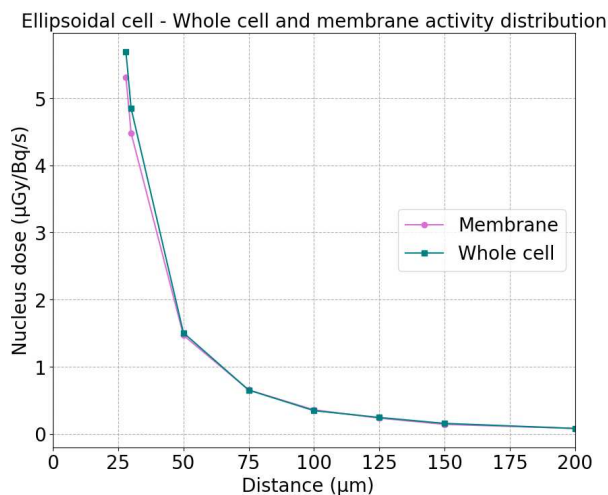
Figure 4.26: Absorbed dose depending on the activity distribution

For the spherical cells one can consider the dose values at distances lower than 150 µm and compare them with the MIRDcell values. In this case the differences range from about 1 to 20%. As it is possible to see in Fig. 4.29, 4.30, 4.31 and 4.32, there is no standard behavior for percentage difference between the MIRDcell and Geant4 values estimations. As in the case of self-absorbed dose, the differences are in accordance with the literature [42].
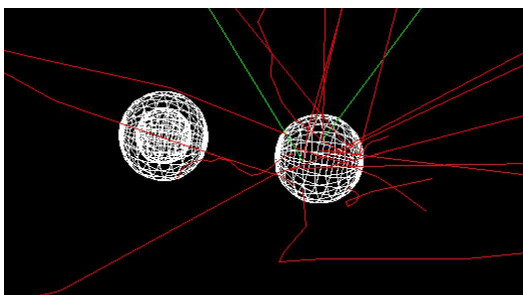
Figure 4.27: Graphic interface of Geant4
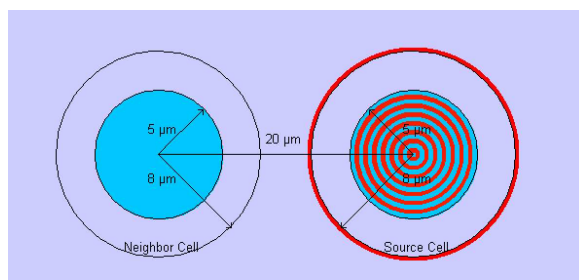
Figure 4.28: MIRDcell interface
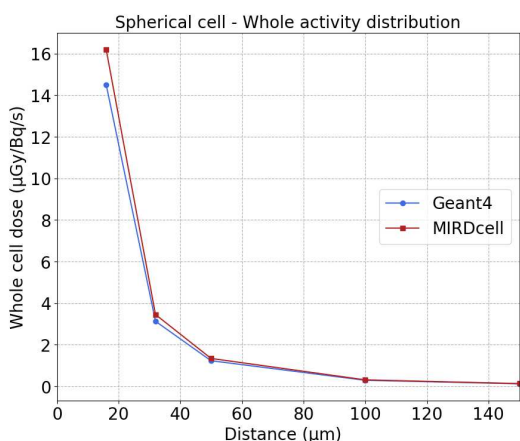
Figure 4.29: Comparison between Geant4 and MIRDcell values
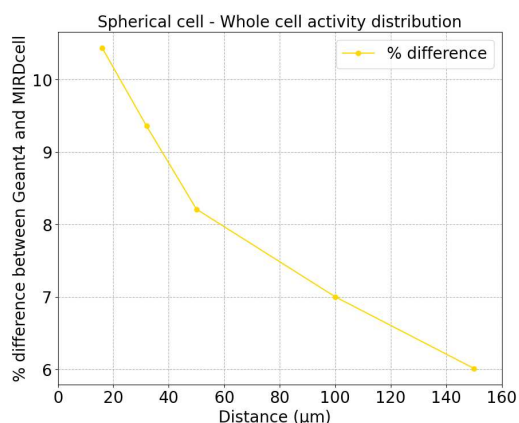
Figure 4.30: % difference between MIRDcell and Geant4 values
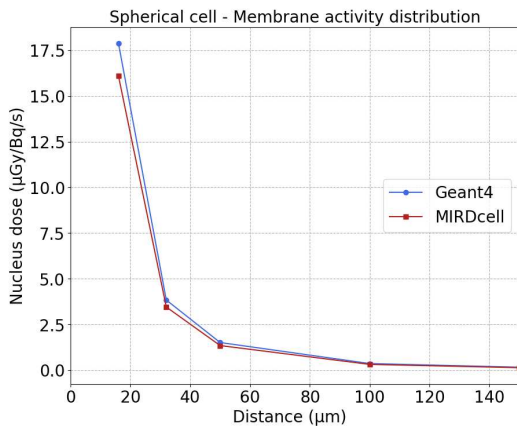
Figure 4.31: Comparison between Geant4 and MIRDcell values
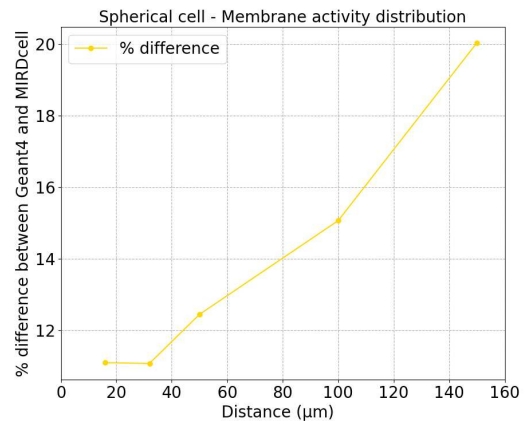
Figure 4.32: % difference between MIRDcell and Geant4 values

It is now possible to compare the self-absorbed dose with the crossed one. As it is shown in Fig. 4.33, in the case of cytoplasm and whole cell activity distribution, the dose intake is the highest. This is due to the properties of ^{111}Ag. Its decay releases more energy at the beginning of the β path. Looking at Fig. 4.19, one can also notice that at distances of about 3 mm the γ does not contribute to the absorbed dose. But, even if one considered the γ contribution, it is possible to deduce from the graph that the energy given by the photons would be way smaller than the one from the β.

In conclusion, to develop a radiopharmaceutical with ^{111}Ag, one should take into consideration the fact that the dose given by a nearby cell is negligible after a few mm. This is a useful information also to understand at which distance the healthy tissues surrounding the disease site are almost completely spared from the radiation.
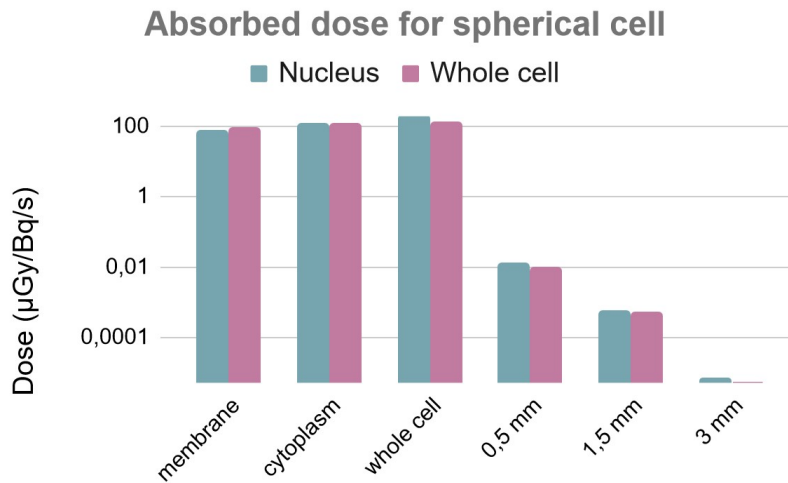
Figure 4.33: Comparison of self-absorbed and cross-absorbed dose

41

4.2.4   Environment evaluation

Another important task to develop RNT dosimetry is the study of the dose absorbed by the cell when the radiopharmaceutical is placed in the environment.
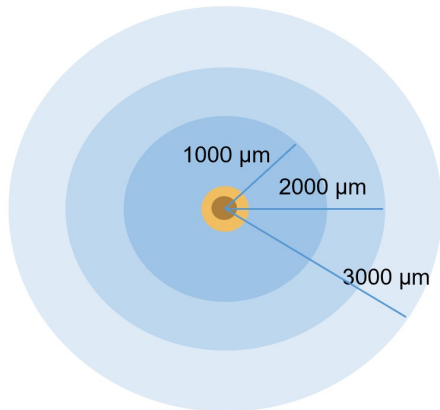
Figure 4.34: Scheme of the simulation

To study at which distance the events do not influence anymore the dose intake, one can consider a spherical environment with a certain radius, evaluate the dose taken by the spherical cell, and then increase the radius until the dose stabilisation (that could be considered a *plateau*).

During this process the density of events for different sizes of environment needs to be kept constant. The value that is obtained is a dose normalised per unit of events and per unit of volume: $(Gy/Bq/s)\cdot\mu m^3$. The distance at which it is possible to have the *plateau* is strongly correlated to the chosen radionuclide.

As one can see in Fig. 4.35, the dose stabilises itself at a distance of about 3 mm. As one can verify looking at Fig.4.19, at these distances the energy released in the cell comes only from the β-decay. One needs to reach distances of about 5 mm to have the contribution of the γ.

The nucleus dose has more fluctuations. To have a more stable dose, one should increase the number of events. This kind of study can also be done for the ellipsoidal cell but, after the dose differences for small radii, one will obtain the same result as for the spherical one.
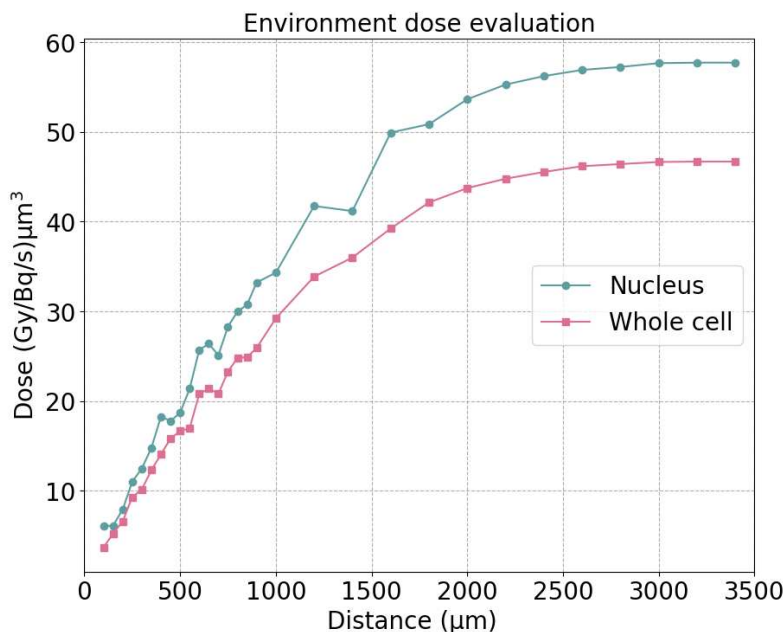
Figure 4.35: Absorbed dose by a spherical cell with events in the external environment

4.3 ^{177}Lu studies

^{177}Lu is a widely used radionuclide in the medical physics field, in particular for radionuclide therapy. It is in fact used to treat a wide range of diseases.

76% of times, it decays β^- to the stable nucleus ^{177}Hf, while in the other cases it decays to one of its excited states and then, via γ emission, it de-excites to the ground state. The ^{177}Lu emissions are mainly β^- with an average energy of 497 keV in 78.6% of the cases, 384 keV for 9.1% and 176 keV in 12.2%. There can be also the emission of a photon of 113 or 208 keV [46].
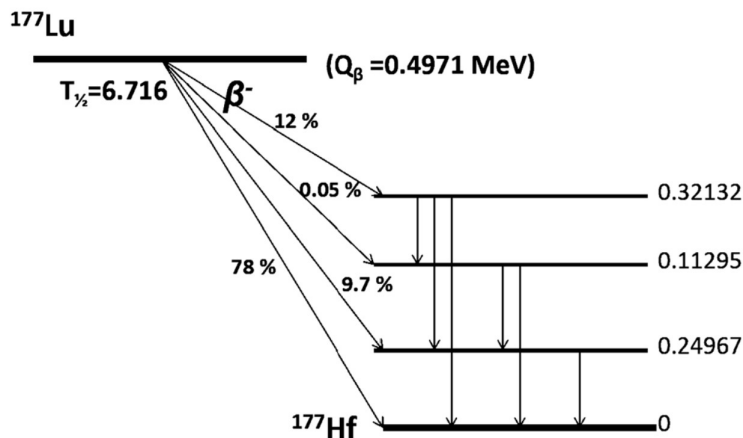
Figure 4.36: ^{177}Lu simplified decay scheme [46]

This radionuclide is a good candidate for nuclear medicine for various reasons. First of all, the mean range of penetration (in soft tissues) is 670 µm. This range is good for small tumors and disease cells situated in the surface of cavities. Moreover, the emission of photons allows to have also diagnostic studies, while the fact that both β^- and γ have a low/moderate energy allows to have a low radiation dose. This means that it is possible to work with high ^{177}Lu activities when the radiopharmaceutic is prepared and administrated.

Due to its chemical properties, it is also possible to radiolabel a wide range of molecular carriers with this nucleus. Another important characteristic is its half-life of 6.65 days. This relatively long half-life allows its preparation and transport also in the cases of sophisticated preparation and administration techniques [46].

Due to its characteristics, ^{177}Lu can be used as a comparison to evaluate the ^{111}Ag properties. To do so, one needs to simulate the self-absorbed, the cross-absorbed dose and the dose coming from the environment for the same types of cells used in the case of ^{111}Ag simulations.

4.3.1 Self-absorbed dose

As in the case of ^{111}Ag, the geometries considered are ellipsoidal and spherical. The self-absorbed dose is simulated with the membrane, cytoplasm and whole cell activity distributions.

For the spherical cell one can compare the dose given by lutetium and the silver isotope:

Spherical cell		D_{Ag-111} (µGy/Bq/s)	D_{Lu-177} (µGy/Bq/s)
Membrane	Nucleus	74	146
	Whole cell	83	224
Whole cell	Nucleus	192	472
	Whole cell	126	314
Cytoplasm	Nucleus	118	243
	Whole cell	114	290

Table 4.3: Comparison between the self-absorbed doses with ^{111}Ag and ^{177}Lu irradiation and different activity distributions for a spherical cell

Ellipsoidal cell		D_{Ag-111} (µGy/Bq/s)	D_{Lu-177} (µGy/Bq/s)
Membrane	Nucleus	236	542
	Whole cell	90	213
Whole cell	Nucleus	149	381
	Whole cell	98	258
Cytoplasm	Nucleus	75	157
	Whole cell	91	243

Table 4.4: Comparison between the self-absorbed doses with ^{111}Ag and ^{177}Lu irradiation and different activity distributions for a ellipsoidal cell

As one can see in Table 4.3, the absorbed dose for ^{177}Lu is higher of a factor $\simeq 2$ respect to the dose for ^{111}Ag for both nucleus and whole cell. Also in the case of ellipsoidal cell (see Table 4.4), the doses differ for a factor a bit higher than 2. This observation is valid also in the case of whole cell activity distribution. This difference is in agreement with the one visible in Fig. 4.19.

Considering only the ^{177}Lu, one can compare the different doses absorbed by both the nucleus and the whole cell in the case of different activity distributions. As one can observe in Fig. 4.37, the higher dose obtainable with self-irradiation is the one with whole cell activity distribution for the cell and its nucleus. Instead, in the case of ellipsoidal cell (see Fig. 4.38), the nucleus and the whole cell absorb more dose when the radionuclide decay on the cell membrane.

It can be noted that the ^{111}Ag and ^{177}Lu have the same dose behavior for different cellular geometries and activity distribution. This can be addressed to the fact that the ^{177}Lu emission loses more energy than ^{111}Ag, but not enough for the electrons to stop within the cell. This implies that the geometric factor does not need to be taken into consideration because its range is wider than the cellular dimensions.
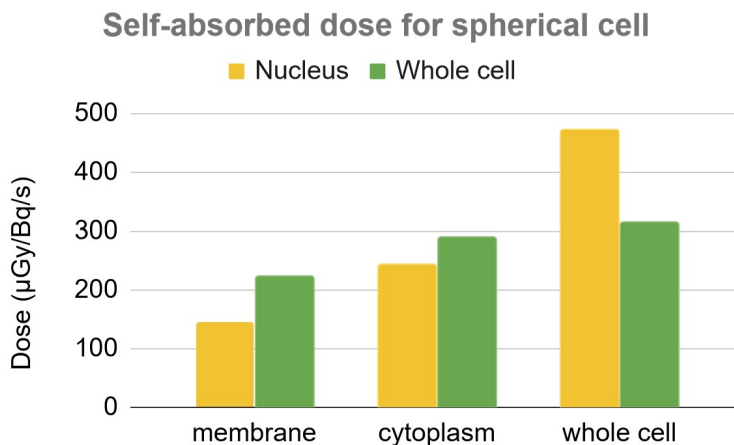
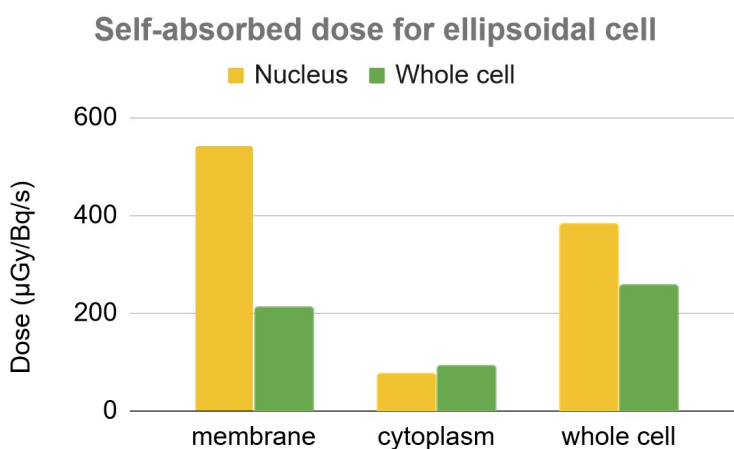Figure 4.37: Comparison between the different activity distributions for a spherical cell irradiated with ^{177}Lu

Figure 4.38: Comparison between the different activity distributions for an ellipsodial cell irradiated with ^{177}Lu

In conclusion, comparing the absorbed dose given by ^{177}Lu and ^{111}Ag, one has that they differ of about a factor 2 at short distances, as it is for the self-absorbed dose. This factor difference is valid as long as the initial quantity and the purity of the radionuclides are the same. In cases in which the lutetium purity and its quantity result lower than the silver ones, the latter could result more advantageous.

4.3.2   Cross-absorbed dose

One can also evaluate the absorbed dose of the cell and its nucleus when the radionuclide is distributed inside another cell. This process allows to study at which distance d_D the dose given is less than 1% respect to the dose absorbed when the cells are adjacent d_0 and to evaluate the dose behavior depending on the distance.

Also in this case the cytoplasm activity distribution is not calculated. This is due to the fact that the whole cell activity nicely approximate the cytoplasm one. After a distance of a couple of diameters the same can be observed for the membrane activity distribution.

Considering for example the ellipsoidal cell in the case of whole cell activity distribution (for the other combinations of geometries/activity distributions see the Appendix):
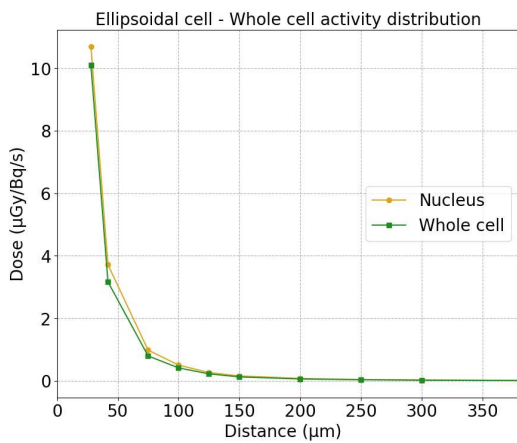
Figure 4.39: Absorbed dose at different distances (range $\simeq$ 0-350 µm)
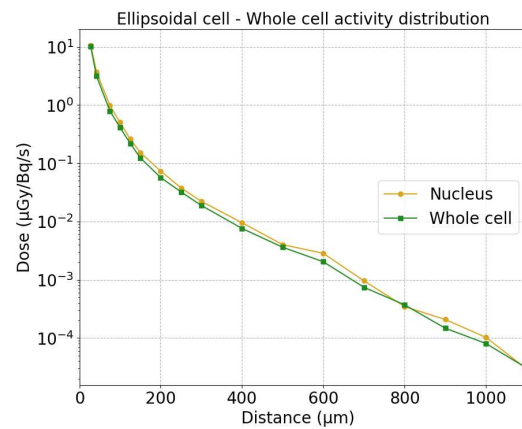
Figure 4.40: Absorbed dose at different distances (range $\simeq$ 0-1100 µm)

For this radionuclide the distance when $d_D \simeq 1\%$ of d_0 is reached at:

- 175 µm for ellipsodial membrane activity and 150 µm when the events are in the whole cell;

- for spherical cell this value is reached in the first case at 125 µm, while for decays in the whole volume at 150 µm.

One can see that the dose behavior resembles ^{111}Ag, but the dose given by ^{177}Lu is lower for higher distances. This fact can be seen when comparing directly the S-values (see Fig. 4.41).
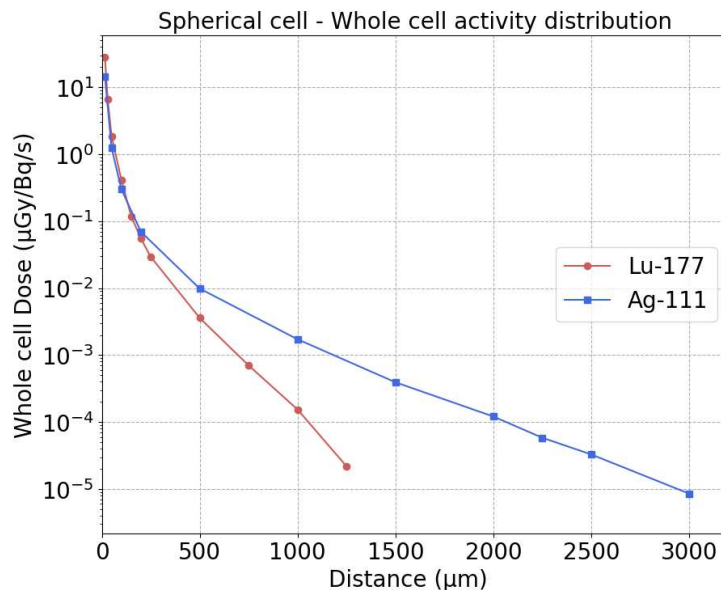
Figure 4.41: Comparison between the different doses at different distances depending on the radionuclide

Looking in particular at lower distances (as it is shown in Fig. 4.42), it is noticeable that the ^{111}Ag dose intake increases respect to the one due to ^{177}Lu. Depending on the cellular geometry and the activity distribution, this "changing point" ranges between 150 and 200 µm. This property of the silver could be useful in case of more extended diseases.
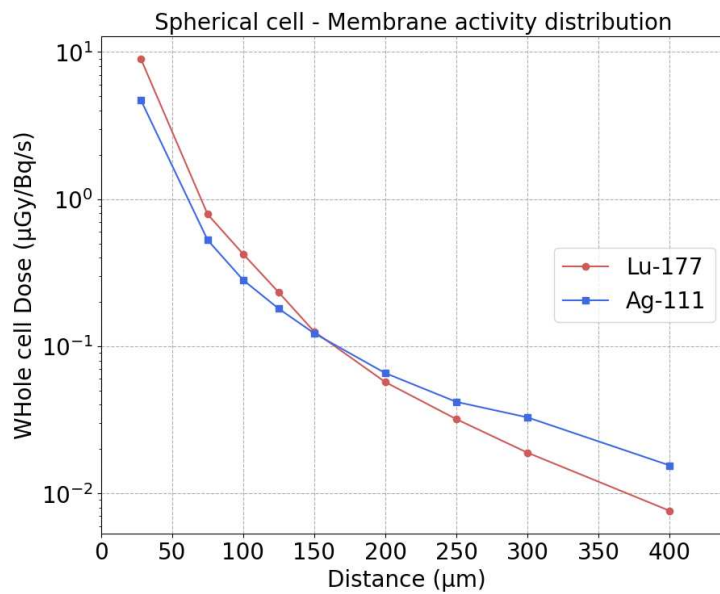
Figure 4.42: Comparison between the different doses at different distances depending on the radionuclide

Looking at the histogram it is clear that the differences in the absorbed dose between the two radioactive nuclei depend on the type of activity distribution. These results show that the silver could be a good candidate for radionuclide therapy for example when the dose is supposed to be absorbed in a wider range.
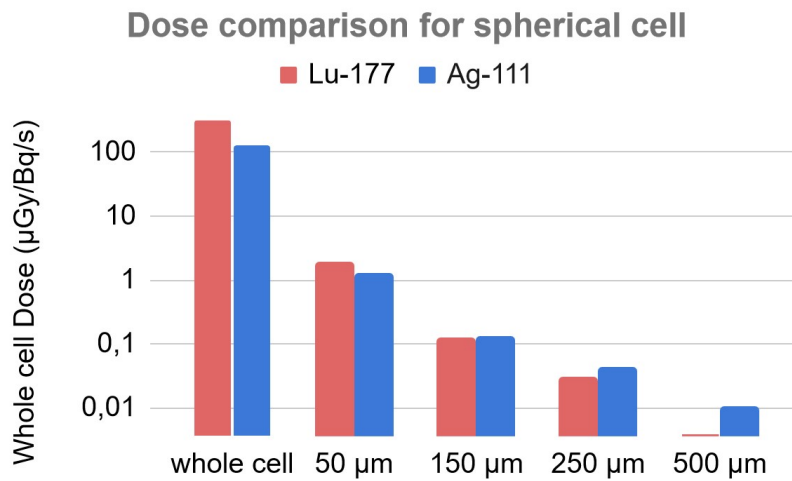
Figure 4.43: Comparison between different absorbed doses depending on the radionuclide and on the type of irradiation

4.3.3 Environment evaluation

To estimate at which distance the decay of the radionuclide does not contribute anymore to the absorbed dose of the cell, one can adopt the same procedure that is used in the case of ^{111}Ag. The result can be seen in Fig. 4.44 and in this case the *plateau* is reached at $\simeq 1$ mm, that is about one third of the distance for silver (see Fig. 4.45). This kind of result is in agreement with the behavior obtained in the previous section: for the cross-absorbed dose it is in fact observed that at higher distances the dose given by lutetium is lower than the one due to the silver.
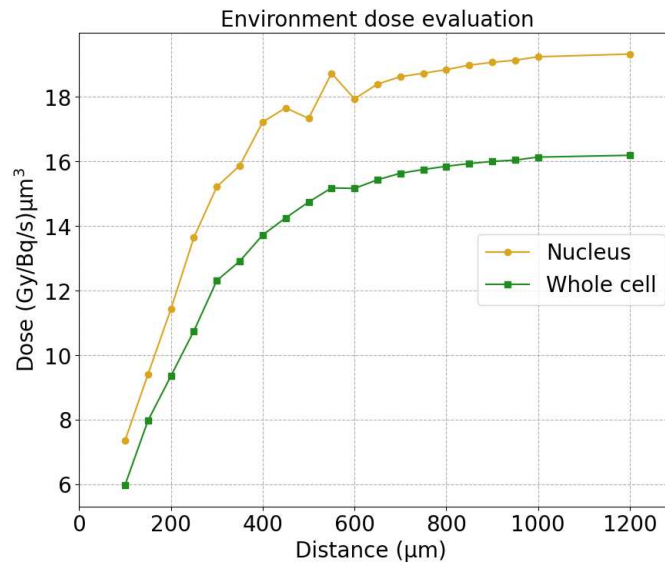
Figure 4.44: Dose absorbed by a spherical cell and its nucleus when the decays happen in the external environment with a constant density
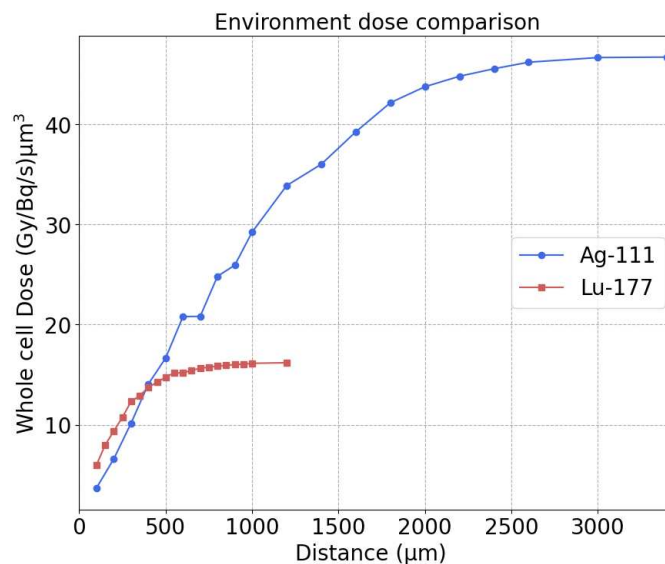
Figure 4.45: Dose absorbed by a spherical cell and its nucleus when the decays happen in the external environment with a constant density

4.4   Final considerations

Considering the results obtained in this chapter, it is possible to observe that ^{111}Ag could be a good candidate for RNT. For self-irradiation activity distributions, it seems to give half of the dose given by the commonly used ^{177}Lu. This means that the silver isotope could be more efficient than lutetium when, for example, its production purity may be higher than the lutetium one. This could be the case of the ^{111}Ag production in the context of the ISOLPHARM project: one of the aims of the SPES cyclotron is in fact the production of radionuclides with high purity (see Fig. 4.46).
Considering the cross-absorbed dose and the activity distributed in the environment, after a couple of diameters of distance, the dose given by the ^{111}Ag dominates over the ^{177}Lu. This could be an advantage when the silver isotope is positioned in the inner part of a tumour of some mm.
Another characteristic of the silver isotope that, depending on the situation, could be an advantage is its half-life. $t_{1/2}$ of ^{111}Ag is about half a day longer than the one of ^{177}Lu. This property could be useful in cases of long transportation or when elaborated processes are needed.
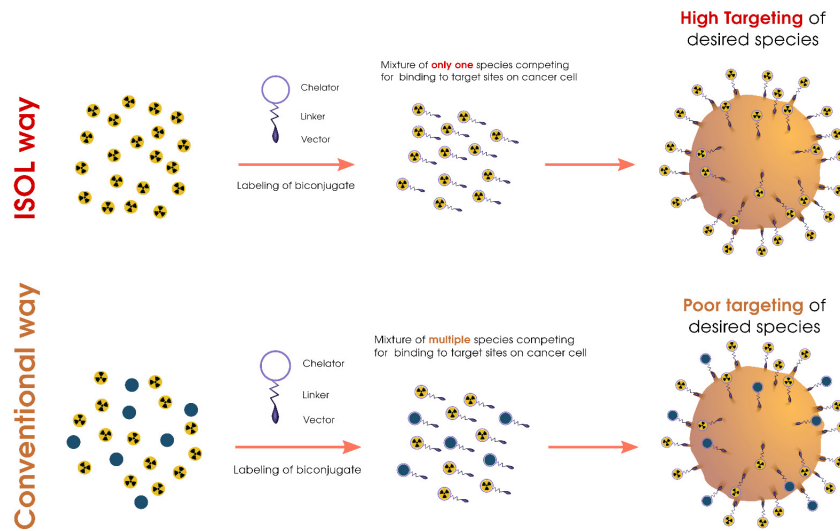
Figure 4.46: Schematic differences between the ISOL method and the conventional way purity

Finally, the doses estimated with the Geant4-developed code can be compared with other estimations obtained with different MC codes, for example with MCNP6 (see Fig. 4.47) and Geant4-DNA (see Fig. 4.48).
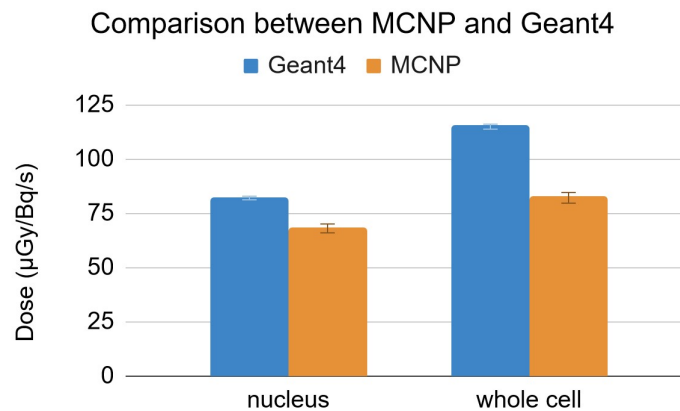
Figure 4.47: Comparison of the absorbed dose of a spherical cell with cytoplasm activity distribution of ^{111}Ag estimated with two different simulators: MCNP and Geant4
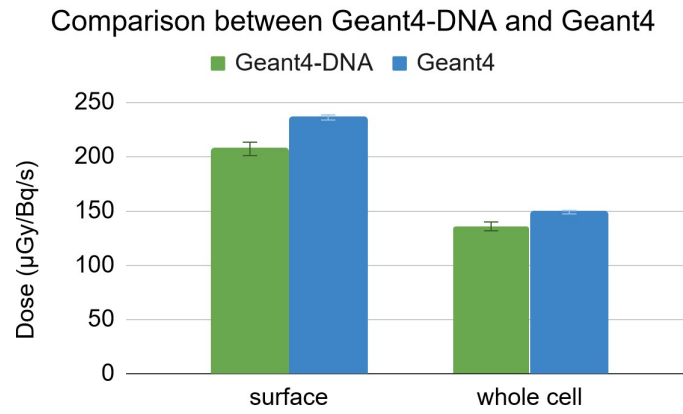
Figure 4.48: Comparison of the nucleus absorbed dose of an ellipsoidal cell with membrane and whole cell activity distribution of ^{111}Ag estimated with two different simulators: Geant4-DNA and Geant4

Considering the comparison of the absorbed dose simulated with Geant4 with the ones obtained with MCNP and Geant4-DNA, it is possible to observe that the Geant4 code developed in this thesis predicts generally dose values slightly higher, with a more significant difference in the case of MCNP.

Chapter 5

Survival fraction estimation

This section of the thesis has the aim to study the dose absorbed by a cell colony and the related survival fraction. This kind of study can be useful to obtain biological parameters that could be used for a preliminary study of the survival curve in the case of irradiation made with [111]Ag. It takes into account two different experiments, both conducted at the LENA nuclear reactor in Pavia. The cell colonies employed are originated from two separate cell lines: U-87 GM and UMR-106. In the first case, the colonies are contained in different flasks, while in the second they are enclosed within various Petri dishes. Both sets of colonies undergo irradiation using ^{60}Co as the radiation source.

In the first experiment one can compare the dose obtained for different irradiation times by the system calibration with the simulated one to validate the developed code. This code could be in fact useful for next studies regardins the silver isotope.

The second experiment involves irradiating cell colonies with varying doses and measuring the amount of DSBs after different times. Depending on the dose applied, the amount of damage to the cells will be different and so the survival fraction. The correlations between the absorbed dose and the survival fraction has been described in literature with different models; in particular, this thesis will consider the Linear-Quadratic and the Lethal and Potentially Lethal ones. As mentioned above, the commonly used Linear-Quadratic model depends on two parameters: α and β, both already studied for the considered cell line in the case of γ irradiation [47]. The knowledge regarding this model and the data acquired in the experiment can be used to estimate the parameters of the LPL model.

In both the experiments the colonies absorb the energy that comes from the decay of [60]Co. This radionuclide (see Fig. 5.1) decays in the 99.9% of the cases with the emission of a β^- to an excited state of [60]Ni. This process is followed by the emission of two γ, respectively of 1.1732 MeV and 1.3325 MeV, to the stable state of the nickel isotope. In the remaining cases, ^{60}Co decays β^- to an intermediate excited state of [60]Ni, which goes through the de-excitation process emitting γ of 1.3325 MeV [48].

Considering the set-up of both the experiments (view Fig. 5.4 and 5.5), the energy absorbed by the colonies comes mainly from the γs, which pass through air with few interactions and have a range in water of $\simeq$ 10 cm.
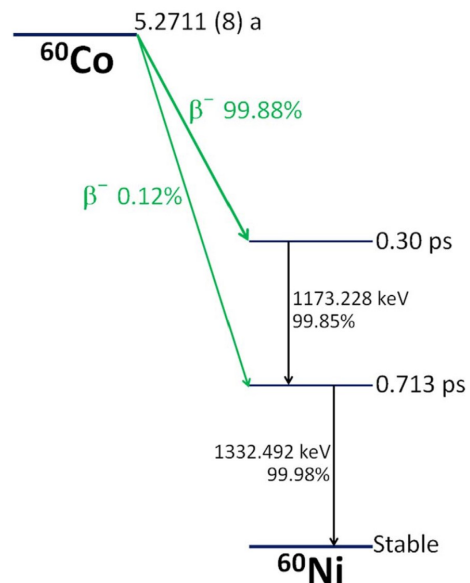

Figure 5.1: [60]Co decay scheme [48]

5.1 Experimental validation

The colonies chosen in this experiment come from the line U-87 GM. This line is one of the reference lines used for the study of the Multiform Glioblastoma, which is one of the most aggressive brain's tumor. An important characteristic of this line is its bimodal behavior: in the first phase of their growth they grow attached to the flask and they form a small layer, while in the second part of their life they generate spherical bodies of hundreds of µm that detach themselves from the layer. In the experiment the colonies are in the early phase, while the late phase is not considered [49].
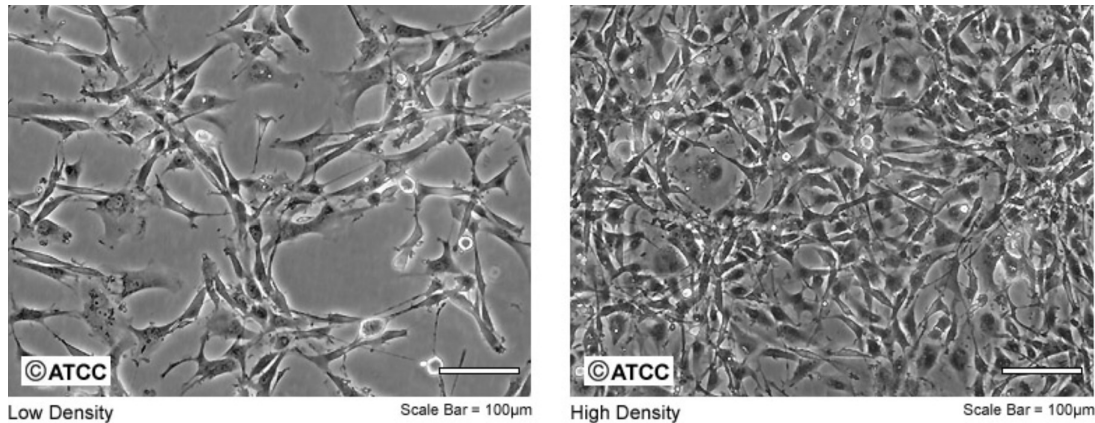
Figure 5.2: U-87 GM images taken with microscope for low and high density [50]

This 2D *in vitro* colonies are situated inside 4 different flasks and are irradiated by 13 ^{60}Co bars, as it can be seen in Fig. 5.4.

These bars (height h=15 cm and external radius r_e=0.775 cm) are accommodated inside containers excavated in a cylindrical structure of Aluminium (inner radius r_i=6.95 cm and outer radius r_o=8.75 cm). The structure has 26 hollow cylinders equally spaced and the radioactive sources are placed alternately. This system is located inside an underground cockpit at LENA. As it can be seen in Fig. 5.3, the structure containing the cells can be dropped inside the cockpit with a pulley. The same mechanism is used to take them out.

Every colony is grown inside a T25 flask (see Fig. 5.6), for a total of 4 colonies. The flasks are positioned in vertical and the colonies develop on one of the vertical faces (the flasks are made of plexiglass with a thickness of 1 mm and they are approximated as a parallelepiped which has a height of 5.9 cm, while the other sides are respectively of 1.8 and 3.8 cm); the rest of the flask is filled with cellular liquid, which can be approximated to water. The cells layer thickness is about 10 µm and it is positioned in the inner part of the flask, as it can be seen in Fig. 5.4. In this way, the cellular layers are surrounded by a layer of the order of cm of cellular liquid.

Figure 5.3: Photo of the external system

In total there are 5 flasks: 4 with cells colonies and one filled only with cellular liquid. The latter

allows the colonies 1, 2 and 3 to be surrounded by water. The evaluation of the dose given to the flasks is made with the supposition of electronic equilibrium. This allows to have a homogeneous energy deposition on the volume [49].
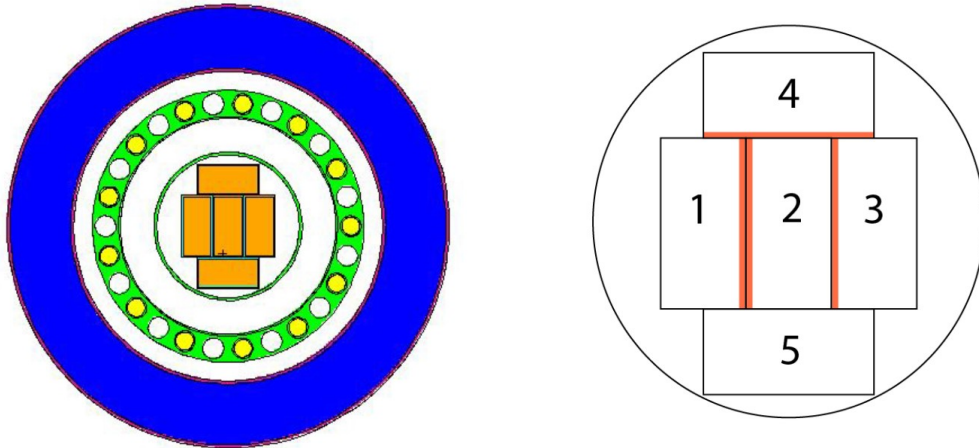

Figure 5.4: On the right: transversal section of the experimental set-up. On the left: zoom on the flasks disposition inside the cylinder. The red layers represent the cells [49]

To obtain different values of dose, each flask is irradiated for a different irradiation time. The latter time is chosen based on a previous calibration to get the wanted dose. The calibration was previously done in two ways: at first with the use of a ionization chamber and then with dosimeters made of alanin in different positions.

Figure 5.6: Photo of an empty and horizontal T25 flask [51]

To shield the external environment from the ^{60}Co decay, the overall system is set inside a lead container covered by a small layer of steel (see Fig. 5.5). This container has an entrance on the top that allows to insert the cylinder with the colonies. This shield does not lead to relevant changes in the dose absorbed by the colonies. On the top of the flasks and of the bars containers there is a steel plug to cover the structure [49].

This external structure could be not considered in the simulation but, due to the fact that is does not influence of a big factor the simulation speed, in this thesis it will be taken into consideration.
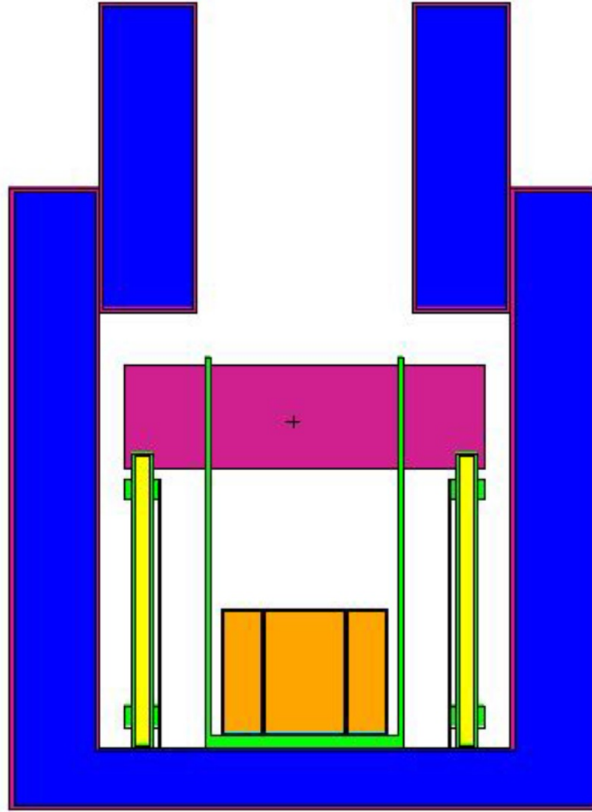
Figure 5.5: Longitudinal section of the experimental set-up [49]

The flasks are positioned inside the experimental set-up for different irradiation times. The experimental absorbed dose can be calculated with a calibration process. A first validation of the code can be done comparing the experimental doses given to the colonies for different irradiation times and the doses obtained with the simulation on Geant4 for the same irradiation times.

Knowing the initial activity of the ^{60}Co sources, that is equal to $2.11 \cdot 10^{11}$ Bq [49], one can simulate the system considering a high number of events and then normalize the value obtained for a wanted activity and exposition time.

Comparing now the dose obtained from the experiment (the data are taken from the master thesis of E. Simeone [49]) and the one from the simulation one has the following values:

Irradiation time (min)	Dose (Gy)	σ_D (Gy)	Dose$_{Geant4}$ (Gy)
1.85	2.00	0.23	2.34
3.28	3.50	0.55	4.15
4.53	5.00	0.47	5.74
6.37	7.50	0.53	8.06
9.23	10.00	0.97	11.68

Table 5.1: Comparison between doses obtained from calibration (with dose error σ_D) and doses obtained via simulations for different irradiation times

Considering a statistical uncertainty of about 1% for the dose calculated with Geant4, one can say that the compatibility between the experimental and simulated doses vary from 1.2 to 1.7. This result shows a good compatibility between the values.

The simulated dose values can be compared also with the values obtained via MCNP6 in the master thesis of E. Simeone [49] and they result to have a good agreement (see Fig. 5.7). As already pointed out in the previous chapter, our Geant4 values are in general slightly higher than the corresponding

MCNP predictions.
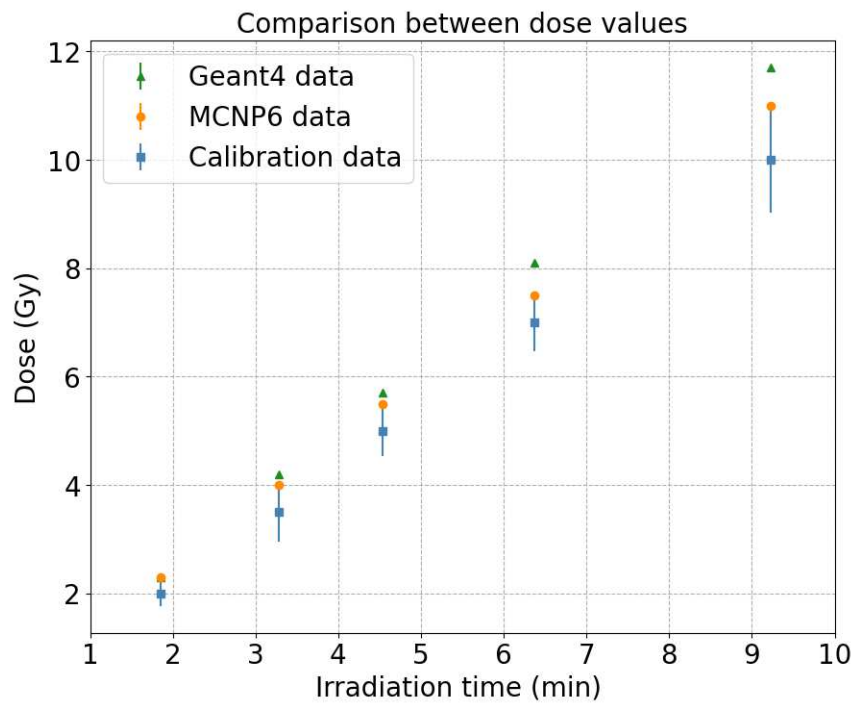
Figure 5.7: Dose comparison between experimental and simulated data

5.2 Repair parameters

Another experiment has been conducted inside the LENA in Pavia with the use of the same experimental set-up. As in the other experiment, the cells are accommodated inside a cockpit where they are irradiated by γ from the decay of ^{60}Co, as it can be observed in Fig. 5.4 and 5.5.

The cell line chosen for the experiment is the UMR-106. This line is a clone of the cells taken from a rat Osteosarcoma. Osteosarcoma is a bone tumor that, due to the high speed of reproduction, is considered really aggressive. Depending on its location, it can be more frequent in children and teenagers or in elderly people [47].

This line presents the typical characteristics of cancerous cells and it is easier to work with, with respect to the cell line used in the previous experiment. The cells present in fact a more regular shape (see Fig. 5.8). Moreover, the U-87 GM have two different development phases; in the late one, in particular, there is the formation of spherical bodies that need to be taken into consideration.
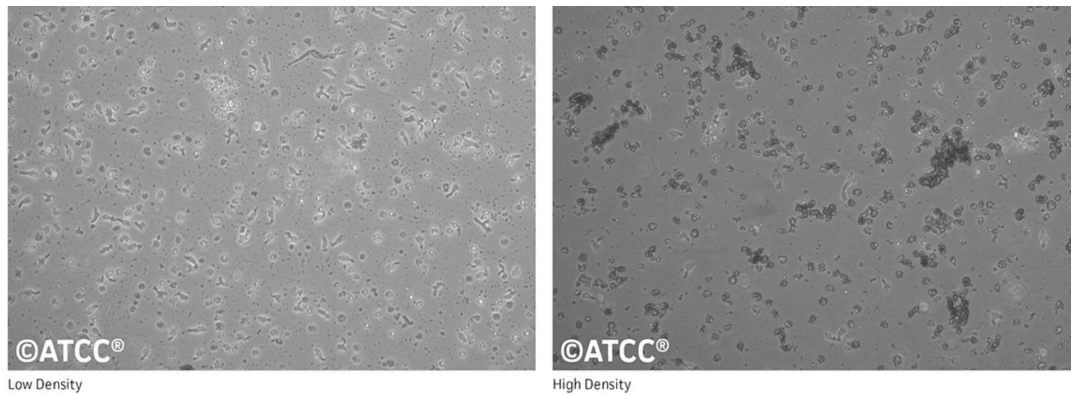
Figure 5.8: UMR-106 images taken with a microscope for high and low density [52]

Figure 5.9: Picture of the Petri dish used for the irradiation [53]

Unlike the previous experiment, each cell colony is positioned on the lower face of a Petri dish (with height h=10 mm and diameter d=35 mm [53]) with the help of a thin squared layer of plastic and they are homogeneously distributed on the dish surface. On average each cell colony is formed by 30000 cells.

The Petri dishes are then divided into 2 columns of 6 each (a couple of Petri dishes were not irradiated to be kept as "control" colonies) and positioned inside an Aluminium container. Another column made of a cylinder of water of the same dimensions of the other two is inserted inside (a schematic view of the set-up containing the colonies can be seen in Fig. 5.10. Disclaimer: this picture wants to give an idea of the set-up and it does not reproduce the right proportions).

On the top and on the bottom of the system there is a layer of water. This is done to have the electronic equilibrium and to have a homogeneous distribution of the energy.

The container is then closed and dropped inside the cockpit thanks to a pulley (see Fig. 5.3). The first column of cells is kept inside the experimental apparatus for half minute and receives 0.5 Gy, while the second one has an irradiation time of 2 minutes and an absorbed dose of 2.0 Gy.
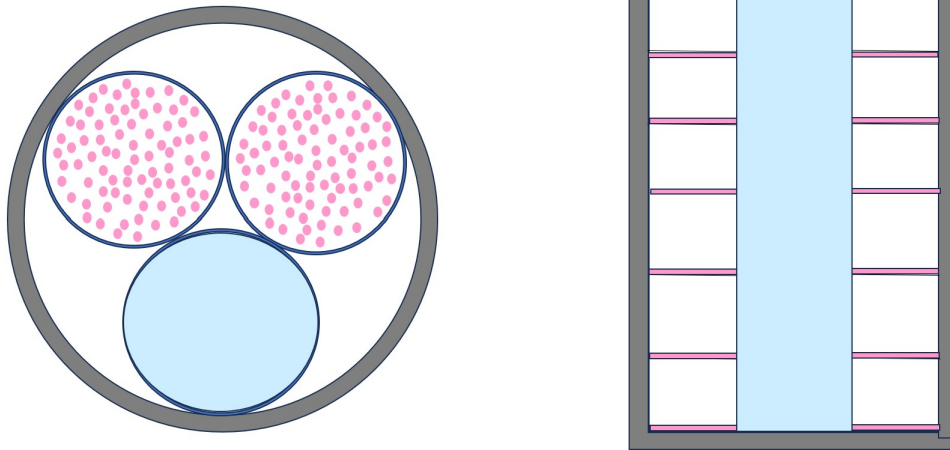
Figure 5.10: Transversal (on the left) and longitudinal (on the right) schematic view of the cells contained inside the Petri dishes and inserted with the water cylinder in the Aluminium container

Depending on the irradiation time and on the initial activity of the ^{60}Co source, the cells absorb a different dose which brings to the death of a certain amount of them. The relation between the given dose and the amount of cells that remain alive, the so-called survival fraction (SF), is described by different models. This thesis considers the models explained in the "Survival Models" chapter that are the LQ model, a "classic" model, and the LPL model, a more sophisticated system that takes into considerations also biochemical factors.

Before studying the survival fraction with the LQ and the LPL models, there can be a further validation of the Geant4 code. This validation can be done comparing the estimated dose (the dose obtained knowing the initial activity of the source and the irradiation time) and the dose obtained with the simulation of the system on Geant4.

Figure 5.11: Picture of the Aluminium container with the cilinders before the irradiation

5.2.1 Linear-Quadratic Model

As mentioned above, the relation between the dose D and the survival fraction SF (in the case in which the dose is given in one fraction) can be written as:

$$SF = e^{-\alpha D - \beta D^2} \tag{5.1}$$

the parameters α and β depend on biological factors and on the type of radiation. For the UMR-106 cell line in the case of γ irradiation coming from the decay of the ^{60}Co, they are estimated in the Master thesis of B. Marcaccio [47]:

$$\alpha = 0.14 \pm 0.05$$

$$\beta = 0.05 \pm 0.01$$

For both the quantities the unit is Gy^{-1}.

This experiment has its focus on the study of the Double-Strand Breaks caused by radiation and there are no available data about the survival fraction. However, there are enough information to simulate the survival fraction behavior.
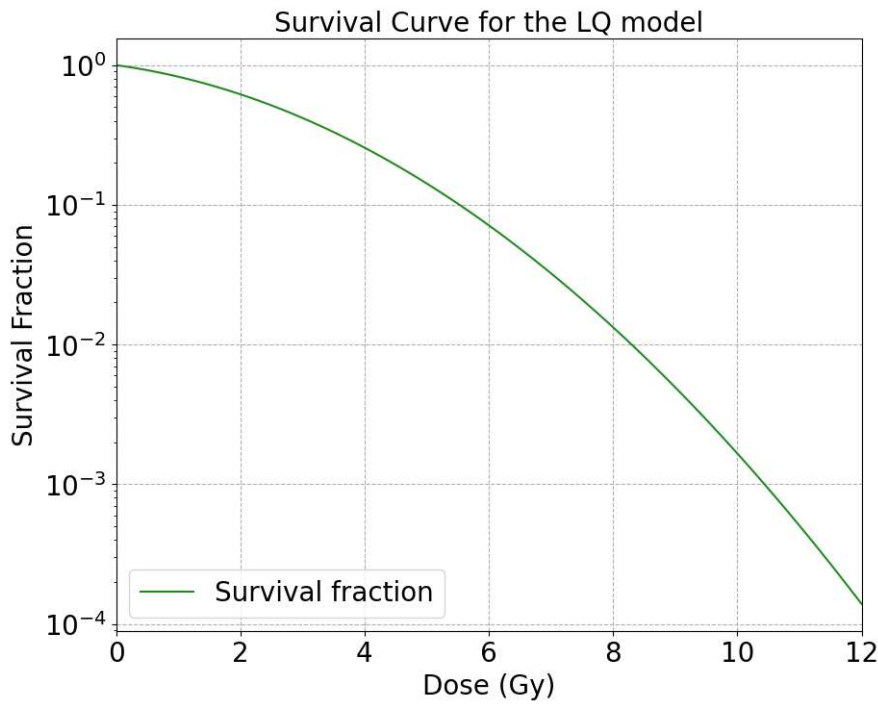
Figure 5.12: Survival curve of the Linear-Quadratic model in the case of the ^{60}Co

In particular, for the doses of 0.5 Gy and 2 Gy the estimated cell survival fraction is the following:

Irradiation time (sec)	Dose (Gy)	SF (%)	σ_{SF} (%)
30	0.5	92	2
120	2.0	62	6

Table 5.2: Cell survival fraction (with the associated error σ_{SF}) for different doses

5.2.2 Lethal and Potentially Lethal Model

As mentioned above, the general form of the survival fraction for the LPL model can be written as:

$$S = e^{-\bar{L}_{tot}(T)} \left[1 + \frac{\bar{L}_{dsb}(T)}{\epsilon}(1 - e^{-\lambda_{dsb}t_r}) \right]^{\epsilon} \tag{5.2}$$

where $\epsilon = \lambda_{dsb}/\eta_{dsb}$. $\bar{L}_{dsb}(T)$ represents the amount of DSBs at the end of the irradiation and it can be obtained from Equation (3.4) when considering the terms of repair and misrepair negligible at the end of the irradiation. In this case in fact $\bar{L}_{dsb}(T)$ becomes:

$$\bar{L}_{dsb}(T) \simeq 2Y\Sigma_{dsb} \int_0^T \dot{D}(t)dt = 2Y\Sigma_{dsb}D \tag{5.3}$$

and the survival fraction can be rewritten as a function of the dose D:

$$S = e^{-2Y(\Sigma_{dsb}+\Sigma_f)D} \left[1 + \frac{2Y\Sigma_{dsb}D}{\epsilon}(1 - e^{-\lambda_{dsb}t_r}) \right]^{\epsilon} \tag{5.4}$$

To obtain the cellular survival curve, it is necessary to estimate the parameters. The first terms taken into consideration are the ones related to the amount of DSBs and fatal lesions after the irradiation time: $2Y\Sigma_{dsb}$ and $2Y\Sigma_f$.

The terms Σ_{dsb} and Σ_f can be obtained as an output of the example code "molecularDNA", available on Geant4-DNA. This code simulates the DNA and the damages inflicted by the radiation. It includes a library containing pre-existing geometries, between which there is also the human cell [35–37]. The simulation will consider a human cell (with the same volume considered for the cell irradiated by ^{111}Ag and ^{177}Lu) irradiated by the γs coming from the decay of the ^{60}Co.

It is important to highlight that the cell line considered in this experiment comes from a rat. Taking into consideration the differences between the healthy human cell and the tumorous rat cell, one will expect an over- or under-estimation of the amount of the damages, but the overall behavior will be the same. The output of "molecularDNA" will be considered but it has to be multiplied by a constant that will be estimated.
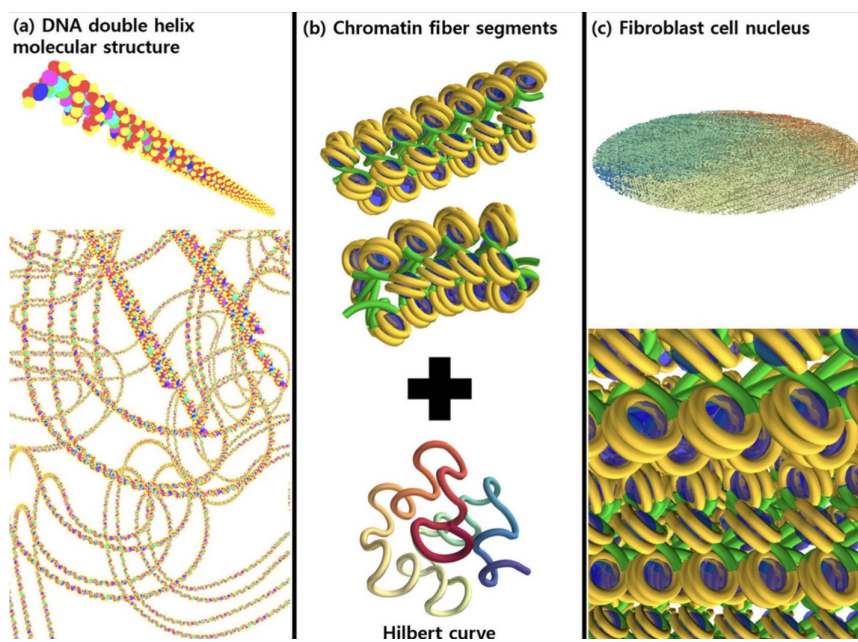
Figure 5.13: Picture of 3 different kinds of geometries pre-existing in "molecularDNA" [54]

The total amount of DSBs after the irradiation of the human cell is:

- for 0.5 Gy $\Sigma_{dsb} = (6.0 \pm 0.2)$ Gy^{-1}·Gbp^{-1}, where bp is a unit used in DNA studies and it stands for "base pair", and the value is associated to an error of 3%;

- in the case of 2 Gy the value is (6.5 ± 0.2) Gy^{-1}·Gbp^{-1}.

Considering that in this model the parameters do not depend on the dose and they can be considered constants, one can estimate the mean value between the ones obtained for 0.5 and 2 Gy. Knowing that on average a rat cell has Y $= 2.65 \cdot 10^9$ pb, the parameter representing the average amount of DSBs per absorbed dose unit is:

$$2Y\Sigma_{dsb} = (33.2 \pm 0.7) \ Gy^{-1} \tag{5.5}$$
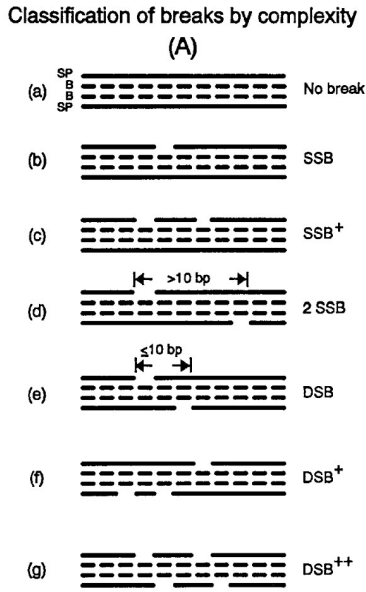
Figure 5.14: DNA damages classification in "molecularDNA" [55]

The same code can also give information about the term related to the fatal lesions $2Y\Sigma_f$. The output of the code classifies the different kind of damages depending on their complexity. Looking at Fig. 5.14, one can distinguish two different kind of damages that could be considered fatal: DSB+ and DSB++. The first ones are lesions made of a DSB and one or more SSB within a segment of DNA of 10 bp, while DSB++ comprehend at least 2 DSBs in a segment of 10 pb of wider [55].

Considering the hypothesis of the LPL model, the DSB will not be considered as a fatal lesion and the term $2Y\Sigma_f$ will comprehend only DSB+ and DSB++. It results to be (1.27 ± 0.04) for 0.5 Gy and (1.38 ± 0.04) for 2 Gy. The average value results to be:

$$\Sigma_f = \Sigma_{dsb+} + \Sigma_{dsb++} = (1.33 \pm 0.03) \ Gy^{-1}Gbp^{-1} \tag{5.6}$$

The term related to the fatal lesions becomes:

$$2Y\Sigma_f = (7.00 \pm 0.15) \ Gy^{-1} \tag{5.7}$$

Figure 5.15: Geant4-DNA logo [56]

To estimate the constant of proportionality for passing from the human cell to the animal one, one can exploit the Linear-Quadratic survival curve. For low doses in fact the LPL model and the LQ one overlap. Considering the values $2Y\Sigma_{dsb}$ and $2Y\Sigma_f$ multiplied by the constant of proportionality k and the doses extrapolated from the LQ survival fraction for low doses, one can do a fit. This allows to obtain k and ϵ. The repair time is considered $t_r \longrightarrow \infty$.
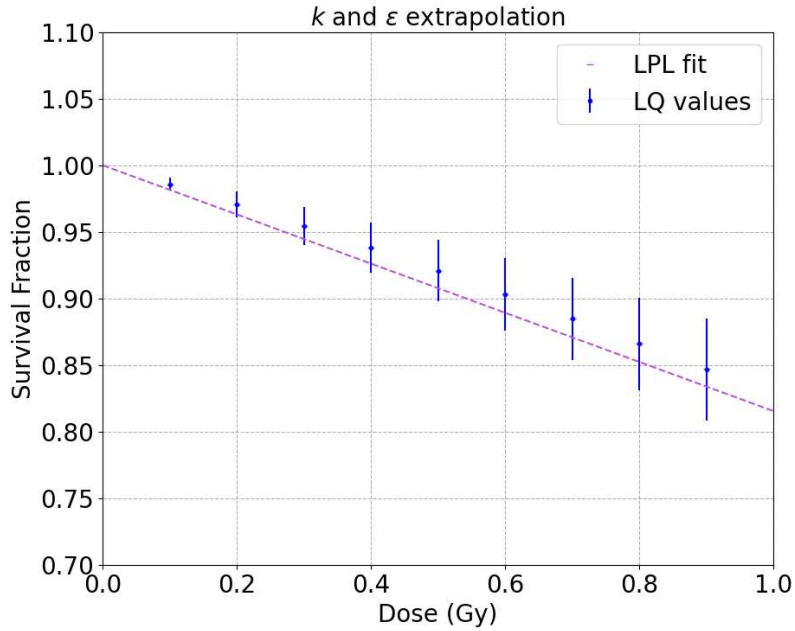
Figure 5.16: LPL fit of the low doses LQ values

The values obtained are:

$$k = 0.01986 \pm 0.00003$$

$$\epsilon = 3.86 \pm 0.05$$

and the amount of DSBs and lethal damages become:

$$k \cdot 2Y\Sigma_{dsb} = 0.657 \pm 0.014 \tag{5.8}$$

$$k \cdot 2Y\Sigma_f = 0.139 \pm 0.003 \tag{5.9}$$

Knowing these values, it is possible to obtain the survival fraction and compare it with the survival curve for the LQ model. It has to be considered that in the Fig. 5.17 the reparation time is taken as $t_r \longrightarrow \infty$.
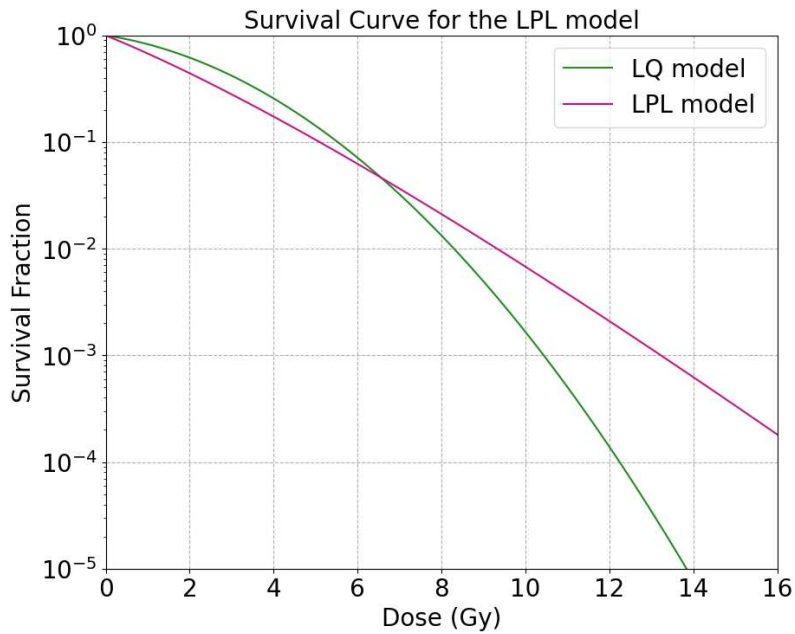
Figure 5.17: LQ and LPL survival curves

The parameters λ_{dsb} and η_{dsb}, related to the repair probability of DSBs, can be obtained experimentally through the *foci* assay. This study regarding the DSBs is based on a technique named IRIF (Ionizing Radiation-Induced Foci). This refers to the individuation of specific proteins related to the repair mechanism of the DSBs. In particular, in the latter experiment, one takes into consideration the phosphorylated histone γH2AX that is a spatial biomark of the lesions. In the *foci* assay this histone is marked with specific antibodies. These antibodies are fluorescent and they can be seen with a fluorescence microscope. The complete process is explained into details in the bachelor thesis of D. I. Filosa [44].

The evaluation of the average amount of *foci* through ImageJ is done in the master thesis of A. Leso [45]. The values are evaluated for two different irradiation doses, 0.5 and 2 Gy, and after 30 minutes and 24 hours. This passage can be done by "freezing" the cell colonies at the wanted time.
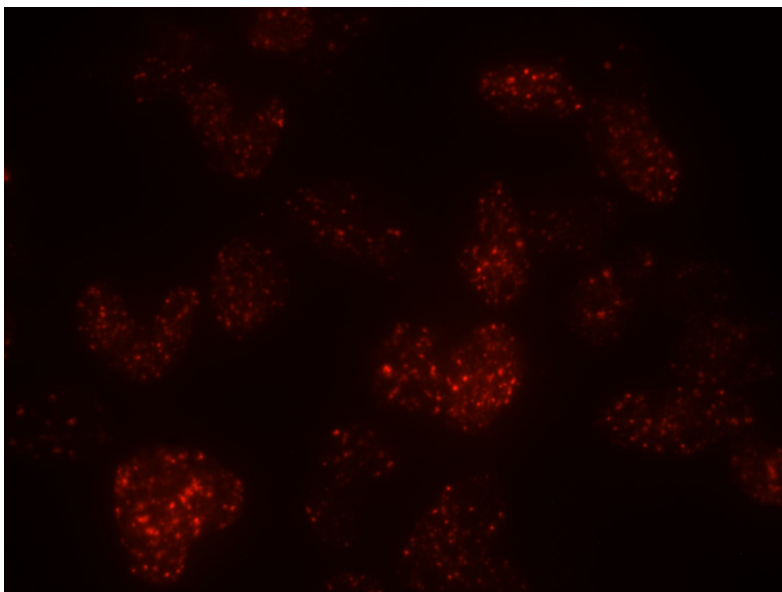
Figure 5.18: Microscope picture at 30 mins after irradiation for a dose of 0.5 Gy
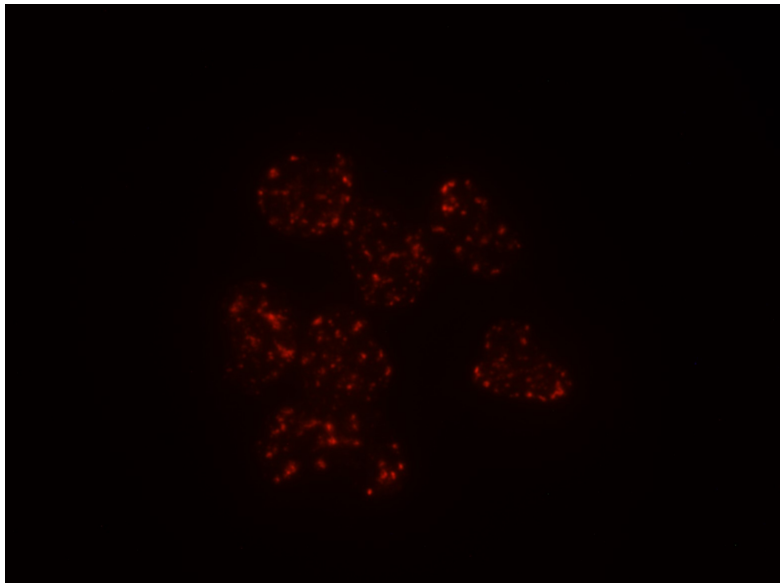
Figure 5.19: Microscope picture at 24 hours after irradiation for a dose of 0.5 Gy

The average values can be seen in the Table 5.3:

Dose (Gy)	30 minutes	24 hours
0.5	32 ± 3	23 ± 3
2	50 ± 7	16 ± 2

Table 5.3: Average amount of γH2AX for different absorbed doses and after different times

It has to be highlighted that the *foci* essay is a semi-quantitative study. This means that it is possible to obtain the behavior of the amount of damages depending on the dose and on the time. To obtain the amount of lesions that will be considered to obtain λ_{dsb}, following the A. Leso master thesis [45] procedure, one can compare the obtained data with the damages behavior simulated with "molecularDNA". This process allows to get the division parameter needed to have the overlapping of the curve with the data, that is 0.55 for 2 Gy and 1.67 for 0.5 Gy. These parameters can then be exploited to get the values of λ_{dsb}.

To obtain the parameter one can consider Equation (3.4) that, when the irradiation is over (t>T), can be simplified as:

$$\bar{L}_{dsb}(t_r) = \frac{\bar{L}_{dsb}(T)e^{-\lambda_{dsb}t_r}}{1 + \bar{L}_{dsb}(T)(1 - e^{-\lambda_{dsb}t_r})/\epsilon} \tag{5.10}$$

Considering the ϵ previously estimated, one can perform a fit for each dose value considering the data contained Table 5.3 divided by the proportional constants mentioned above. This process allows in fact to estimate λ_{dsb}.

In the LPL model does not consider the fact that there is an amount of time after the irradiation when the proteins are not attached to the lesions yet. In this range of time the *foci* assay is not reliable and one needs to wait until the proteins get attached. The data obtained are taken after this range of time and so in this case one can neglect this behavior at small times [45]. Moreover, the values obtained at 30 minutes result to be approximately on the peak of the descendent curve representing the amount of DSBs and so they will be considered as $\bar{L}_{dsb}(T)$.
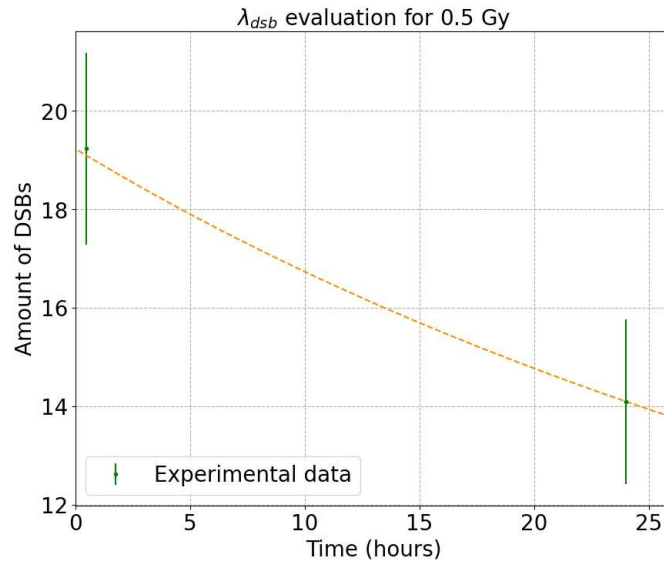
Figure 5.20: Fit of the amount of DSBs with Equation (5.12) for 0.5 Gy
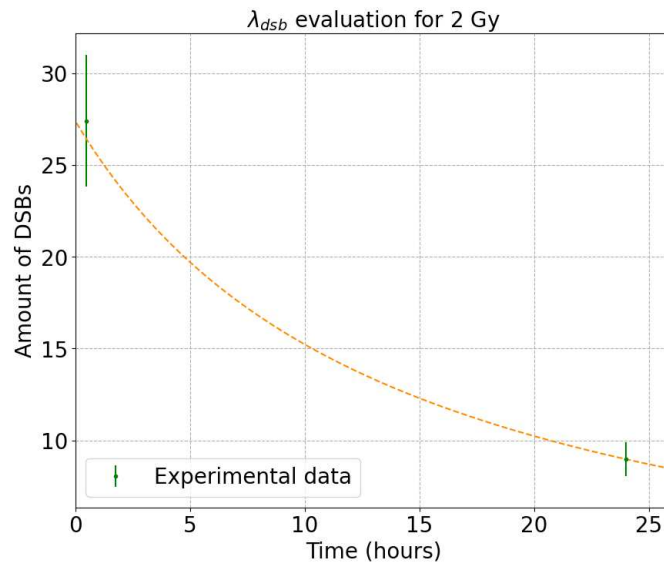
Figure 5.21: Fit of the amount of DSBs with Equation (5.12) for 2 Gy

The estimated λ_{dsb} is obtained through an average of the values for the two doses:

$$\lambda_{dsb} = 0.006 \pm 0.002 \ \frac{1}{h}$$

Knowing this parameter and ϵ one can also estimate the term related to the interactions of the DSBs between each other (binary misrepair):

$$\eta_{dsb} = 0.0016 \pm 0.0005 \ \frac{1}{h}$$

Another interesting study regards the repair time of the cell line UMR-106. One can in fact compare the survival curve for $t_r \longrightarrow \infty$ with the ones for different repair time. In this way one can estimate the order of magnitude of the repair time. As it is shown in Fig. 5.22, the t_r of the cell line UMR-106 seems to be of the order of the hundreds of hours. This kind of estimation can be useful in *in vitro* to understand the amount of time that is necessary to wait before evaluating the survival fraction.
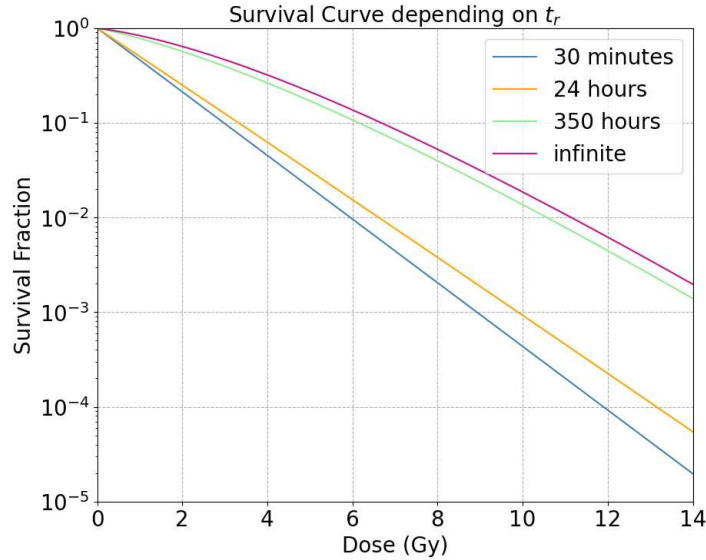
Figure 5.22: Estimation of the repair time in the LPL model

The biological parameters η_{dsb} and λ_{dsb} depend on the cell line and can be used to estimate the survival curve behavior of the UMR-106 line irradiated by the decay of the ^{111}Ag. In this case one should estimate the proportionality constant k with the same fit done in Fig. 5.20 and 5.21 and then multiply it to the simulated $2Y\Sigma_{dsb}$ and $2Y\Sigma_f$. This factor k is in fact calibrated on a survival curve of the UMR-106 cell line for the ^{60}Co irradiation and has to be recalculated in the case of another source.

Conclusions

This thesis comprehends preliminary studies regarding ^{111}Ag in the context of the ADMIRAL experiment. The aim of the project is to study the characteristics of this silver isotope to use it in Radionuclide Therapy. In the first part of the thesis there are different studies regarding the cellular absorbed dose depending on the cell's geometry and on the activity distribution of the radionuclide. These values are compared with the doses simulated in the case of ^{177}Lu, a commonly used radioactive isotope in RNT. It can be seen that for small distances the dose due to the ^{111}Ag decay is half of the one obtained with ^{177}Lu, while after $\simeq 150$ µm ^{111}Ag dominates.

The second part of the thesis includes preliminary studies using the LPL model. The first step is to simulate an experimental set-up that is supposed to be similar to the one that will be conducted using ^{111}Ag with the use of ^{60}Co. This part allows to validate the developed code. After the code validation, one can obtain the biological parameters of cellular repair λ_{dsb} and misrepair η_{dsb} of the colony UMR-106 through the Linear-Quadratic parameters obtained previously. These values, summed to the amount of lethal and potentially lethal damages simulated through Geant4-DNA, allow to estimate the survival fraction of the LPL model. This same process applied in this thesis for ^{60}Co can easily be adapted in the case of ^{111}Ag irradiation to evaluate the UMR-106 survival fraction.

Acknowledgements

Appendix

^{111}Ag studies

- Library evaluation: dose absorbed by the nucleus and the whole cell in the case of ellipsoidal cell with membrane activity distribution (respectively see Fig. A.1, A.2) and in the case of whole volume activity (respectively see Fig. A.3, A.4);
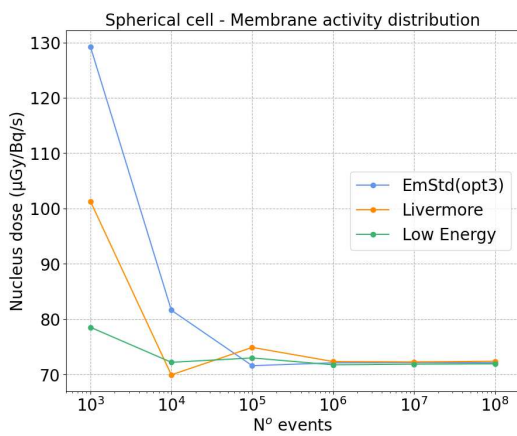

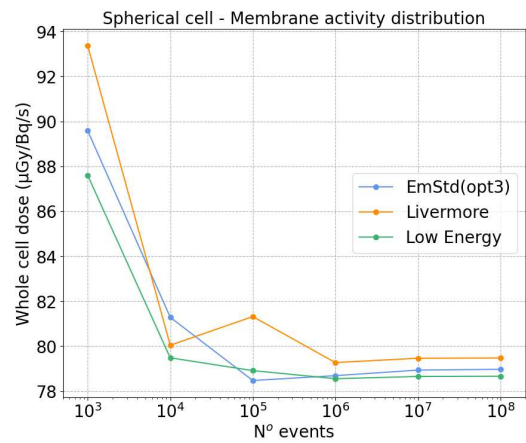Figure A.1: Nucleus normalized absorbed dose
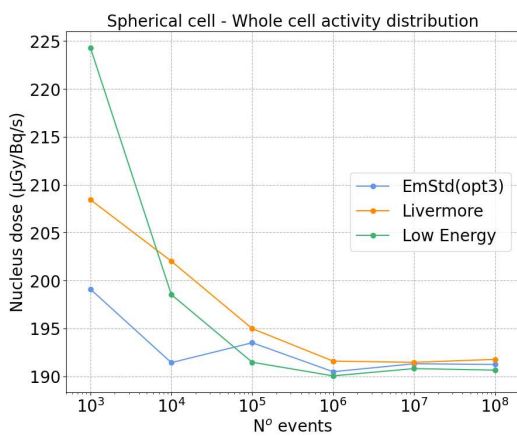

Figure A.2: Cell normalized absorbed dose
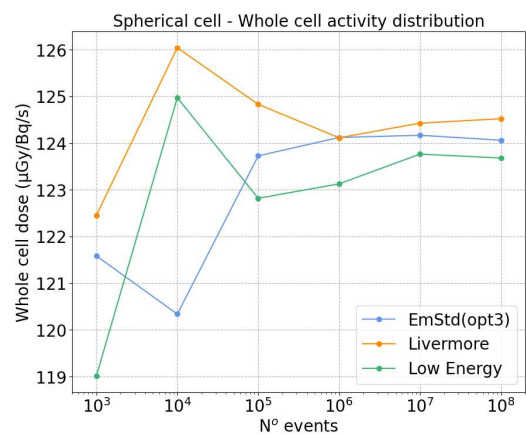

Figure A.3: Nucleus normalized absorbed dose

Figure A.4: Cell normalized absorbed dose

- Stability evaluation: for ellipsoidal cell with whole cell activity distribution (see Fig. A.5) and for spherical cell with membrane (see Fig. A.7) distribution and whole cell (see Fig. A.9) distribution;
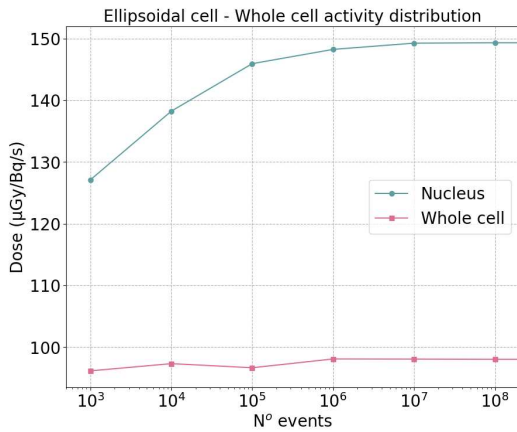
Figure A.5: Nucleus and whole cell dose
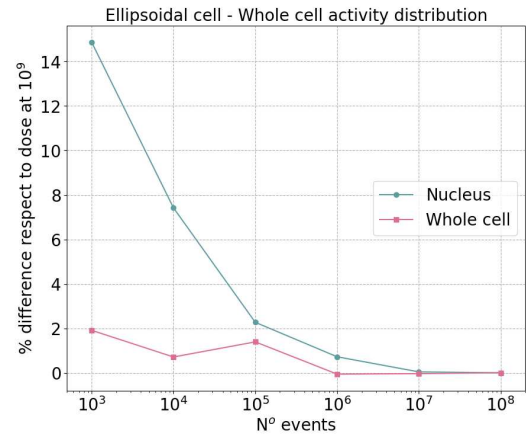
Figure A.6: Percentage difference wrt 10^9 events
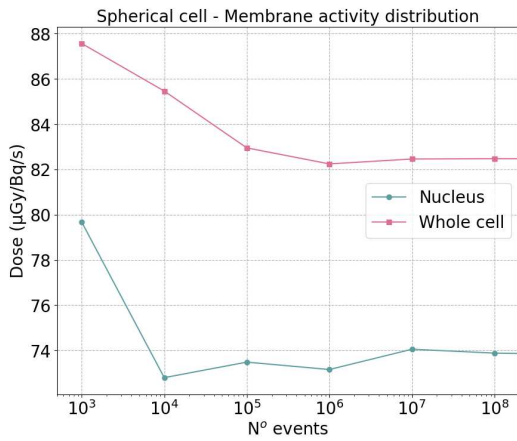
Figure A.7: Nucleus and whole cell dose

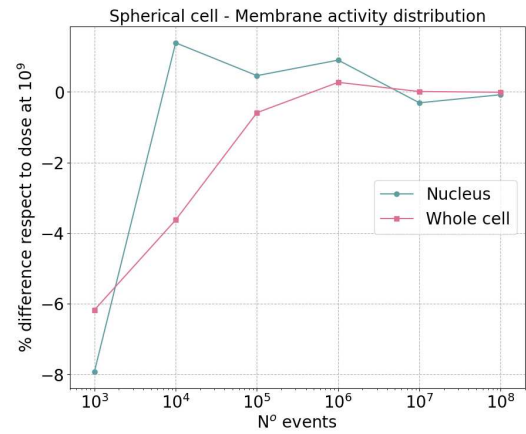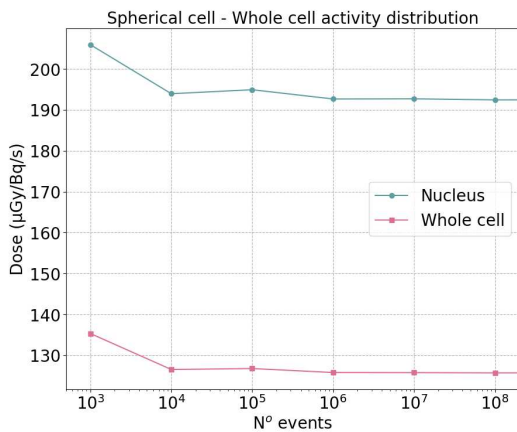Figure A.8: Percentage difference wrt 10^9 event
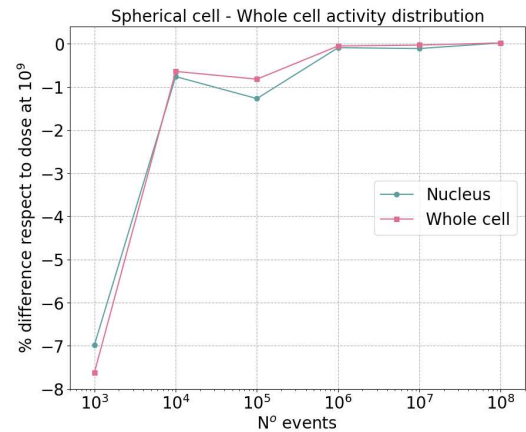

Figure A.9: Nucleus and whole cell dose

Figure A.10: Percentage difference wrt 10^9 events

- Cross-absorbed dose: whole cell activity distribution at difference distances for spherical (see Fig. A.11) and ellipsoidal (see Fig. A.12) cells. Cross-dose for a spherical cell with a membrane distribution for a range of 0-250 µm (see Fig. A.15) for 0-3 mm (see Fig. A.16).
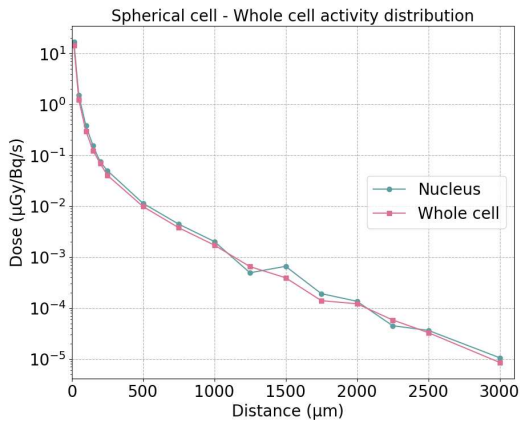

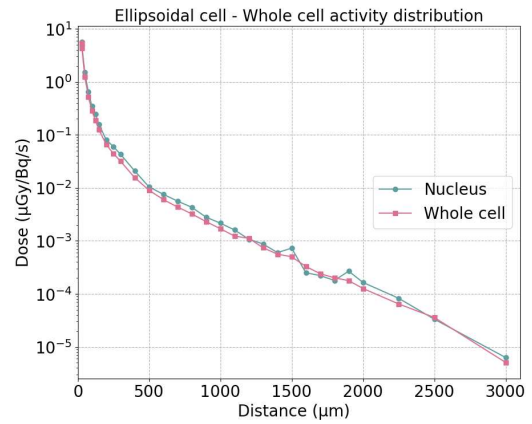Figure A.11: Nucleus and whole cell cross-dose
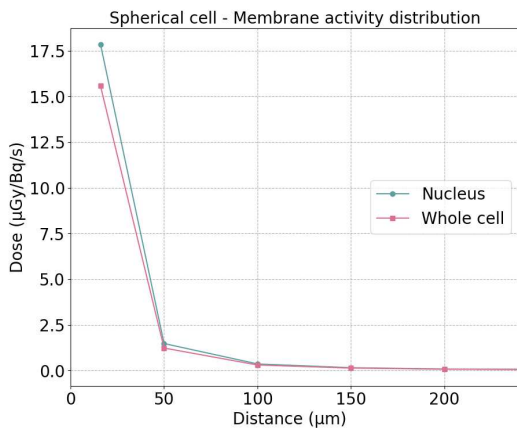

Figure A.12: Nucleus and whole cell cross-dose
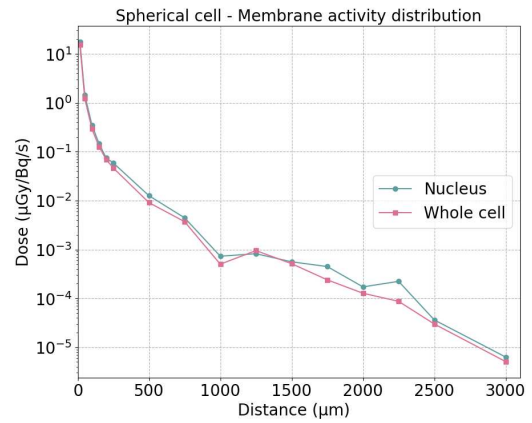

Figure A.13: Cross-dose in a range of $\simeq$ 0-250 µm

Figure A.14: Cross-dose in a range of $\simeq$ 0-3000 µm
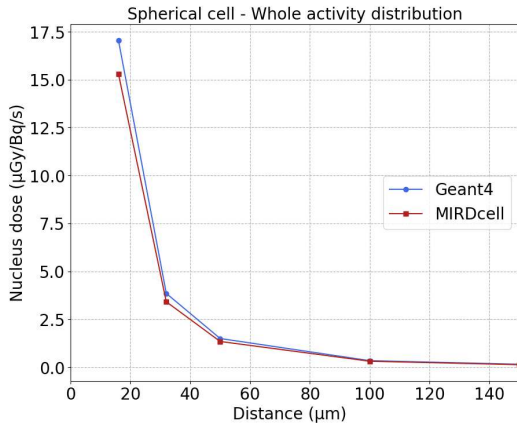
- MIRDcell and Geant4 comparison:

Figure A.15: Comparison between Geant4 and MIRDcell values
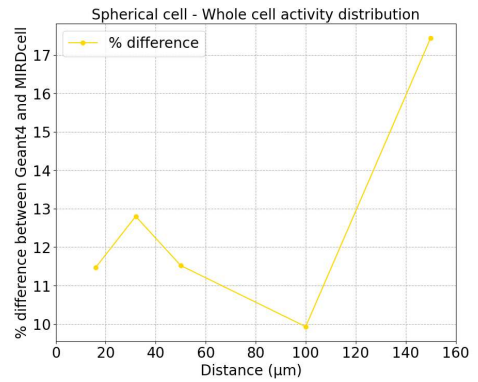

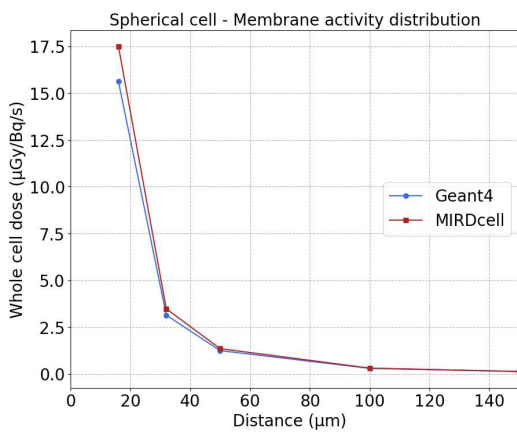Figure A.16: % difference between MIRDcell and Geant4 values

Figure A.17: Comparison between Geant4 and MIRDcell values
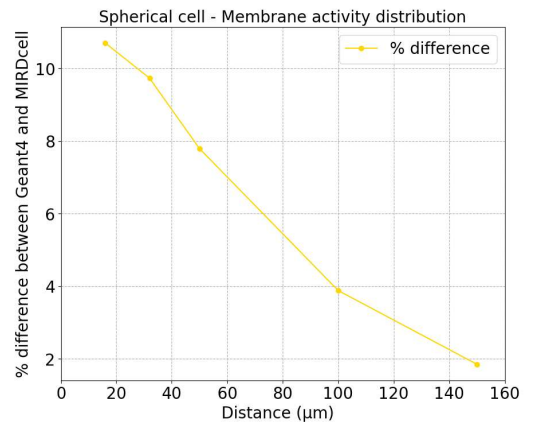
Figure A.18: % difference between MIRDcell and Geant4 values

^{177}Lu studies

- Cross-absorbed dose in the case of ^{177}Lu decay for the cell and its nucleus. In particular, see Fig. A.19 and A.20 for membrane activity distribution for ellipsoidal and spherical cell respectively and comparison with ^{111}Ag.

Figure A.19: Absorbed dose at different distances (ellipsoidal cell)

Figure A.20: Absorbed dose at different distances (spherical cell)

Figure A.21: Absorbed dose at different distances (spherical cell)

- Environment dose evaluation and dose comparison between silver and lutetium for nucleus absorbed dose:

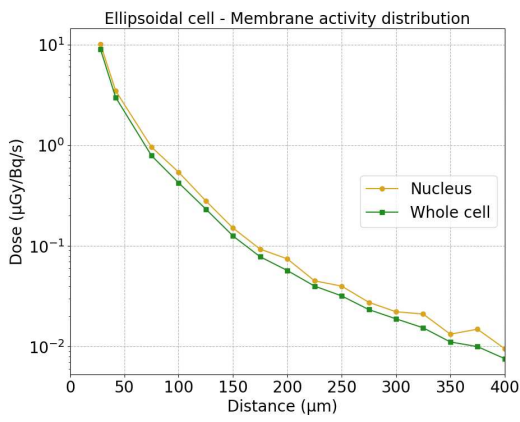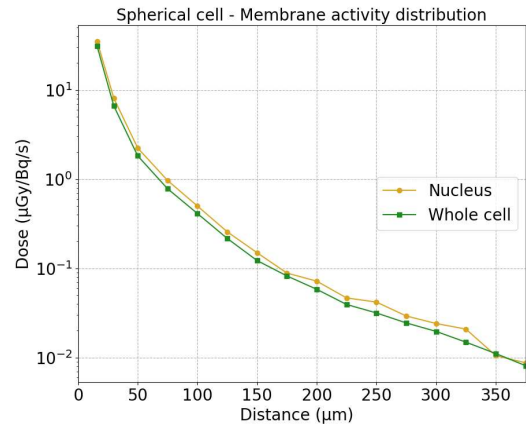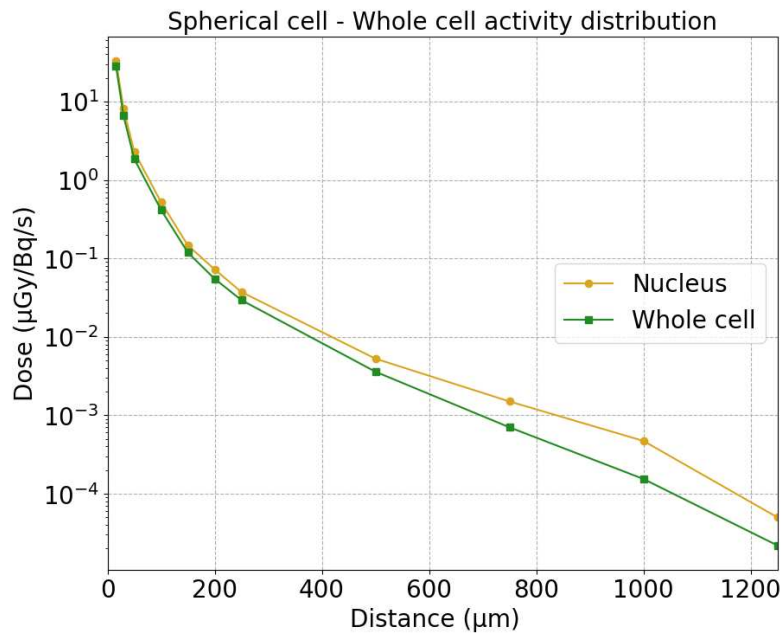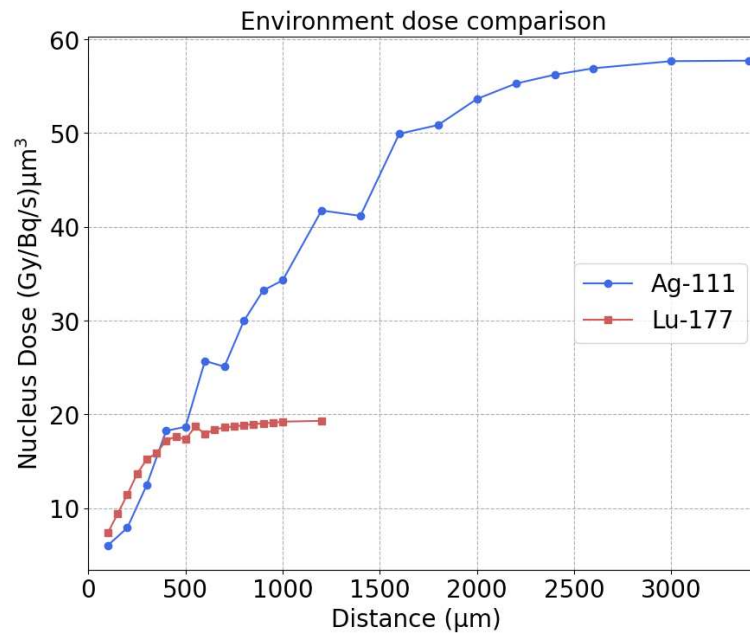Figure A.22: Dose absorbed by a spherical nucleus and its nucleus when the decays happen in the external environment with a constant density

Bibliography

[1] E.Vettorato *et al.*, *A new production method of high specific activity radionuclides towards innovative pharmaceuticals: the isolpharm project*, RAD Conference Proceedings, vol. 6, pp. 8–14, 2022;

[2] A.Andrighetto *et al.*, *The ISOLPHARM project: A New ISOL production method of high specific activity beta-emitting radionuclides as radiopharmaceutical precursors*, Applications of Nuclear Techniques (CRETE17), International Journal of Modern Physics: Conference Series, Vol. 48 (2018) 1860103 (11 pages);

[3] T.Marchi *et al.*, *The SPES facility at Legnaro National Laboratories*, 27th International Nuclear Physics Conference (INPC2019), Journal of Physics: Conference Series, 1643 (2020) 012036;

[4] G.Prete *et al.*, *The SPES project at the INFN- Laboratori Nazionali di Legnaro*, EPJ Web of Conferences, 66, 11030 (2014);

[5] `https://isolpharm.pd.infn.it/web/?page_id=967` (visited on May 2023);

[6] A.Andrighetto *et al.*, *The ISOLPHARM project: ISOL-based production of radionuclides for medical applications*, Vol.:(0123456789)1 Journal of Radioanalytical and Nuclear Chemistry (2019) 322:73–77;

[7] `https://www.lnl.infn.it/en/isolpharm-2/` (visited on May 2023);

[8] M.Ballan *et al.*, *Preliminary evaluation of the production of non-carrier added 111Ag as core of a therapeutic radiopharmaceutical in the framework of ISOLPHARM_ Ag experiment*, Applied Radiation and Isotopes 164 (2020) 109258;

[9] A.Andrighetto *et al.*, *Admiral proposal*, Project Proposal for INFN CSNV Experiment 2022;

[10] `https://geant4.web.cern.ch/about/` (visited on May 2023);

[11] `https://mirdsoft.org/mirdcell` (visited on May 2023);

[12] S.Agostinelli *et al.*, *Geant4—a simulation toolkit*, Nuclear Instruments and Methods in Physics Research A 506 (2003) 250–303;

[13] E.B.Podgoršak, *Radiation Physics for Medical Physicists*, third edition, Springer, ISSN 1868-4513;

[14] A.Dash, F.F.Knapp Jr,M.R.A.Pillai, *Targeted Radionuclide Therapy - An Overview*, Current Radiopharmaceuticals, 2013, 6, 000-000;

[15] J.P.Pouget, *Introduction to radiobiology for targeted radionuclide therapy*, Reviews in Medicine, March 2015, Volume 2, Article 12;

[16] `https://www.cirse.org/patients/general-information/ir-procedures/brachytherapy/` (visited on June 2023);

[17] C.Lawhn-Heath *et al.*, *Dosimetry in radionuclide therapy: the clinical role of measuring radiation dose*, www.thelancet.com/oncology, Volume 23 February 2022;

[18] A.I.Kassis, S.J.Adelstein, *Radiobiologic Principles in Radionuclide Therapy*, The Journal of Nuclear Medicine, Volume 46, No. 1 (Suppl), January 2005;

[19] S.V.Gudkov *et al.*, *Targeted Radionuclide Therapy of Human Tumors*, Int. J. Mol. Sci. 2016, 17, 33;

[20] S.Goldsmith, *Targeted Radionuclide Therapy: A Historical and Personal Review*, Seminars in Nuclear Medicine, Vienna, Austria in October 2017;

[21] D.V.Becker, C.T.Sawin, *Radioiodine and Thyroid Disease: The Beginning*, Seminars in Nuclear Medicine, Vol XXVI,No 3 (July), 1996:pp 155-164;

[22] G.M.Currie *et al.*, *Radionuclide production*, The Radiographer 2011, Volume 58 (3) 2011;

[23] L.Morselli *et al.*, *Production and characterization of 111Ag radioisotope for medical use in a TRIGA Mark II nuclear research reactor*, Applied Radiation and Isotopes 197 (2023) 110798;

[24] `https://lena.unipv.it/il-reattore/` (visited on July 2023);

[25] `https://www.lnl.infn.it/spes-ciclotrone/` (visited on July 2023);

[26] N.Chatterjee and G.C.Walker, *Mechanisms of DNA Damage, Repair, and Mutagenesis*, Environmental and Molecular Mutagenesis, Wiley Online Library, e 9 May 2017;

[27] G.Borrego-Soto *et al.*, *Ionizing radiation-induced DNA injury and damage detection in patients with breast cancer*, Genetics and Molecular Biology, 38, 4, 420-432 (2015);

[28] J.Seco, Lectures notes of the course *Medical Physics 1*, University of Heidelberg, Winter Semester 2022-2023;

[29] `https://en.wikipedia.org/wiki/Homologous_recombination` (visited on July 2023);

[30] `https://en.wikipedia.org/wiki/Non-homologous_end_joining` (visited on July 2023);

[31] S.J.McMahon *et al.*, *The linear quadratic model: usage, interpretation and challenges*, Phys. Med. Biol. 64 (2019) 01TR01 (24pp);

[32] S.B.Curtis, *Lethal and potentially lethal lesions induced by radiation: a unified repair model*, Biology and Medicine Division, Lawrence Berkeley National Laboratory, September 1985;

[33] R.D.Stewart, *Two-Lesion Kinetic Model of Double-Strand Break Rejoining and Cell Killing*, RADIATION RESEARCH 156, 365–378 (2001);

[34] W.E.Bolch *et al.*, *MIRD Pamphlet No. 21: A Generalized Schema for Radiopharmaceutical Dosimetry—Standardization of Nomenclature*, The Journal of Nuclear Medicine, Vol.50, No.3, March 2009;

[35] D.Sakata *et al.*, *Fully integrated Monte Carlo simulation for evaluating radiation induced DNA damage and subsequent repair using Geant4-DNA*, nature research, Scientific Reports, (2020) 10:20788;

[36] D.Sakata *et al.*, *Performance Evaluation for Repair of HSGc-C5 Carcinoma Cell Using Geant4-DNA*, Cancers 2021, 13, 6046. https://doi.org/10.3390/cancers13236046;

[37] W.-G.Shin *et al.*, *A Geant4-DNA Evaluation of Radiation-Induced DNA Damage on a Human Fibroblast*, Cancers 2021, 13, 4940. https://doi.org/10.3390/cancers13194940;

[38] `https://imagebank.hematology.org/image/63363/neutrophil-and-lymphocytes` (visited on July 2023);

[39] `https://editora.pucrs.br/edipucrs/acessolivre/livros/atlas-de-histologia/tecido-conjuntivo-propriamente-dito.html` (visited on July 2023);

[40] C.Janicki, *MIRD Techniques for Internal Dosimetry*, McGill University Health Center, 2004;

[41] `https://geant4-userdoc.web.cern.ch/UsersGuides/PhysicsListGuide/html/index.html` (visited on August 2023);

[42] Z.Cai *et al.*, *Monte Carlo N-Particle (MCNP) Modeling of the Cellular Dosimetry of 64Cu: Comparison with MIRDcell S Values and Implications for Studies of Its Cytotoxic Effects*, The Journal of Nuclear Medicine, Vol. 58, No. 2, February 2017;

[43] A.Arzenton, *Monte Carlo based dosimetry using PET/CT and SPECT/CT imaging in radiopharmaceutical therapy in the context of the ISOLPHARM project*, master thesis, Dipartimento di Fisica e Astronomia "Galileo Galilei", 2021;

[44] D.I.Filosa, *Ottimizzazione del software per la quantificazione del danno radioindotto al DNA visualizzato attraverso il saggio immunofluorescente γH2AX/53BP1*, bachelor thesis, Dipartimento di Fisica "Ettore Pancini", AA. 2019/2020;

[45] A.Leso, *Study of DNA damage by beta radiation using* Geant4-DNA *in the context of the ISOLPHARM project*, master thesis, Dipartimento di Fisica e Astronomia "Galileo Galilei", AA. 2022/2023;

[46] A.Dash *et al.*, *Production of 177Lu for Targeted Radionuclide Therapy: Available Options*, Nucl Med Mol Imaging (2015) 49:85–107;

[47] Master thesis of B.Marcaccio, *From radiobiological experiments to treatment planning in patients: a BNCT dosimetry study*, University of Pavia, Academic Year 2020-2021;

[48] K.Kossert *et al.*, *Activity determination of 60Co and the importance of its beta spectrum*, Applied Radiation and Isotopes 134 (2018) 212–218;

[49] Master thesis of E.Simeone, *Studi dosimetrici per la BNCT del Glioblastoma Multiforme con acceleratore*, University of Pavia, Academic Year 2021-2022;

[50] `https://www.atcc.org/products/htb-14` (visited on August 2023);

[51] `https://shop.gbo.com/en/row/products/bioscience/covid-19/covid-19-tc-flasks/690160.html` (visited on July 2023);

[52] `https://www.atcc.org/products/crl-1661` (visited on August 2023);

[53] `https://shop.gbo.com/it/italy/products/bioscience/covid-19/0110_9000_0040/627160.html` (visited on August 2023);

[54] `https://geant4-dna.github.io/molecular-docs/`(visited on August 2023);

[55] H.Nikjoo *et al.*, *Computational modelling of low-energy electron-induced DNA damage by early physical and chemical events*, Int J Radiat Biol 1997, vol.71, no.5, 467-483;

[56] `http://geant4-dna.org/` (visited on August 2023);

[57] L.Morselli, *Production and Characterization of 111-Ag for radiopharmaceutical applications in the gramework of the ISOLPHARM project*, University of Ferrara, Years 2019/2022;

[58] Ashutosh Dash *et al.*, *Production of 177Lu for Targeted Radionuclide Therapy: Available Options*, Nucl Med Mol Imaging (2015) 49:85–107;

[59] A.Arzenton, *Radiobiological model for β-emitter radiopharmaceutical therapy in dynamic cell cultures in the framework of the ISOLPHARM project*, Il Nuovo Cimento 46 C (2023) 72;

[60] `https://www.culturecollections.org.uk/products/celllines/generalcell/detail.jsp?refId=90111314&collection=ecacc_gc` (visited on August 2023);

[61] `https://it.wikipedia.org/wiki/Cobalto-60` (visited on August 2023);

[62] K.Howe *et al.*, *The genome sequence of the Norway rat, Rattus norvegicus Berkenhout 1769*, Wellcome Open Research 2021, 6:118;